

EXAMINATION OF TOPPLING BEHAVIOUR IN LARGE ROCK SLOPES

USING THE UDEC COMPUTER CODE

by

SUSAN L. NICHOL  
B.A., McGill University, 1988  
B.A.Sc., The University of British Columbia, 1997

A THESIS SUBMITTED IN PARTIAL FULFILLMENT  
OF THE REQUIREMENTS FOR THE DEGREE OF  
MASTER OF APPLIED SCIENCE

in

THE FACULTY OF GRADUATE STUDIES

(Department of Earth and Ocean Sciences)  
(Geological Engineering Program)

We accept this thesis as conforming  
to the required standard

THE UNIVERSITY OF BRITISH COLUMBIA

April 2000  
© Susan L. Nichol

In presenting this thesis in partial fulfilment of the requirements for an advanced degree at the University of British Columbia, I agree that the Library shall make it freely available for reference and study. I further agree that permission for extensive copying of this thesis for scholarly purposes may be granted by the head of my department or by his or her representatives. It is understood that copying or publication of this thesis for financial gain shall not be allowed without my written permission.

Department of Earth + Ocean Sciences

The University of British Columbia  
Vancouver, Canada

Date April 25, 2000

## ABSTRACT

The question of how to predict the catastrophic failure of a slowly deforming rock mass, be it a natural or engineered slope, remains unresolved despite a large body of research on the topic. The transition of the deformation mechanism from slow, self-stabilizing toppling to rapid, catastrophic detachment continues to hold the interest of researchers due to the proximity of many such deforming slopes to vital infrastructure such as major transportation routes and hydroelectric power facilities.

The idea that certain key parameters may influence toppling behaviour in a quantifiable way was examined through a qualitative study of a large rock slope carried out using the Universal Distinct Element Code (UDEC). The slope was modelled using variations of intact rock strength, discontinuity orientation and persistence, and toe conditions. While it was not feasible to consider every possible parameter, this study allowed the influence of small changes to be tracked, and boundaries of behaviour to be mapped.

The study showed that stable flexural toppling develops in rock masses characterized by weak to medium-strength rock with relatively few cross-joints. Stresses in these cases remain sub-parallel to the ground surface in the upper portions of the slope. The study demonstrated that deformation of slopes undergoing flexural toppling is relatively slow and generally does not accelerate. With slow rotation, discontinuity dips become sufficiently shallow that flexural toppling is no longer kinematically feasible and these slopes ultimately stabilize. With more persistent cross-joints and stronger rock, the study showed that deformation generally accelerates and catastrophic brittle toppling failure is more likely to occur. This type of failure is strongly promoted by toe undercutting. Stress distributions show sub-vertical stresses dominating the upper portions of the slope. Simplified models of Mystery Creek (catastrophic failure) and Mount Breakenridge (stabilized) were able to demonstrate these contrasting types of behaviour.

## TABLE OF CONTENTS

	<i>Page</i>
Abstract	ii
List of Figures	v
List of Tables	vii
Acknowledgements	viii
1.0 Introduction	1
2.0 Theory and Analysis of Toppling Behaviour	4
2.1 Toppling Mechanism	4
2.2 Stability Analysis	5
2.3 Discontinuity Strength	8
2.4 Rock Mass Strength	10
2.5 In Situ Stress Conditions	13
3.0 Review of Numerical Modelling Theory	21
3.1 Continuum Methods	22
3.2 Discontinuum Methods	25
4.0 Case Histories from the Literature	31
4.1 Heather Hill, Glacier National Park, British Columbia	31
4.2 Clapière, Southern France	32
4.3 Affliction Creek, British Columbia	34
4.4 Glen Pean, South Inverness-shire, Scotland	35
4.5 Ben Attow, Scotland	37
4.6 Billan, France	38
4.7 Torreggio, Italy	39
4.8 Brenda Mine, Peachland, British Columbia	40
4.9 Luscar Mine, Hinton, Alberta	41
4.10 Chuquicamata Mine, Chile	43
5.0 Numerical Modelling Study - Methodology	55
5.1 General Modelling Procedure	56
5.2 Parametric Modelling	59
5.2.1 Intact Rock Strength	59
5.2.2 Cross-Jointing	60
5.2.2.1 Persistence	61
5.2.2.2 Spacing	61
5.2.2.3 Orientation	62
5.2.3 Toe Conditions	62

	<i>Page</i>
6.0 Numerical Modelling Study - Results	69
6.1 Variation of Intact Rock Strength	69
6.2 Cross-Joints	71
6.2.1 Variation of Persistence	71
6.2.2 Variation of Spacing	73
6.2.3 Variation of Orientation	74
6.3 Variation of Toe Conditions	75
7.0 Mystery Creek Case Study	95
7.1 Background Information	95
7.2 UDEC Modelling	97
8.0 Mount Breakenridge Case Study	109
8.1 Background Information	109
8.2 UDEC Modelling	113
9.0 Discussion	127
10.0 Conclusions and Recommendations	134
10.1 Conclusions	134
10.2 Recommendations for Further Work	136
References	139
Appendix	
Estimation of constants for the Generalised Hoek-Brown failure criterion	145

## LIST OF FIGURES

No.	Title	Page
2-1	Types of toppling	15
2-2	Kinematic test for toppling	16
2-3	Limits of poles to discontinuities that permit common toppling on a 70° slope with $\phi = 30^\circ$	16
2-4	Section through common topples	17
2-5	Joint Roughness Coefficient (JRC) values	18
2-6	Rock Mass Rating (RMR) System classification form	19
2-7	Typical curved shear strength envelope defined by Hoek-Brown theory for rock mass strength	20
4-1	Heather Hill Landslide, location and cross-section	45
4-2	UDEC modelling of Heather Hill Landslide	46
4-3	Failure mechanism of La Clapière	47
4-4	Geology and slope movement features of the Affliction Creek study area	48
4-5	Cumulative normalized slope movements at Affliction Creek	49
4-6	North-south section through Glen Pean slide	50
4-7	Geomorphological map of the southwest slope of Ben Attow	50
4-8	General slope profile of the Billan landslide	51
4-9	Block geometry and assumed water table for UDEC modelling of Brenda Mine	51
4-10	Pure flexural toppling deformation at Brenda Mine	52
4-11	“Graben” toppling deformation at Brenda Mine	53
4-12	Geological structure in Luscar pit	54
5-1	Initial model set up for parametric study	63
5-2	Outer slope geometry for parametric study	63
5-3	Four cases of variation in cross-joint persistence	64
6-1	Block plots for variation of intact rock strength after approximately 20 seconds run time	76
6-2	Detail of displacement vectors for variation of intact rock strength after approximately 20 seconds run time	79
6-3	Detail of principal stresses for variation of intact rock strength after approximately 20 seconds run time	80
6-4	Block plots for variation in cross-joint persistence after approximately 18 seconds run time	81
6-5	Stresses in the slope for Test 0	84
6-6	Velocity history for Test 2	85
6-7	Shear displacement for idealized cross-joints	86
6-8	Block plots for variation in spacing normal to cross-joints after approx. 20 seconds run time	87

No.	Title	Page
6-9	Displacement vectors for a single cross-joint	88
6-10	Test 3 after approximately 20 s run time	89
6-11	Shear plots for horizontal cross-joints (normal spacing 50 m)	90
6-12	Detail of horizontal cross-joints after 70000 cycles	91
6-13	Block plot of oversteepened slope #1 after 40000 cycles	91
6-14	Block plot of oversteepened slope #2	92
6-15	Block plot for GSI = 48, $m_i = 2.5$ , UCS = 10 MPa	93
6-16	X-Displacement Contours for GSI = 48, $m_i = 2.5$ , UCS = 10 MPa; and GSI = 62, $m_i = 12$ , UCS = 10 MPa	94
7-1	Location of Mystery Creek rock avalanche	101
7-2	Mystery Creek rock avalanche	102
7-3	Photo of Mystery Creek rock avalanche	103
7-4	Photographs of toppling in rock mass on southern edge of scar	104
7-5	Structural data collected at: (a) Mystery Creek (by the author); (b) Mt. Currie (by Evans, 1987).	105
7-6	Input geometry for UDEC modelling of Mystery Creek	106
7-7	Displacement and shear without cross-joints in Mystery Creek model.	106
7-8	Block plot of fully continuous cross-joints after 50 000 cycles	107
7-9	Block plot of cliff in Mystery Creek model after 30000 cycles	107
7-10	Block plot of cliff in Mystery Creek model after 49000 cycles	108
8-1	Location of Mount Breakenridge slope movement	117
8-2	Photo of Mount Breakenridge disturbed slope	118
8-3	Geology of Harrison Lake area	119
8-4	Structural data from the Slollicum Formation	120
8-5	Comparison between structural orientations inside and outside of disturbed area	121
8-6	Mount Breakenridge geometry: Section b-b from TCL report (Anon., 1990, Fig. 4)	122
8-7	Initial input geometry for Mount Breakenridge UDEC model	122
8-8	Initial input geometry with joints	123
8-9	Detail of deformation in upper portion of Mount Breakenridge slope	124
8-10	Kink band development near base of columns	125
8-11	Bulging of the toe area	125
A-1	Estimation of constants $m_b / m_i$ , $s$ , $a$ , deformation modulus $E$ and the Poisson's ratio $\nu$ for the Generalised Hoek-Brown failure criterion based upon rock mass structure and discontinuity surface conditions for undisturbed rock mass (Hoek et al., 1995, Table 8-4)	146

## LIST OF TABLES

No.	Title	Page
2-1	Rock mass quality classifications based on Tunnelling Quality Index, $Q$	20
5-1	Monitoring points	66
5-2	Rock strength parameters used in UDEC modelling	66
5-3	Spreadsheet for calculation of Hoek-Brown and Mohr-Coulomb parameters	67
5-4	Parameters for variation of cross-joint persistence	68
7-1	Input parameters for UDEC modelling of Mystery Creek	108
8-1	Initial input parameters for UDEC modelling of Mount Breakenridge	126
8-2	Secondary input parameters for UDEC modelling of Mount Breakenridge	126

## ACKNOWLEDGEMENTS

This work was carried out under the Professional Partnership Program between BC Hydro and the University of British Columbia. I am very grateful for the financial and professional support of BC Hydro. I wish to thank everyone in the Geotechnical and Water Resources Group, and in particular K.Y. Lum, M.K. Lee, L. Cornish, J.K. Lou and K. Ahlfield, for making my experience in the Partnership Program enjoyable and extremely rewarding.

I would like to thank my advisor, Dr. Oldrich Hungr, for his patience, guidance and support (educational and financial). His outlook on life helped to keep my stress level at a minimum. I wish to express my gratitude to the members of my committee for their time and effort on my behalf: Dr. L. Kennedy and Dr. R. Chase (UBC Department of Earth and Ocean Sciences), Dr. M. Bovis (UBC Department of Geography), Dr. R. Pakalnis (UBC Department of Mining and Mineral Processing Engineering), and Dr. S.G. Evans (Geologic Survey of Canada, Ottawa). As well, I thank the faculty and staff in the Department of Earth and Ocean Sciences for creating a great environment for learning.

Dr. S.G. Evans of the GSC generously allowed access to data for the Mystery Creek case study. D. Smith, P.Eng, of Thurber Engineering kindly provided information on the Mount Breakenridge site. R. Enegren, P.Eng., of BC Hydro graciously arranged a field trip to the Wahleach Hydroelectric Project, although the site was ultimately not included in this research. Dr. B. Ripley, P.Eng., of BC Hydro provided support and encouragement.

Various people provided assistance in one form or another over the last few years and I greatly appreciate and acknowledge their efforts: N. Rose for UDEC support; T. Good for field assistance; D. Weir for keeping me out of the river; N. Young for inspiration and perspective; Dr. B. Mackay for providing writing tools and encouragement; J. Steele for graphics help; EBA Engineering Consultants for flexibility and use of their scanner; L. Fletcher and D. Ayotte for interesting conversations and kind support; and J. Schrank for friendship.

My friends and my family (Nichol and Scott) have been incredibly loving and supportive of all my undertakings and I thank them for helping me to achieve my goals.

Finally, this work would not have been possible without the incredible love, patience and support of my husband, Peter Scott.

## 1.0 INTRODUCTION

Natural hazards pose increasing risk to people and infrastructure as population expands. The damage caused by natural hazards is often severe, and as population increases the cost to repair the damage and the potential for lives to be lost also increase. Underestimating the impact of an event may lead to loss of human life or expensive legal responsibility. The main challenge presented by natural hazards is that, to a large extent, many events are unpredictable. This complicates the design of mitigation strategies. The overriding factor in the mitigation of the risk due to natural hazards is economics. Understanding the cause(s) of a landslide requires data, which often are expensive to obtain. As well, the cost of safety structures and other methods of risk reduction must be balanced with the cost of the risk to downslope resources.

Extremely slow ( $< 16$  mm/year) to slow ( $< 1.6$  m/year) landslides, as defined by Cruden and Varnes (1996), do not pose a serious threat to resources and lives downslope and can be managed. However, when a landslide is extremely rapid ( $> 5$  m/s), there is essentially no possibility of escape for structures or people in its path. Of various possible failure mechanisms, toppling is particularly interesting because some slopes experiencing toppling behaviour slowly stabilize over time, while toppling movements on other slopes result in extremely rapid, highly destructive landslides. The question of how to predict the potential for catastrophic failure of a slowly deforming rock mass, be it a natural or engineered slope, remains unresolved despite a large body of research on the topic. The transition of the deformation mechanism from slow, self-stabilizing toppling to rapid, catastrophic detachment continues to hold the interest of researchers due to the proximity of many such

deforming slopes to vital infrastructure such as major transportation routes and hydroelectric power facilities. There is a need to understand when and why certain slopes stabilize in order to assess which cases will fail and which will not.

Predicting catastrophic failure of toppling slopes is difficult, mainly due to the variability that occurs in nature. For the various methods of slope stability analysis, there are many parameters that must be quantified, but seldom is it possible to actually measure each parameter in the field. Economics usually determines the amount of information that is obtained from an unstable slope. Even with extensive financial resources, the amount of information acquired is usually limited, and subsurface conditions must be interpolated between a few drill holes or estimated from surface information. From surficial structural data, it is possible to predict whether toppling is a possible failure mechanism, e.g., using a stereonet, but whether the deformation will lead to catastrophic failure is generally unknown.

With improvements in computer technology, it is now possible to carry out detailed studies of deforming slopes, and to back-analyze failed slopes, in a relatively short amount of time. Numerical modelling methods, originally developed to analyze civil structures, have been successfully adapted to soil and rock mechanics problems. Although numerical methods are powerful, they still require a number of assumptions about subsurface conditions; thus, they should be considered only as an additional analysis tool and not as a substitute for traditional geotechnical engineering practice. One notable improvement of numerical methods over limit equilibrium methods is that the failure mechanism is identified from the analysis rather than being one of the input parameters. Numerical methods also allow for creation of a virtual laboratory where the influence of various parameters can be studied.

Two failure mechanisms associated with toppling, which involves rotation of columns or blocks of rock about some fixed base, are examined in this study: a ductile mechanism (flexural toppling) and a brittle mechanism (block toppling). It can be shown that these two mechanisms have significantly different stress distributions that result in fundamentally different behaviour. The idea that certain key parameters may influence the toppling failure mechanism in a quantifiable way is the hypothesis behind this study. A qualitative study of a large rock slope was carried out using the Universal Distinct Element Code (UDEC), a software package developed by Itasca Consulting Group. The slope was modelled using variations of intact rock strength, discontinuity orientation and persistence, and toe conditions. It was not feasible to consider every possible parameter. While perhaps somewhat simplistic, this study allowed the influence of small changes to be tracked, and boundaries of behaviour to be mapped. Mystery Creek and Mount Breakenridge, two slopes with fundamentally different behaviour, were then examined and compared in terms of the results of the parametric study.

This document provides the following information: the theory of toppling behaviour (Chapter 2) and the theory of numerical modelling (Chapter 3) are reviewed; case histories from the literature are described (Chapter 4); the methodology (Chapter 5) and results (Chapter 6) of the study are given; Mystery Creek (Chapter 7) and Mount Breakenridge (Chapter 8), are examined in terms of the results of the study; a detailed discussion of all aspects of the research is provided (Chapter 9); and conclusions and recommendations for further work are summarized (Chapter 10).

## 2.0 THEORY AND ANALYSIS OF TOPPLING BEHAVIOUR

Landslides have been recorded for centuries. However, significant developments in the field of rock mechanics have occurred only over the last several decades. A number of catastrophic failures, e.g., Vaiont in Italy in 1963, and Nevado Huascarán in Peru in 1962 and 1970, encouraged research in this area, in order to improve understanding of failure mechanisms and prevent such catastrophes from reoccurring.

Four primary failure mechanisms in rock have been identified: planar, wedge, circular and toppling (Hoek and Bray, 1981). Many landslides involve complex combinations of these primary mechanisms. Toppling is perhaps the most difficult of these to analyze, as it involves the mechanical interaction of rock fragments separated by discontinuities.

### 2.1 *Toppling Mechanism*

Three types of toppling behaviour have been defined by Goodman and Bray (1976): block toppling, flexural toppling and block flexure toppling (Figure 2-1). Block toppling is the result of widely-spaced joints which divide the rock mass into columns. Cross-joints provide release surfaces (Figure 2-1a). The columns rotate forward out of the slope, and stability is dependent on the location of the centre of gravity of the columns. Where the centre of gravity falls outside the base of the column, the column is normally free to overturn. Once the outermost column fails, the second column is free to rotate further forward. Such systems are usually open, due to the release surfaces, and pore water pressure is normally free to drain.

Such systems also tend to fail catastrophically, for once the columns begin to tip, there is no stabilizing force. Block toppling is analogous to the instability of a row of books on a shelf.

Flexural toppling occurs where there is one dominant, relatively closely-spaced set of steeply-dipping discontinuities dividing the rock mass into columns (Figure 2-1b). There may be some cross-jointing, though not sufficient to permit free rotation of the blocks. The columns bend out of the slope like cantilever beams. The bending is accommodated by slip between the columns. Groundwater pressures may vary significantly throughout the slope due to the limited number of flow paths through the columns. Slopes undergoing flexural toppling often self-stabilize, once the dips of the discontinuities become sufficiently shallow due to rotation, and do not fail catastrophically.

Block flexure toppling is a combination of the two types, characterized by the bending of long columns and motion along numerous cross-joints (Figure 2-1c). Sliding becomes possible on the cross-joints due to oversteepening caused by bending of the columns.

## 2.2 *Stability Analysis*

Various methods exist to analyze slope stability with respect to sliding. Empirical methods, developed predominantly for mining applications, attempt to group data for similar slopes. Charts have been developed to assess slope height – slope angle stability relationships (e.g., Hoek and Bray, 1981, Figure 7). The notable problem with these methods is that, due to the variability found in nature, it is often not possible to determine precise groupings. While

previous experience is always valuable, it does not necessarily provide sufficiently detailed information.

Limit equilibrium methods have also been developed to assess the stability of slopes subject to block toppling (Goodman and Bray, 1976). These methods assume rigid blocks, and are thus not as effective for flexural toppling. As well, a failure surface must be assumed as one of the input parameters, rather than determined from the analysis.

Block theory, developed by Goodman and Shi (1985), is a method that identifies the types of blocks that can be formed in a jointed rock mass and which are potentially moveable. It can handle an unlimited number of joint sets, but assumes that all joint surfaces are perfectly planar and infinitely long.

In order for flexural toppling failure to occur, movement must be kinematically feasible. Goodman and Bray (1976) defined the conditions that must be satisfied in order for toppling to occur:

$$H / B > \cot (90 - \psi) \quad [1]$$

$$\beta \geq \phi + (90 - \psi) \quad [2]$$

H and B are the height and width of the block,  $\psi$  is the dip of the discontinuity,  $\beta$  is the slope angle, and  $\phi$  is the friction angle along the discontinuity. Equation [1] determines whether rotation is possible, i.e., whether the centre of gravity lies outside the base of the block, and [2] defines the potential for inter-layer (flexural) slip. Equation [2] assumes that principal

stresses in the slope are parallel to the slope face, which was shown to be reasonable for gravitational stresses in long, steep slopes by Savage et al. (1985), among others.

Stereonets, specifically equatorial equal-area stereonets, offer a simple way of compiling and analyzing discontinuity data. Failure modes can be predicted based on the orientation of discontinuities, slope orientations and frictional properties under dry conditions. Goodman and Bray (1976) used equation [2] to demonstrate that for toppling to occur in a slope where the main principal stress is parallel to the slope, the pole to the discontinuity set must lie outside a great circle that is  $\phi$  degrees beyond the slope face (Figure 2-2). Goodman and Bray (1976) argued that, because the discontinuity set must strike roughly parallel to the slope face, this test should only be used where the discontinuities strike within  $10^\circ$  of the strike of the slope, i.e., their poles lie in the shaded region shown in Figure 2-2. While this region was expanded to  $20^\circ$  (Matheson, 1983) and  $30^\circ$  (Goodman, 1980), Cruden (1989) pointed out that these values were arbitrary and demonstrated that toppling may occur in a significantly wider range of discontinuity orientations than acknowledged by Goodman and Bray (1976). The limits of the poles to discontinuities allowing common toppling as determined by Cruden (1989) are shown in Figure 2-3. Note that Cruden (1987) defined anaclinal slopes as those where discontinuities dip into the slope (Figure 2-4a), and underdip cataclinal slopes as those where discontinuities dip parallel to and more steeply than the slope (Figure 2-4b), while plagioclinal slopes are those between  $20^\circ$  and  $70^\circ$  to the strike of the discontinuities. Cruden (1989) argues that toppling under gravity alone on underdip cataclinal slopes is probably confined to flexural toppling, because in order for columns oriented as shown in Figure 2-4b

to topple as blocks, other processes such as creep must help to rotate the columns through the vertical.

### 2.3 *Discontinuity Strength*

Rock joints provide most of the weakness, deformability and conductivity of typical rock masses (Barton, 1986). The strength of individual discontinuities obviously plays an important role on the amount of deformation that can take place. The relationship between shear strength and normal stresses acting on a joint surface is usually expressed as:

$$\tau = c + \sigma \tan\phi \quad [3]$$

where  $\tau$  is the failure shear stress (“strength”),  $c$  is cohesion,  $\sigma$  is the normal stress, and  $\phi$  is the angle of friction on the discontinuity surface. Rock discontinuities generally do not have true cohesion. The factor “ $c$ ” therefore represents either intact rock “bridges” caused by limited joint persistence or an apparent cohesion caused by curvature of the strength envelope. The friction angle may be broken down into a basic friction angle,  $\phi_b$ , and a roughness component,  $i$ , related to asperities on the surface, as demonstrated by Patton (1966). As forces resisting movement on the surface are overcome, shear stress gradually reaches a maximum (peak shear strength), and thereafter the shear stress required to cause further shear displacement drops rapidly and levels out at a constant value called the residual shear strength (Hoek and Bray, 1981). For residual strength, apparent cohesion no longer exists (i.e., equal to zero), and the residual friction angle is lower than the peak friction angle.

Most rocks have a basic angle of friction the same as the residual angle for natural joints, lying between approximately 25° and 35° (Barton 1973).

Ladanyi and Archambault (1970) proposed the following equation for peak shear strength:

$$\tau = [\sigma (1 - a_s) (\nu + \tan\phi) + a_s \tau_r] / [1 - (1 - a_s) \nu \tan\phi] \quad [4]$$

where  $a_s$  is the proportion of the discontinuity surface over which asperities of intact rock material have been sheared through,  $\nu$  is the dilation rate  $dv/du$  (change in vertical displacement/change in horizontal displacement) at peak shear strength, and  $\tau_r$  is the shear strength of the intact rock material. Hoek and Bray (1981) comment that  $a_s$  is not easy to measure, even under laboratory conditions, and that while the dilation rate can be measured, it has not been standard practise to measure it. Hence,  $\nu$  only exists for a small proportion of published data. Empirical relationships for  $\nu$  and  $a_s$  were later proposed by Ladanyi and Archambault (1972) in order to make equation [4] more useful.

An alternative empirical relationship for predicting shear strength was proposed by Barton (1973, 1986):

$$\tau = \sigma_n \tan[\phi_b + JRC \log_{10}(JCS/\sigma_n)] \quad [5]$$

where  $\sigma_n$  is the normal stress acting on the surface,  $\phi_b$  is the basic friction angle, JRC is the joint roughness coefficient, and JCS is the joint wall compressive strength. Joint roughness coefficients are shown in Figure 2-5. The  $JCS/\sigma_n$  term gives a measure of the strength of the asperities, i.e., whether dilation up and over asperities will occur (low normal stress) or whether the asperities will be sheared off (higher normal stress).

Hoek and Bray (1981) point out that Barton's original studies were carried out at very low normal stress levels, and equation [5] is probably applicable in the range  $0.01 < \sigma_n/JCS < 0.3$ ; however, as most rock slope stability problems fall within this range, Hoek and Bray (1981) considered Barton's relationship to be useful for slope problems.

#### 2.4 *Rock Mass Strength*

The Geomechanics Classification or Rock Mass Rating (RMR) system was developed empirically by Bieniawski in 1973. This system has been revised over time, and Bieniawski has made significant changes to the original system (Bieniawski, 1989). The system uses six factors: the strength of the intact rock (point load index or UCS); rock quality designation (RQD); discontinuity spacing; discontinuity conditions; groundwater conditions; and an adjustment for discontinuity orientations. A sample of a rock mass classification form is shown in Figure 2-6. RQD was developed by Deere et al. (1967) as a quick and objective technique for estimating rock mass quality from drill core, and is calculated as the ratio of the sum of the lengths of all pieces of core greater than 10 cm to the total length of the core run. In the absence of drill core, Palmstrom (1982) suggested the following relationship for clay-free rock masses:

$$RQD = 115 - 3.3 J_v \quad [6]$$

where  $J_v$  is the sum of the number of joints per unit length for all joint (discontinuity) sets known as the volumetric joint count. As RQD is directionally dependent, use of the volumetric joint count may be helpful in reducing this dependence (Hoek et al., 1995).

Barton et al. (1974) used a large number of underground excavation case histories to develop the Tunnelling Quality Index,  $Q$  for determining rock mass characteristics and tunnel support requirements, as defined in the following equation:

$$Q = (RQD / J_n) (J_r / J_a) (J_w / SRF) \quad [7]$$

where RQD is the rock quality designation described above,  $J_n$  is the joint set number,  $J_r$  is the joint roughness number,  $J_a$  is the joint alteration number,  $J_w$  is the joint water reduction number, and SRF is the stress reduction factor. The value of the index  $Q$  varies from 0.001 to 1000 on a logarithmic scale. It is possible to consider RQD/ $J_n$  a very crude representation of average block size, and  $J_r/J_a$  to represent joint surface integrity and strength. Tables exist for determining values for each of the parameters (e.g., Hoek et al., 1995, Table 4.6). The SRF term is set equal to 1 for the purpose of analytical or numerical modelling, where the influence of stress is taken into account within the model, and the index should be referred to as  $Q'$  (Modified Rock Quality Index) when this is the case. The classifications in Table 2-1 of rock mass quality based on the evaluation of  $Q$  were proposed by Barton et al. (1974).

Another empirical method was developed by Hoek and Brown (1980, 1988, 1997; Hoek et al., 1992, 1995) using observations from field and laboratory studies and a strength criterion derived from the Griffith crack theory of rock fracture. Three parameters are required to define the curved (i.e., non-linear) strength envelope: the uniaxial compressive strength of the intact rock, and two dimensionless material constants,  $m$  (dependent on rock type) and  $s$  (dependent on degree of fracturing). A typical curved shear strength envelope is shown in Figure 2-7. In the equation given in Figure 2-7,

$$\tau = [\cot (\phi_i') - \cos (\phi_i')] m \sigma_c / 8 \quad [8]$$

$\phi_i'$  is the instantaneous friction angle at given values of  $\tau$  and  $\sigma'$ . At low normal stresses, blocks are interlocked and  $\phi_i'$  is high. At higher normal stresses, shearing of the rock is started, which lowers the friction angle. Instantaneous cohesion ( $\tau - \sigma' \tan(\phi_i')$ ), which is initially low, progressively increases with increasing normal stress as a result of greater confinement and tighter interlocking.

Use of the RMR system to estimate the material constants  $m$  and  $s$ , assuming completely dry conditions and a very favourable joint orientation, had been suggested by Hoek and Brown (1988). This process is satisfactory where the RMR is greater than about 25, but is unacceptable for poor rock masses (the minimum value for RMR is 18 (Hoek et al., 1995)). Hoek et al. (1995) describe the Geologic Strength Index (GSI) as an alternative to Bienieawski's RMR system. GSI is linked to both versions of Bieniawski's RMR system:

for  $RMR_{76} > 18$ :

$$GSI = RMR_{76} \quad [9]$$

for  $RMR_{89} > 23$ :

$$GSI = RMR_{89} - 5 \quad [10]$$

A general form of the Hoek-Brown failure criterion was presented by Hoek et al. (1995), and is written as:

$$\sigma'_1 = \sigma'_3 + \sigma_c \{m_b (\sigma'_3 / \sigma_c) + s\}^a \quad [11]$$

To estimate the material constants  $m_b$ ,  $s$  and  $a$ , the following relations were suggested (Hoek et al., 1995; Hoek and Brown, 1997):

$$m_b = m_i \exp [(GSI - 100) / 28] \quad [12]$$

for  $GSI > 25$  (undisturbed rock masses):

$$s = \exp [(GSI - 100) / 9] \quad [13]$$

$$a = 0.5 \quad [14]$$

for  $GSI < 25$  (undisturbed rock masses):

$$s = 0 \quad [15]$$

$$a = 0.65 - (GSI / 200) \quad [16]$$

Tables for estimating  $m_i$  based on rock type and GSI based on rock mass structure and surface conditions of discontinuities were presented by Hoek and Brown (1997). GSI ranges from about 10 for extremely poor rock masses to 100 for intact rock. Using estimated values for  $m_i$  and GSI, and the intact rock strength, it is possible to derive the Mohr-Coulomb envelope. This is described further in Chapter 5.

## 2.5 *In Situ Stress Conditions*

Measurements of in situ horizontal stresses at civil and mining sites around the world have shown that the ratio of horizontal to vertical stresses tends to be high at shallow depths and decreases at depth (Hoek et al., 1995). The direction of measurement is particularly important in layered sedimentary or metamorphic rocks, because the deformation moduli are likely to be significantly different in different directions.

Stress conditions at a particular site are not easy to determine. The geologic history of the site may have resulted in residual stresses; for example, stress changes were induced by

glaciation, and many landslides are the result of re-equilibration of in situ stresses, as well as unloading in the direction of the valley remaining after glacial retreat. It is also possible that sufficient time has passed since glaciation to have allowed a significant portion of any residual stresses in such slopes to dissipate.

If stresses are due to gravity alone, for long steep slopes the principal compressive stress near the slope surface is assumed to be parallel to the face of the slope, which has been shown to be reasonable by Savage et al. (1985), among others. This stress state sets up conditions favourable to toppling, as illustrated in Figure 2-4.

All of the above conditions must be considered when setting up numerical models. In the majority of cases, assumptions need to be made regarding in situ conditions, as it is usually not economically feasible to collect all of the necessary data in the field.

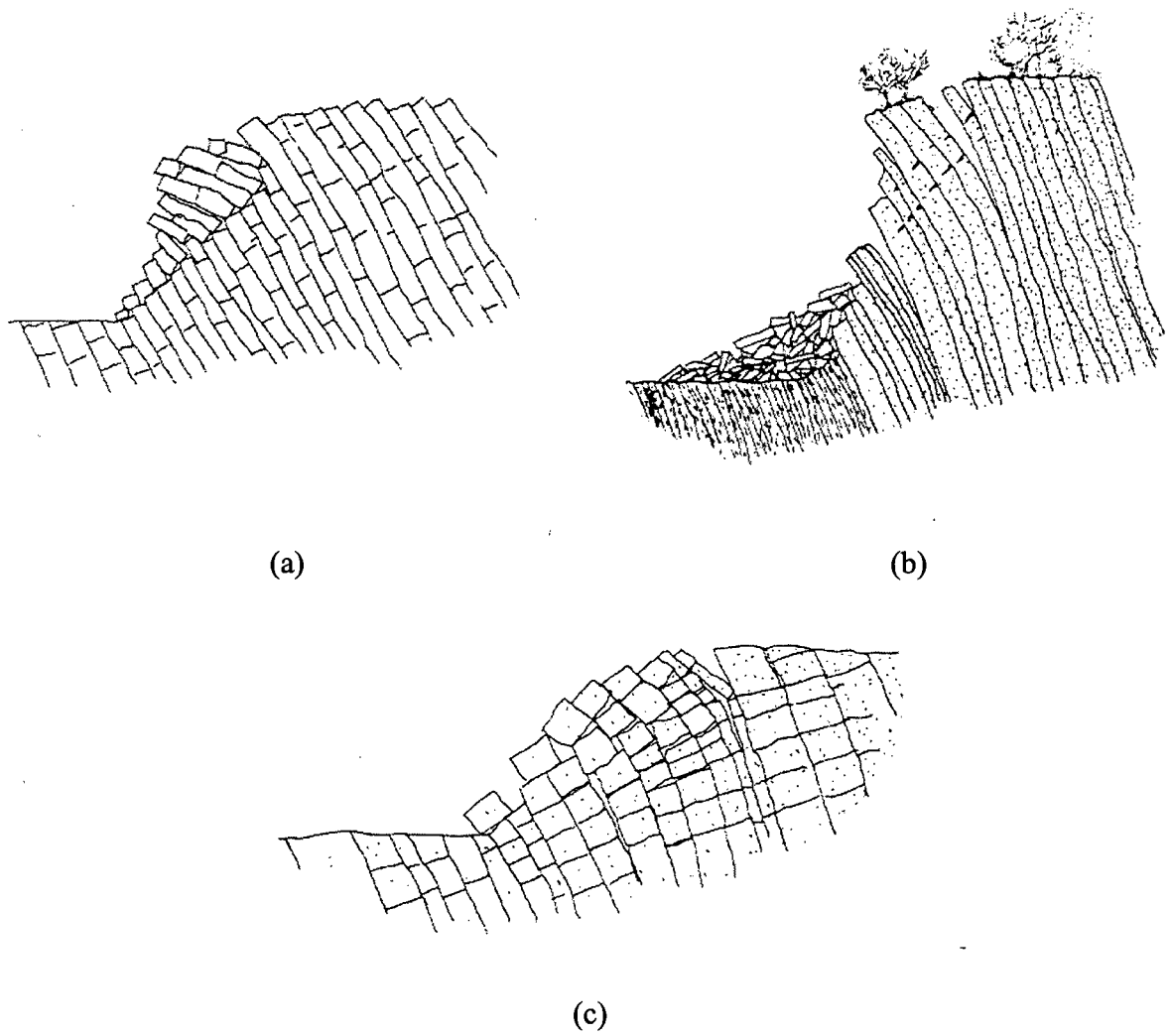


Figure 2-1: Types of Toppling: (a) block toppling; (b) flexural toppling; (c) block flexure toppling (after Goodman and Bray, 1976, Fig. 1).

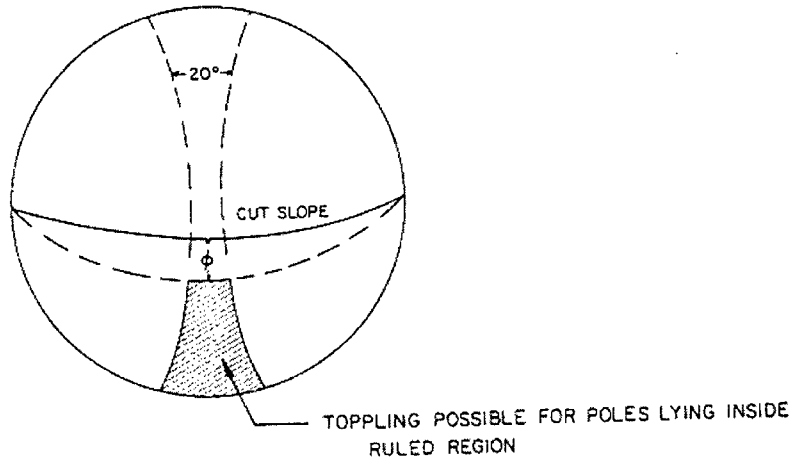


Figure 2-2:  
Kinematic test for toppling  
(Goodman and Bray,  
1976).

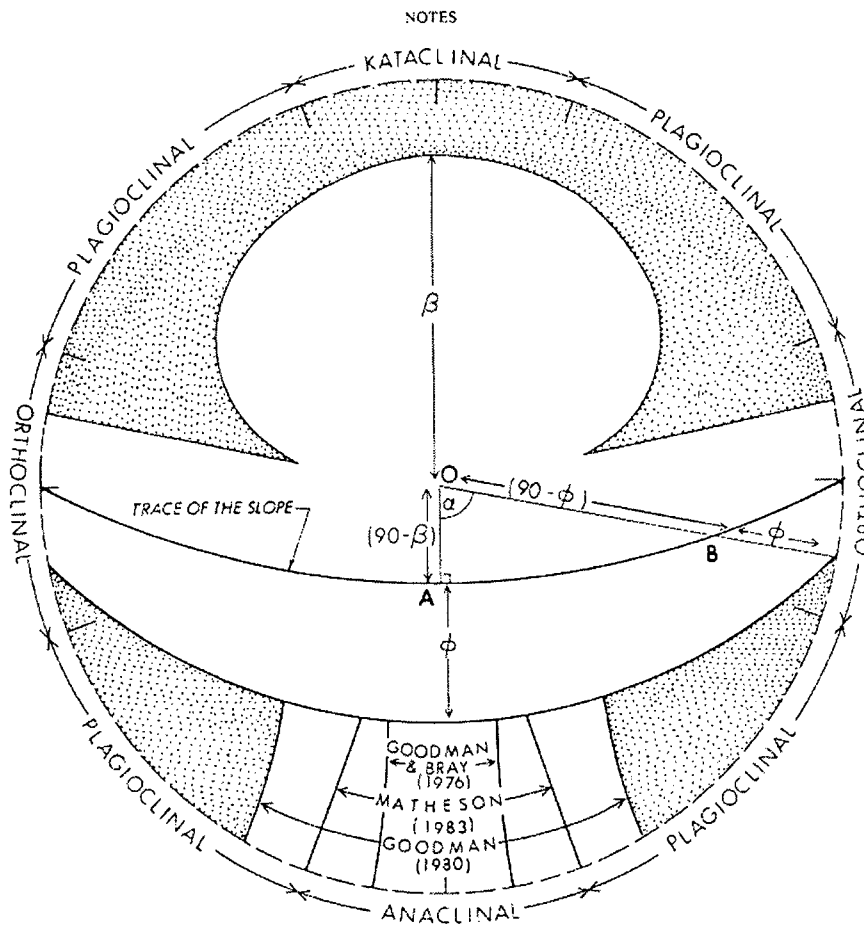


Figure 2-3: Limits of poles to discontinuities that permit common toppling on a 70° slope with  $\phi = 30^\circ$  (Cruden, 1989, Fig. 4).

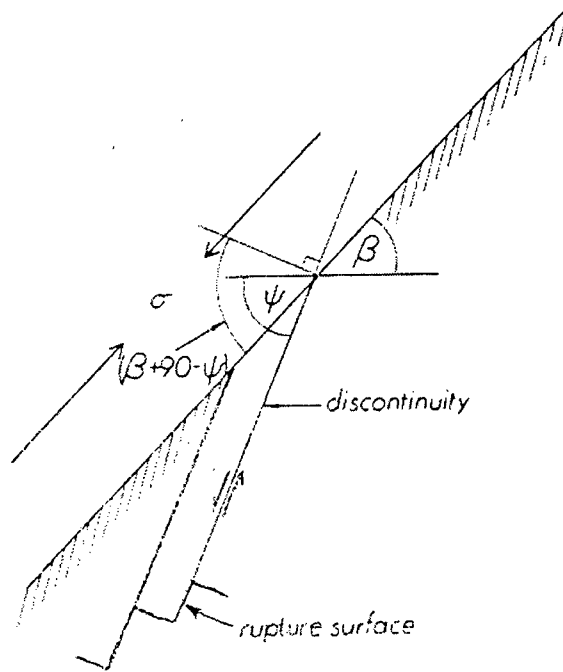
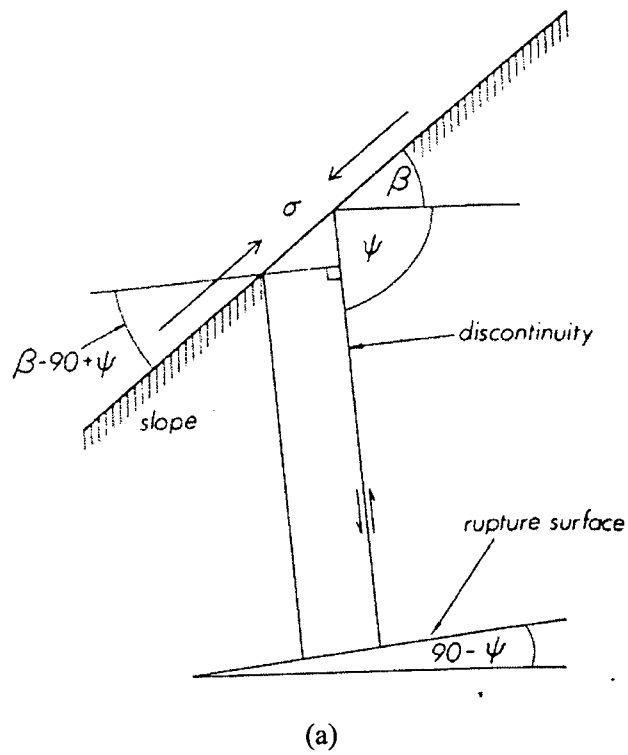


Figure 2-4: Section through common topples: (a) anaclinal slope; (b) cataclinal slope (Cruden, 1989, Figs. 3, 5).

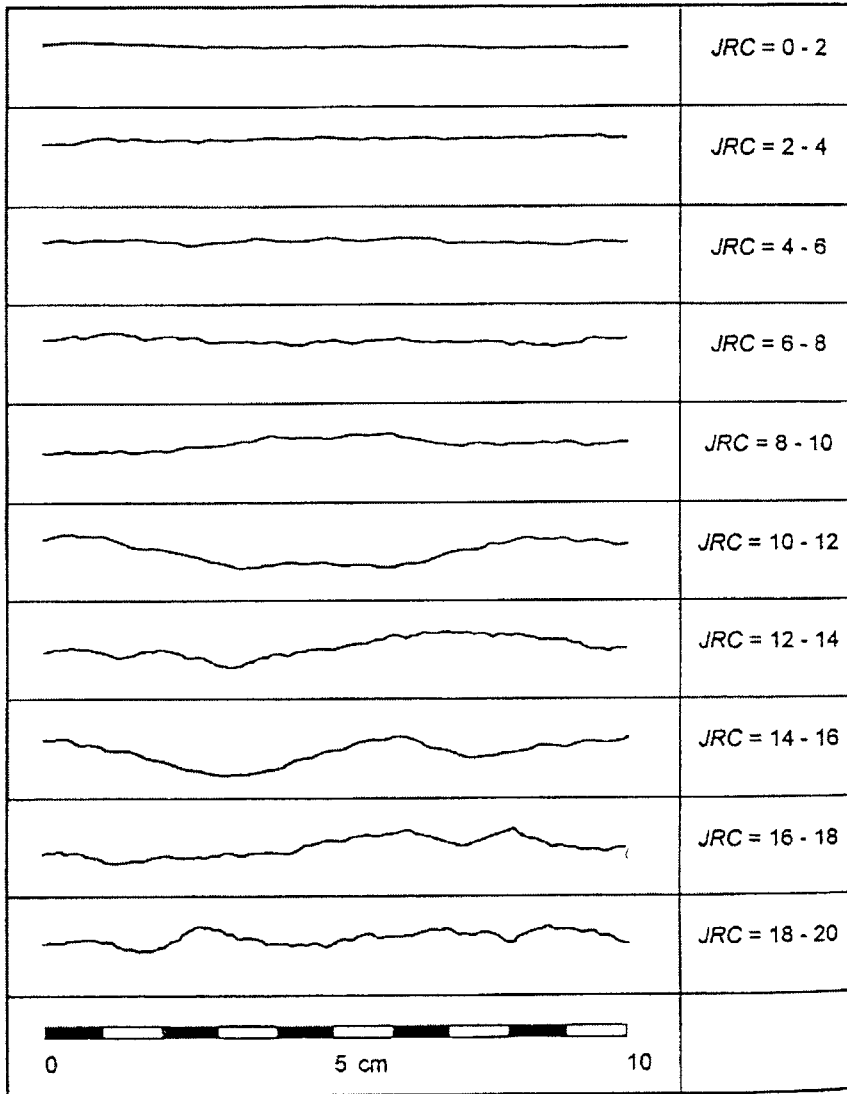


Figure 2-5: Joint Roughness Coefficient (*JRC*) values (from Hoek et al., 1995, after Barton and Choubey, 1977).

A. CLASSIFICATION PARAMETERS AND THEIR RATINGS									
Parameter			Range of values						
1	Strength of intact rock material	Point-load strength index	>10 MPa	4-10 MPa	2-4 MPa	1-2 MPa	For this low range - uniaxial compressive test is preferred		
		Uniaxial comp. strength	>250 MPa	100-250 MPa	50-100 MPa	25-50 MPa	5-25 MPa	1-5 MPa	< 1 MPa
		Rating	15	12	7	4	2	1	0
2	Drill core Quality <i>RQD</i>		90%-100%	75%-90%	50%-75%	25%-50%	< 25%		
	Rating		20	17	13	8	3		
3	Spacing of discontinuities		> 2 m	0.6-2 . m	200-600 mm	60-200 mm	< 60 mm		
	Rating		20	15	10	8	5		
4	Condition of discontinuities (See E)		Very rough surfaces Not continuous No separation Unweathered wall rock	Slightly rough surfaces Separation < 1 mm Slightly weathered walls	Slightly rough surfaces Separation < 1 mm Highly weathered walls	Slickensided surfaces or Gouge < 5 mm thick or Separation 1-5 mm Continuous	Soft gouge >5 mm thick or Separation > 5 mm Continuous		
	Rating		30	25	20	10	0		
5	Ground water	Inflow per 10 m tunnel length (l/m)	None	< 10	10-25	25-125	> 125		
		(Joint water press)/(Major principal $\sigma$ )	0	< 0.1	0.1-0.2	0.2-0.5	> 0.5		
		General conditions	Completely dry	Damp	Wet	Dripping	Flowing		
		Rating	15	10	7	4	0		
B. RATING ADJUSTMENT FOR DISCONTINUITY ORIENTATIONS (See F)									
Strike and dip orientations		Very favourable	Favourable	Fair	Unfavourable	Very Unfavourable			
Ratings	Tunnels & mines	0	-2	-5	-10	-12			
	Foundations	0	-2	-7	-15	-25			
	Slopes	0	-5	-25	-50				
C. ROCK MASS CLASSES DETERMINED FROM TOTAL RATINGS									
Rating	100 ← 81		80 ← 61		60 ← 41		40 ← 21		< 21
Class number	I		II		III		IV		V
Description	Very good rock		Good rock		Fair rock		Poor rock		Very poor rock
D. MEANING OF ROCK CLASSES									
Class number	I		II		III		IV		V
Average stand-up time	20 yrs for 15 m span		1 year for 10 m span		1 week for 5 m span		10 hrs for 2.5 m span		30 min for 1 m span
Cohesion of rock mass (kPa)	> 400		300-400		200-300		100-200		< 100
Friction angle of rock mass (deg)	> 45		35-45		25-35		15-25		< 15
E. GUIDELINES FOR CLASSIFICATION OF DISCONTINUITY conditions									
Discontinuity length (persistence)	< 1 m		1-3 m		3-10 m		10-20 m		> 20 m
Rating	6		4		2		1		0
Separation (aperture)	None		< 0.1 mm		0.1-1.0 mm		1-5 mm		> 5 mm
Rating	6		5		4		1		0
Roughness	Very rough		Rough		Slightly rough		Smooth		Slickensided
Rating	6		5		3		1		0
Infilling (gouge)	None		Hard filling < 5 mm		Hard filling > 5 mm		Soft filling < 5 mm		Soft filling > 5 mm
Rating	6		4		2		2		0
Weathering	Unweathered		Slightly weathered		Moderately weathered		Highly weathered		Decomposed
Rating	6		5		3		1		0
F. EFFECT OF DISCONTINUITY STRIKE AND DIP ORIENTATION IN TUNNELLING**									
Strike perpendicular to tunnel axis				Strike parallel to tunnel axis					
Drive with dip-Dip 45-90°		Drive with dip-Dip 20-45°		Dip 45-90°		Dip 20-45°			
Very favourable		Favourable		Very favourable		Fair			
Drive against dip-Dip 45-90°		Drive against dip-Dip 20-45°		Dip 0-20-Irrespective of strike°					
Fair		Unfavourable		Fair					

Figure 2-6: Rock Mass Rating System (Hoek et al., 1995, after Bieniawski, 1989).

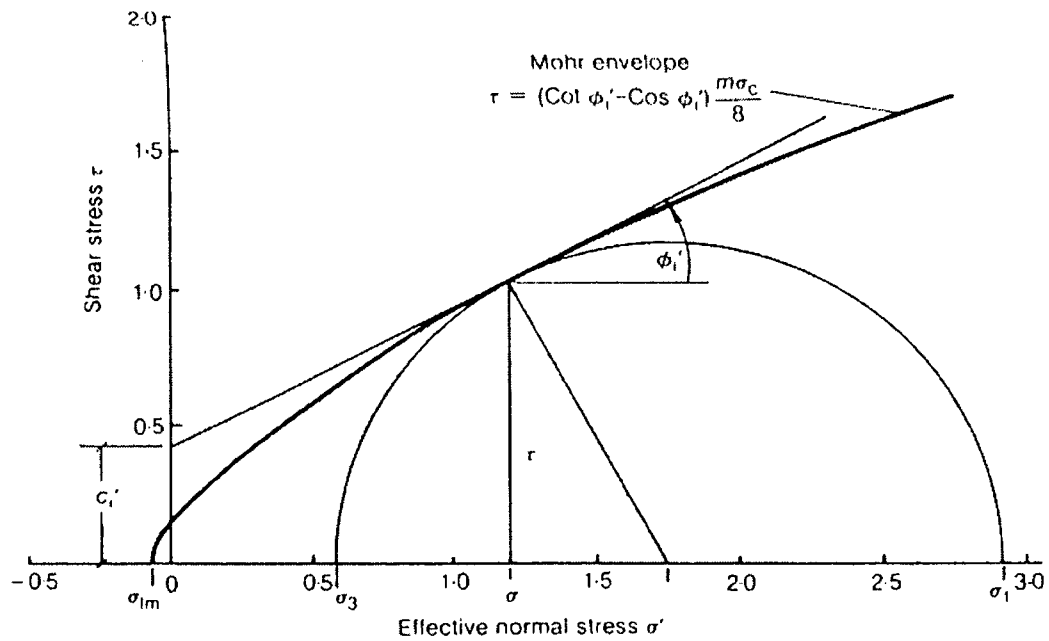


Figure 2-7: Typical curved shear strength envelope defined by Hoek-Brown theory for rock mass strength (Hoek, 1983, Fig. 3).

Table 2-1: Rock Mass Quality Classifications Based on Tunnelling Quality Index,  $Q$

<u>Tunnelling Quality Index, <math>Q</math></u>	<u>Rock Mass Description</u>
0.001 – 0.01	Exceptionally Poor
0.01 – 0.1	Extremely Poor
0.1 – 1	Very Poor
1 – 4	Poor
4 – 10	Fair
10 – 40	Good
40 – 100	Very Good
100 – 400	Extremely Good
400 – 1000	Exceptionally Good

### 3.0 REVIEW OF NUMERICAL MODELLING THEORY

Numerical modelling has become a common tool in the analysis of the stability of soil and rock foundations and slopes, in large part due to advances in computer technology. With sophisticated, user-friendly software and faster personal computing hardware currently available, it is possible to model virtually any scenario and analyze behaviour under various loading conditions in a relatively short period of time. This essentially turns the desktop computer into a laboratory. Slopes that have already failed can be back-analyzed in order to better understand failure conditions, existing slopes can be studied and the model calibrated with observed movements to help predict future behaviour, or a large number of parametric studies may be carried out which would not be feasible to perform in the lab.

One advantage that numerical modelling methods have over traditional limit equilibrium methods is that the failure mechanism is determined during modelling rather than required as an input parameter. This allows failure modes to be identified which might not have been considered. As well as being useful for predicting under what conditions failure may occur, numerical modelling allows the magnitude of deformations to be estimated. It must be kept in mind, however, that modelling is only one of the tools available and should not be considered as a substitute for traditional engineering methods.

There are a number of modelling methods in use via different software packages, each having inherent advantages and disadvantages. The appropriate method and software to use depend predominantly on the physical conditions to be modelled, and to a much lesser extent on

personal preference. Numerical methods and programs associated with them are described briefly below. More detailed information may be obtained either from the manual provided with the software by the manufacturer or from the cited references.

### *3.1 Continuum Methods*

The finite element method was developed for structural engineering and has in the last number of decades emerged as a valuable tool for foundation and slope stability problems. Full details about the development of the method and its applications are given by Zienkiewicz (1977). The method involves dividing the model into relatively small elements that are joined together at the corners or nodes. Increasing the number of elements used to model the problem improves the solution but this must be balanced with reasonable computing times. Material properties are assigned to each element. Stresses are calculated at one or more points inside each element. Displacements at the nodes are unknown and are solved for using a large set of simultaneous equations. Problems may be formulated either implicitly or explicitly. An implicit formulation derives a set of equations that is solved to determine a new state at some given time, while an explicit formulation effectively freezes the state of the system at each time step and determines a new condition at each calculation point directly from values at adjacent points (Brown, 1987). An advantage to the explicit formulation is that it does not need to establish, store and solve a new set of simultaneous equations at each time step (Brown, 1987).

The model is treated as a continuum, i.e., there is no separation at nodes or along the sides of the elements, so no actual failure surface discontinuity is formed. The failure surface must be interpreted based on shear strain concentrations in the model. For modelling jointed rocks, special joint elements of zero thickness may be used to simulate the discontinuities (see, e.g., Wang and Garga, 1993). However, because the mass is treated as a continuum, large displacements cannot easily be simulated. As well, the number of joint elements required to model a heavily jointed rock mass greatly increases the number of degrees of freedom required to solve the problem, significantly lengthening the computing time (Wang and Garga, 1993). Discontinuum methods, described in the next section, are perhaps more suitable for these types of problems.

One problem that arises is the need to arbitrarily define the outer boundary of the analysis, which may introduce inaccuracies because the far-field stress conditions may not be satisfied completely (Brown, 1987). This can be overcome by extending the model far enough that the boundary conditions do not affect the area of interest, but again, this must be balanced with reasonable computing times. Another option is the use of infinite elements or finite elements linked to boundary elements (Brown, 1987).

Considerable effort is usually required to prepare data for a problem and this is one disadvantage of the finite element method. An advantage of this method is its capability of modelling a wide variety of loading and construction sequences as well as heterogeneous problems (Pande et al., 1990).

Similar in concept, yet somewhat less flexible, is the boundary element method, where only the boundaries of the problem are discretized into elements. The mass is treated as a continuum. Data preparation is generally simple, unless there are a number of layers of material, each separated by a boundary. The advantage of this method is its efficiency for homogeneous, linear elastic problems (Pande et al., 1990).

The finite difference method also treats the mass as a continuum and problems may be formulated implicitly or explicitly. It is used more for solving transient or dynamic problems than for steady-state or static problems (Brown, 1987).

The Fast Lagrangian Analysis of Continuum (FLAC) is a commercially available program developed by Itasca (1995) which uses an explicit finite difference method and plasticity theory to model material failure. The solid body is divided into a mesh of quadrilateral elements, each subdivided by the program into two overlain sets of constant-strain triangular elements. Stresses and strains are calculated for each of the four triangles and averaged to give stress and strain for that element. There are a large number of constitutive models available. FLAC is capable of doing calculations in large strain mode, i.e., coordinates of nodes are updated and the mesh moves and deforms with the material. Results must be interpreted by the user to assess whether the system is stable, unstable or in steady-state plastic flow (Sjöberg, 1999).

For some rock slope problems, it may be possible to use a continuum method where the block size is sufficiently small in comparison to the overall size of the problem area.

However, where continuum behaviour cannot be assumed, it is more appropriate to use a discontinuum approach.

### 3.2 *Discontinuum Methods*

Discontinuous Deformation Analysis (DDA) was developed by Shi (1988). It is based on dynamic equilibrium and considers both friction and the kinematics of motion of individual blocks. It incorporates all of the primary factors that control the stability of rock slopes: dynamics, kinematics, friction and deformability (MacLaughlin, 1997). The displacements and deformations of the blocks are the result of the accumulation of a number of small increments, corresponding to small time steps. The method is based on the minimization of the total potential energy of a system of blocks. The mechanical interactions of the blocks and their surroundings are formulated in terms of a displacement parameter set. For each block, x- and y-translations, rotation, x- and y-components of normal strain, and shear strain are used to describe the displacement of the centre of mass of the block, from which the corresponding locations of the block vertices can be determined.

Kinematic constraints of the system are imposed using numerical penalties analogous to stiff springs applied at the contacts between vertices of one block and edges and vertices of other blocks to prevent interpenetration of the blocks (MacLaughlin and Sitar, 1995). Tension or penetration at the contacts results in expansion or contraction of these springs, adding energy to the block system. The minimum energy solution is one with no tension or penetration, and is found by setting the partial derivatives of the total potential energy function (the sum of the

individual energy contributions) equal to zero, resulting in a system of linear equations. Solution of the system of equations is an iterative procedure in which contact springs are repeatedly added and subtracted in one timestep until each of the contacts converges to a constant state, at which point the block vertices are updated according to the displacement function. A complete description of the formulation of the equations, including derivations of each of the energy terms, can be found in Shi (1993).

DDA uses an implicit formulation, meaning that the equations are set up so that equilibrium is satisfied at the end of the timestep, guaranteeing numerical stability. One limitation of DDA is the inability to model stress concentrations within the blocks, resulting in limited block deformability and complete absence of crushing or fracturing of the blocks. This limitation (block rigidity) was the main reason this method was not used in this study. As well, the program is not designed to inherently model pore water pressures; water forces must be added explicitly (MacLaughlin, 1997). An advantage of DDA is that it models the kinematics of motion along discontinuities and thus is not limited to analysis of initiation of failure, but may be used to study the behaviour of the slope after the onset of motion.

The Block-Spring Model (BSM) was developed by Wang and Garga (1993), and simulates the jointed rock mass by an assemblage of blocks separated by joints and interacting through contacts. The blocks are assumed to be rigid, which is a drawback of the model. The contact forces are related to the relative displacements between blocks and equilibrium equations are directly applied, which allows the displacements of the blocks and subsequently the contact

forces to be determined. An iterative procedure is applied to describe the progressive failure along the joints.

BSM assumes that the blocks are in contact along their surfaces with corner-to-edge and edge-to-edge contacts. A pair of springs aligned in the normal and shear directions of the contact surface is used to represent the point contact. Edge-to-edge contact is simplified as two point contacts at the two corners. As a result, the model deals with forces directly rather than stresses distributed along the contact area. The deformations of the springs are determined from the relative displacements between blocks. The spring (contact) forces are then evaluated from the stiffness and deformations of the springs. The system is considered initially to be in equilibrium. A change in load conditions disturbs the original state, the blocks displace and a set of new contact forces results. A set of equilibrium equations for all the blocks is obtained by considering all of the forces on the blocks. Assuming boundary conditions are known, the equations can be solved to determine the displacements of the blocks. To model groundwater pressures, BSM assumes a single steady water table. The linearly distributed water pressure on the face of a submerged block is determined by the depth of the two corners below the water table and is considered to be two concentrated forces acting on the two ends.

The coordinates of the blocks are updated after each cycle of computation, when block-to-block contact is checked. If blocks lose their contacts with other blocks, the computation is terminated and the unstable blocks are identified. This aspect of BSM was the main reason it was not chosen to be used for this study.

The distinct element method utilizes an explicit time-stepping algorithm developed by Cundall (1971) that allows large displacements and rotations by treating the model as a discontinuum. When loads are applied, changes in contact forces are tracked with time. The equations of dynamic equilibrium for each element are repeatedly solved until the laws of contacts and boundary conditions are satisfied (Pande et al., 1990). The acceleration, velocity and displacement of each block are determined based on the time interval adopted using the finite difference approximation. The blocks oscillate due to repeated balance and unbalance of the contact forces; therefore, a damping procedure has to be used to dissipate the kinetic energy and to make the blocks converge to a statically stable state (Wang and Garga, 1993).

The Universal Distinct Element Code (UDEEC) is a program based on the distinct element method for discontinuum modelling (Itasca, 1997). The general characteristics of the program are outlined below. The information is taken predominantly from the UDEEC manual, which should be consulted if more detailed information is desired.

UDEEC is a discrete element program, in that it allows finite displacements and rotations of discrete bodies, including complete detachment, and automatically recognizes new contacts. The rock mass is modelled as a set of discrete rigid or deformable blocks separated by joints, which are considered to be interfaces (i.e., the discontinuity is treated as a boundary condition). A "soft-contact" approach is used to treat the behaviour in the normal direction of motion at contacts. A finite normal stiffness is used to represent the measurable stiffness that exists at a contact or joint. Realistic representation of crushing of the corners of the blocks, which would occur as a result of stress concentration, is achieved by rounding the corners so

that blocks can smoothly slide past one another when two opposing corners interact. In order not to introduce inaccuracy in the solution, the rounding length should be kept to approximately 1% of the representative block edge length in the model.

Explicit time-marching is used to directly solve the equations of motion. Numerically, a time-stepping algorithm is used to represent dynamic behaviour. Velocities and accelerations are assumed to be constant within a time-step, limiting the size of the time-step so that it is sufficiently small that propagation of disturbances cannot occur between one discrete element and its immediate neighbours. This corresponds to the fact that there is a limited speed at which information can be transmitted in any physical medium. For rigid blocks, the block mass and interface stiffness between blocks define the size of the time-step; for deformable blocks, the size of the time-step is defined by the size of the deformable zones.

The calculations performed by UDEC alternate between application of a force-displacement law at all contacts and Newton's second law ( $F = ma$ ) at all blocks. The force-displacement law is used to find contact forces from known (and fixed) displacements. Newton's second law gives the motion of the blocks resulting from the known (and fixed) forces acting on them. If the blocks are deformable, motion is calculated at the gridpoint of the triangular finite-strain zones within the blocks. Then, the application of the block material constitutive relations gives new stresses within the elements.

There are seven block constitutive models provided in UDEC, arranged into three groups: null, elastic and plastic. The *null model* is used to represent material that is removed or

excavated. The *elastic, isotropic model* provides the simplest representation of material behaviour, and is valid for homogeneous, isotropic, continuous materials that exhibit linear stress-strain behaviour with no hysteresis on unloading. The plastic model group contains the remaining five models: the *Mohr-Coulomb model* is the conventional model used to represent shear failure in soils and rocks; the *ubiquitous-joint model* is an anisotropic plasticity model that includes weak planes of specific orientation embedded in a Mohr-Coulomb solid; the *strain-softening/hardening model* allows representation of non-linear material softening and hardening behaviour; the *double-yield model* is intended to represent materials in which there may be significant irreversible compaction in addition to shear yielding; the *Drucker-Prager plasticity model* is included to permit comparison with other numerical program results and may be useful to model soft clays with low friction angles, but is not generally recommended for application to geologic materials.

UDEC allows static and dynamic analyses, and can model groundwater conditions. The small time-step required has a direct impact on the time required to run models, but with modern computers this is not the drawback it once was. Of the available methods, UDEC was found to be the most applicable to conditions to be examined in this study. Further information is found ahead in Chapter 5.

## 4.0 CASE HISTORIES FROM THE LITERATURE

Past experience is invaluable in the quest to understand the behaviour of large rock slopes. While it is beyond the scope of this paper to review every documented toppling failure, those discussed below highlight significant issues that must be addressed when trying to assess the potential for catastrophic failure. The reader is referred to Sjöberg (1999) for an extensive review of case histories of large rock slopes.

### 4.1 *Heather Hill, Glacier National Park, British Columbia*

Situated at the northern end of Glacier National Park in eastern British Columbia, the Heather Hill landslide is one of several ancient landslides in the Beaver Valley (Figure 4-1a). Slope stability is of particular concern as the valley forms part of a major east-west transportation corridor, and some of the slides have been reactivated by construction activity (Anon., 1976).

Lithologies are intercalated, with quartz biotite schist and minor metaquartzite (referred to as grit) at the base of the slope to predominantly grit with minor schist above the headscarp (Pritchard et al., 1990). Dominant structure includes bedding foliation (S0) and crenulation cleavage (S2), both of which generally dip into the slope at about 65°, as well as two joint sets. The data for both S0 and S2 sets indicate a reduction in dip from 66° and 62°, respectively, at Creek A, to 46° and 51°, respectively, at Creek C (Figure 4-1a). This reduction is considered to be the result of toppling and not due to a natural structural

variation. Bedding thickness spacing is roughly 25 m in the lower portion of the slope, and gradually increases moving upslope. The upper slope dips toward the river at about 25°, while the lower portion of the slope has been steepened by glacial erosion to about 45° (Figure 4-1b).

Rapp (1987) determined that large scale toppling failure was possible in the valley slopes. The landslide was modelled by Pritchard (1989) using UDEC (Figure 4-2). Toppling was assumed to have started or accelerated due to the oversteepening of the lower portion of the slope. Back analysis found that failure of the slope initiated at the toe of the slope and progressed upslope. A distinct failure zone, based on nodes that are in a plastic condition, developed in the upper 100 m of the slope, with a base dipping toward the valley at roughly 40°, which closely approximated the observed failure geometry and headscarp location. The upslope limit of the failure was found to be related to gradational change in rock type from foliated pelitic rock at the base of the slope to feldspathic grit above the headscarp, which is supported by the distribution of other landslides in the valley. It was also suggested that the area to the north of the Heather Hill slide and other slopes in the valley may be in the early stages of deep seated toppling failure (Pritchard, 1989).

#### 4.2 *Clapière, Southern France*

This landslide illustrates the dilemma faced by authorities when the behaviour of a large rock slope experiencing a significant amount of deformation cannot be predicted. Located near Nice in southern France, the Clapière landslide occurs in the metamorphic rocks of the

northeast valley wall of the Tinée River. The rock is mostly muscovite schist, with schistosity and relict bedding dipping at 60° to 70° into the slope. In the slide area, dips have been reduced to nearly horizontal by widespread flexural toppling (Anon., 1992). The upper part of the slope is at about 20°, while the lower 800 m of the slope, where toppling is occurring, has been oversteepened to about 40° by glacial erosion.

The failure is considered to have developed in three stages: first, the toe of the slope was oversteepened by glacial erosion; next, widespread flexural toppling occurred in the slope; finally, discrete sliding surfaces developed (Figure 4-3) (Follacci, 1987). Present displacement of the slope is greater than 100 m.

Between the end of 1982 and the end of 1986, the moving mass, which has an estimated volume of more than 50 million cubic metres, moved more than 13 metres, and during three months in 1987 moved an average of 80 mm/day (Follacci et al, 1988). The landslide threatened to block the Tinée valley and dam the river, flooding villages upstream. A dynamic analysis of a potential catastrophic failure was carried out in 1987, resulting in some houses and a road being relocated. As well, two drainage bypass tunnels were designed beneath the slope on the opposite side of the valley, to prevent upstream flooding should the Tinée be dammed. The first tunnel was completed, being 2.6 km long and 10 m<sup>2</sup> in cross-section, at significant cost (Anon., 1992). After completion of the first tunnel movement velocities decreased, leading authorities to believe that the urgency of the hazard had been reduced, and the second tunnel was not constructed.

The slope has not failed to date. At the time, however, movement velocities were such that catastrophic failure was considered imminent. Better predictive capabilities may have been able to lower the cost of mitigation measures.

#### 4.3 *Affliction Creek, British Columbia*

An 18-year movement record exists for deformation occurring at Affliction Creek, located on the western margin of the Meager Creek Volcanic Complex in southwestern British Columbia (Bovis, 1982; Bovis, 1990; Bovis and Stewart, 1998). The rock types consist of porphyritic basalt overlying biotite quartz monzonite. The basalt outcrops across a broad terrace-like feature and is traversed by a series of tension cracks, which in 1982 showed recent signs of spreading (Figure 4-4). Within the basalt there is a predominantly vertical joint pattern and poorly developed columnar structure. The quartz monzonite is traversed by three relatively smooth joint sets showing oxide staining from alteration and weathering but having little or no cementation. The downslope margin of the monzonite is a highly fractured rock face, with an average slope angle of 60°. The main joint set strikes roughly parallel to the rock face (N15°E), with dip angles ranging from 35°W to 70°W (into the slope), with many of the lower angles occurring in outcrops where incipient toppling is apparent. An orthogonal cross-joint set strikes roughly parallel to the main set, with an average dip of 50°E. The third set is less well defined, and strikes N20°E dipping 75°N (Bovis, 1982).

A prominent set of antisllope scarps about 1 to 3 m high trends roughly north-south, with scarps occurring in both the basalt and the quartz monzonite. The development of these scarps is considered to be influenced by a strong planar anisotropy that exists. Other landforms include wide tension cracks, elongated grabens and collapse pits, and a large block field produced by extensive sliding and toppling of material in the northern part of the site (Bovis, 1982). The estimated volume of material affected by slope movement is  $30 \times 10^6 \text{ m}^3$  (Bovis, 1990).

Modelling of the slope using UDEC successfully reproduced the observed movements and features (Figure 4-5), and indicated that deformation of the slope dominated by flexural toppling failure was feasible under gravitational stresses alone (i.e., without seismic or tectonic driving forces). Modelling also demonstrated that the slope was sensitive to fluctuating groundwater levels due to annual variations (Bovis and Stewart, 1998).

#### 4.4 *Glen Pean, South Inverness-shire, Scotland*

De Freitas and Watters (1973) describe a failure that occurred on the north slope of the glaciated WSW-ENE-trending Pean River valley (the age of failure was not discussed). The rocks are metamorphosed sediments (granulites and schists) of late Precambrian age known as the Moine Series. Three major types of schist are present (mica, granular and migmatized), with thin schistose laminae within the granulites themselves and all occurring in varying amounts as a layered sequence reflecting the original bedding. Alignment of minerals still reflects the former presence of the bedding planes, which have been largely obliterated by

metamorphism, and this foliation dips approximately 80°NW (i.e., into the slope, which has an angle of about 40°) due to folding associated with metamorphism. Well-developed jointing strikes mainly E-W or NNE-SSW, with the former set tending to be nearly vertical and the latter set dipping on average around 38°ESE (i.e., out of the slope) (De Freitas and Watters, 1973).

The failure extends from the Pean River at the toe of the slope to the summit at Càrn Mór, approximately 740 m above. Three regions of movement were identified in the field (Figure 4-6):

- (1) a wedge-shaped mass at the toe that detached along foliation surfaces and slid as a monolith along the joints dipping into the valley, leaving a small scarp and a marked break in slope;
- (2) an area, rectangular in plan view, divided into steeply dipping rectangular plates that have toppled toward the valley which produced a series of small scarp faces, with heights of 1.5 to 7 m, dipping toward the summit; this area comprises most of the failure; and
- (3) two regions, both triangular in plan view, extending from the upper most scarp faces to just below the summit of Carn Mor, identified as screens.

No exposure was identified in the field which showed the base of the slide, but De Freitas and Watters (1973) carried out stability calculations indicating that the failure surface probably lies between 50 and 60 m below present ground level. With the failure surface so located, the volume of material involved was estimated at roughly  $1.5 \times 10^9 \text{ m}^3$ .

From Figure 4-6, it is evident that the toe wedge offers stability to the plates higher up the slope, and has prevented catastrophic failure. Deformation appears to be controlled by the presence of the joint set dipping toward the valley, which offers release surfaces, and by the relative weakness of the foliation planes.

#### 4.5 *Ben Attow, Scotland*

Holmes and Jarvis (1985) describe the southwest slope of Ben Attow as exhibiting “the largest extent of obsequent-scarplets in Scotland” (Figure 4-7), and consider the likeliest cause to be block-flexural toppling. The extent of the scarps illustrates the role that joint persistence plays in deformation. The geology consists of coarse psammites of varying metamorphic grade. There are four joint sets: one parallel to foliation (essentially horizontal); one striking parallel to and dipping steeply into the slope (the scarps strike subparallel to this set); and two sets dipping gently to the west. Unlike the conditions at Glen Pean, no sliding toe block exists at the base of the slope, and Holmes and Jarvis (1985) do not consider it likely that there was a toe block on the basis that in situ rock outcrops across the base of the slope, and glacial erosion of an existing toe block would also have removed the scarps. The deformation is thus considered to postdate the last glaciation in the area. The slope shows no signs of recent movement, with partly infilled slope trenches and vegetation on the upslope faces of the scarps.

Holmes and Jarvis (1985) make an important observation: if toppling is occurring from the base of the slope upward, an apparently minor topple could affect a massive area of the slope.

In other words, support which currently exists at the toe would be removed if development (a new road, for example) involved cutting into the base of the slope. Thus, a catastrophic failure might be man-made.

#### 4.6 *Billan, France*

This landslide is located on the northwest bank of the Grande-Maison reservoir, approximately 1.5 km upstream of the dam near Isère. The slope, with an average angle of about 35°, consists of schist and gneiss in the upper part, with slate at the base (Figure 4-8) (Giraud et al., 1990). Schistosity and the contact of the units are nearly vertical; however, the beds are rotated outwards by flexural toppling, lying at a dip of 35° to 45° (Anon., 1992). Seismic profiling showed a progressive increase in seismic velocity with depth, demonstrating the effect of toppling over a depth of about 100 m (Giraud et al., 1990).

A crack developed above a bulge in the slope during filling of the reservoir in May 1986. A road located just above the unit contact subsided by 240 mm over a one-month period (Anon., 1992). In order to mitigate the hazard, that summer Electricité de France installed an 850 m long drainage gallery with a total of 1300 m of drain holes, and movement rates dropped to acceptable levels. Peak drainage flow from the gallery was 150 litres/second in the spring of 1987.

This case, like Clapière, illustrates the measures that must be taken (i.e., expensive drainage works) to prevent a slide which could cause widespread damage and potential loss of life

(here, a landslide-induced wave could overtop the dam; at Clapière, potential damming of the river which would flood upstream communities, and downstream communities when the dam is breached).

#### 4.7 *Torreggio, Italy*

The Torreggio landslide is located in Val Malenco in northern Italy. The rock types consist of muscovite schist with gneissic interbeds. The slide took place in the lower 600 m of the slope, which lies at about 36° (Anon., 1992). Widespread flexural toppling has reduced the dip of the schistosity, which originally dipped steeply into the slope. Toppling had gradually developed into a slump based below the stream bed, with cumulative displacements up to many tens of metres by 1987. A major storm affected the region in July 1987, causing a sudden substantial displacement of the slide mass which gradually constricted the Torreggio channel, but did not involve catastrophic velocities. There was no runup on the opposite bank. The channel was already under flooding conditions and the subsequent rapid erosion of the slide debris triggered a major debris flow which resulted in severe damage downstream (Anon., 1992).

The slide mass likely experienced elevated pore pressures due to the precipitation influx from the storm, and the toe may have been undercut by the flooding in the channel. Toppling of the rock mass had gradually terminated in a slumped area, possibly the result of prolonged weathering and weakening of the toppled region, but did not result in catastrophic detachment. This illustrates that while slope undergoing flexural toppling may gradually

stabilize, the toppled mass is potentially more susceptible to the negative impact of weathering and extreme storm events, and stability of the slope may still be in question.

#### 4.8 *Brenda Mine, Peachland, BC*

The original slope of the east-west trending south wall of the Brenda open pit mine near Peachland, British Columbia, experienced significant toppling deformation when mined at 40° to a depth of approximately 200 m (Pritchard, 1989). The rock forming the slope is hard, fractured quartz diorite with three major discontinuity sets. Set A discontinuities are continuous gouge-filled faults that trend approximately east west and dip 70° to 80° to the south (i.e., into the wall), with spacing at 15 to 27 m in the vicinity of the south wall. Set B consists of joints and faults that strike approximately north-south and dip moderately to steeply to the northeast. Set C joints trend east-west and dip from 23° to 50° to the north (i.e., out of the wall). Toppling is accommodated by flexural slip along Set A discontinuities, which are also believed to act as low permeability barriers to groundwater flow (Pritchard, 1989).

The slope was modelled using UDEC by Pritchard (1989). The block geometry and assumed groundwater level are shown in Figure 4-9. The analysis identified two modes of toppling failure: one purely flexural topple and one “graben” topple, with the difference in input parameters being a small increase in the block internal friction angle and a decrease in cohesion and tensile strength by two thirds for the “graben” model. For the flexural toppling model, Figure 4-11(a) indicates grid point velocities attenuating with depth, as expected for

toppling, while Figure 4-10(b) shows a circular failure surface. Pritchard (1989) states that the addition of pore pressures did not affect the shape of the failure surface, but an increase in friction angle was required to maintain stability. The “graben” model (Figure 4-11(a)) is initially a pure flexural topple, but after some rotation the blocks begin to fail by sliding, with the sliding surface developing through the point of bending in each column. Pritchard (1989) compares this failure mode to that described by Nieto (1987), illustrated in Figure 4-11(b).

Pritchard (1989) concludes that the geometry and location of the failure surface in larger slopes is dependent on the combination of block cohesion, block tensile strength, and the joint friction angle. As well, pore pressure was found to significantly affect the stability of toppling slopes.

#### 4.9 *Luscar Mine, Hinton, AB*

The Luscar open pit mine, located in the Inner Foothills Belt of the Rocky Mountains near Hinton, Alberta, experienced toppling deformation as a result of progressive slope excavation (Benko and Stead, 1999). The rock types consist mainly of massive siltstones and sandstones with minor shale and coal beds (Figure 4-12). Bedding dips into the south wall of the mine at 60° to 70°, and a joint set orthogonal to the bedding dips between 25° to 40° to the north. Joint spacing in the Torrens Member is 1 m, and in the Moosebar, Gladstone and Nikanassin Members is 0.5 m. The pit design called for an overall slope angle of 45° for the south wall, with benches 12 m high and 6 m wide. Slope movement was first detected after the second

bench had been excavated. Uphill-facing scarps appeared on benches and on the slope crest, and gradually progressed upslope. Two periods of accelerated movement occurred which were deduced to be related to spring ice breakup.

Benko and Stead (1999) modelled the slope using UDEC. The UCS for the Luscar Formation ranges from 25-50 MPa for the Moosebar shales to 150 MPa for the Torrens sandstone, with 25-70 MPa for the interbedded sequences. Bulk (K) and shear (G) moduli were selected from typical values, with K ranging from 3.3 GPa for coal to 23.3 GPa for conglomerate, and G ranging from 1.5 GPa for coal to 14 GPa for conglomerate. Rock mass strength was back-analyzed in order to reproduce the major instability resulting from the excavation of the second bench. To reproduce this instability, block cohesion of 45 kPa or less was required in the model for dry conditions. Most of the deformation during this stage stopped against the Cadomin Conglomerate in the middle of the hill, which is relatively strong compared to the formations downslope.

The basal surface of the failing mass was found to be approximately 20 m below the ground surface, starting at the base of the second bench. Using a constant water table located 5 m below the ground surface, it was found that block cohesion of 65 kPa initiated toppling (45% higher than the dry case). Benko and Stead draw attention to the fact that the same section of the slope is affected in both the wet and dry cases, with the failure stopping at the Cadomin Conglomerate layer. Wet conditions produced a slightly deeper location of the failure surface in the toe area. After excavation of the third and successive benches, toppling (and the basal

failure surface) propagated to the top of the hillside above the pit, with the failure surface approximately 50 m below the ground surface.

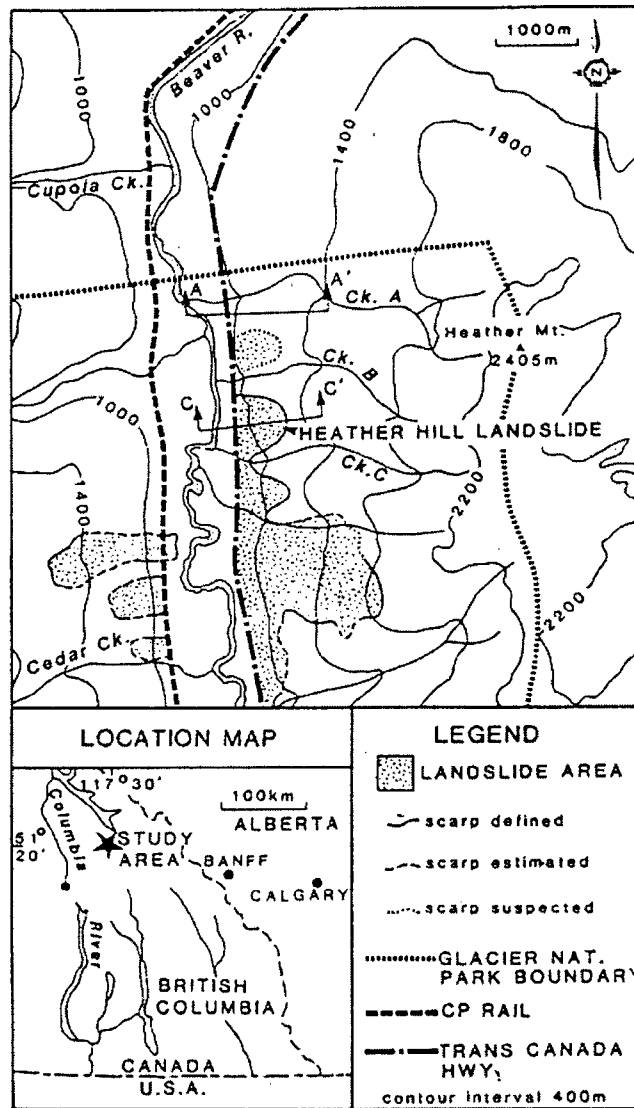
Benko and Stead (1999) point out that there seemed to be a wide range of strength parameters that could reproduce the slope failure observed at the mine. They also note that the use of the ubiquitous joint model did not provide significantly improved insight into the failure mechanism than the Mohr-Coulomb criterion. The influence of cross-joints was included by using a low value for block cohesion rather than explicitly including the joints (which they argue would not be continuous in sedimentary formations), yet the model still produced good agreement with the observed failure surface.

#### *4.10 Chuquicamata Mine, Chile*

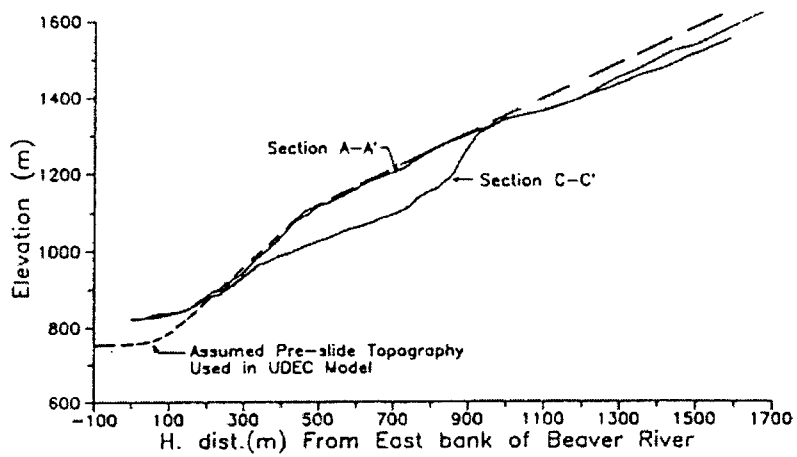
The failure mechanism of the west wall of the Chuquicamata open pit mine in Chile involves quasi-stable toppling of the upper 100 m or so. The behaviour of the wall was found to be controlled mainly by a set of steeply dipping joints and a weak zone near the bottom of the pit based on a comparative analysis carried out by Board et al. (1996), described below. The upper part of the slope consists of granodiorite containing two prominent and continuous joint sets, the first dipping 70°W to 90°, the second dipping roughly 35°E (into the pit), and both striking north-south (parallel to the slope face). The weak zone is known as the Zona Plastica.

Board et al. (1996) modelled the slope using both FLAC (with the ubiquitous joint model) and UDEC, and found generally that the results were the same in both cases. They indicate that computational considerations favoured the use of continuum over discontinuum methods. Both models reproduced the general features of the observed failure. Initial toppling lead to slumping, with the west wall moving slowly downslope as the Zona Plastica compresses. Board et al. (1996) found that the conceptual model of the west wall as a slumping, active wedge in contact with the Zona Plastica, which acts as a passive wedge, represents the failure process reasonably well. These results compare to those of Pritchard (1989). The main conclusion reached by Board et al. (1996) is that toppling would not occur in the west wall if the Zona Plastica did not compress.

Figure 4-1:  
Heather Hill  
Landslide:  
(a) location;  
(b) cross-  
sections  
shown in (a)  
(Pritchard et  
al., 1990).



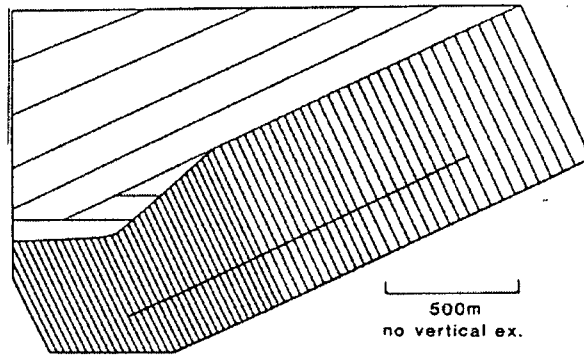
(a)



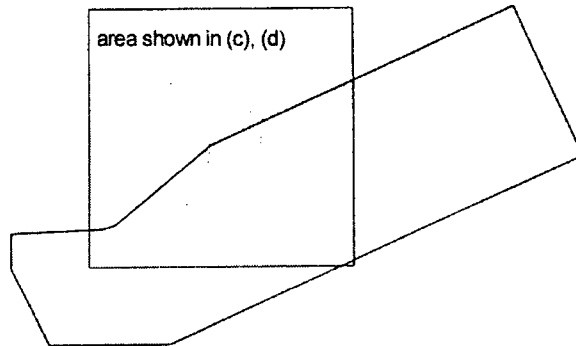
(b)

Figure 4-2:  
Heather Hill modelling  
(Pritchard et al., 1990).

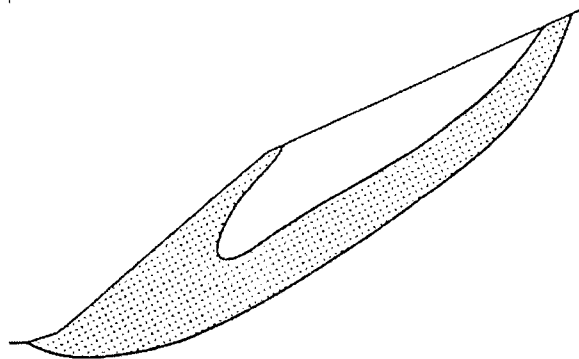
(a) discretized slope model;



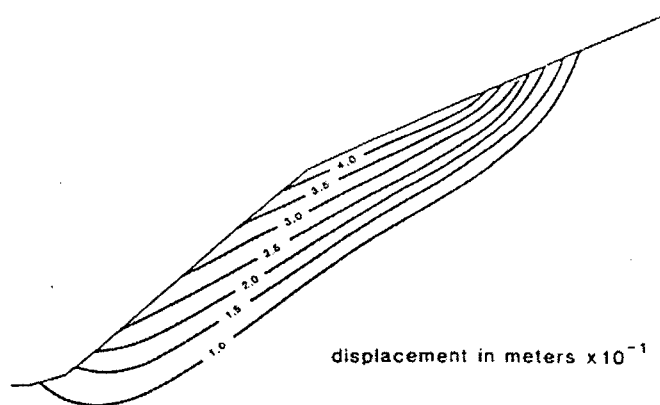
(b) index to (c) and (d);



(c) zone of failure (plastic condition);



(d) horizontal displacement contours.



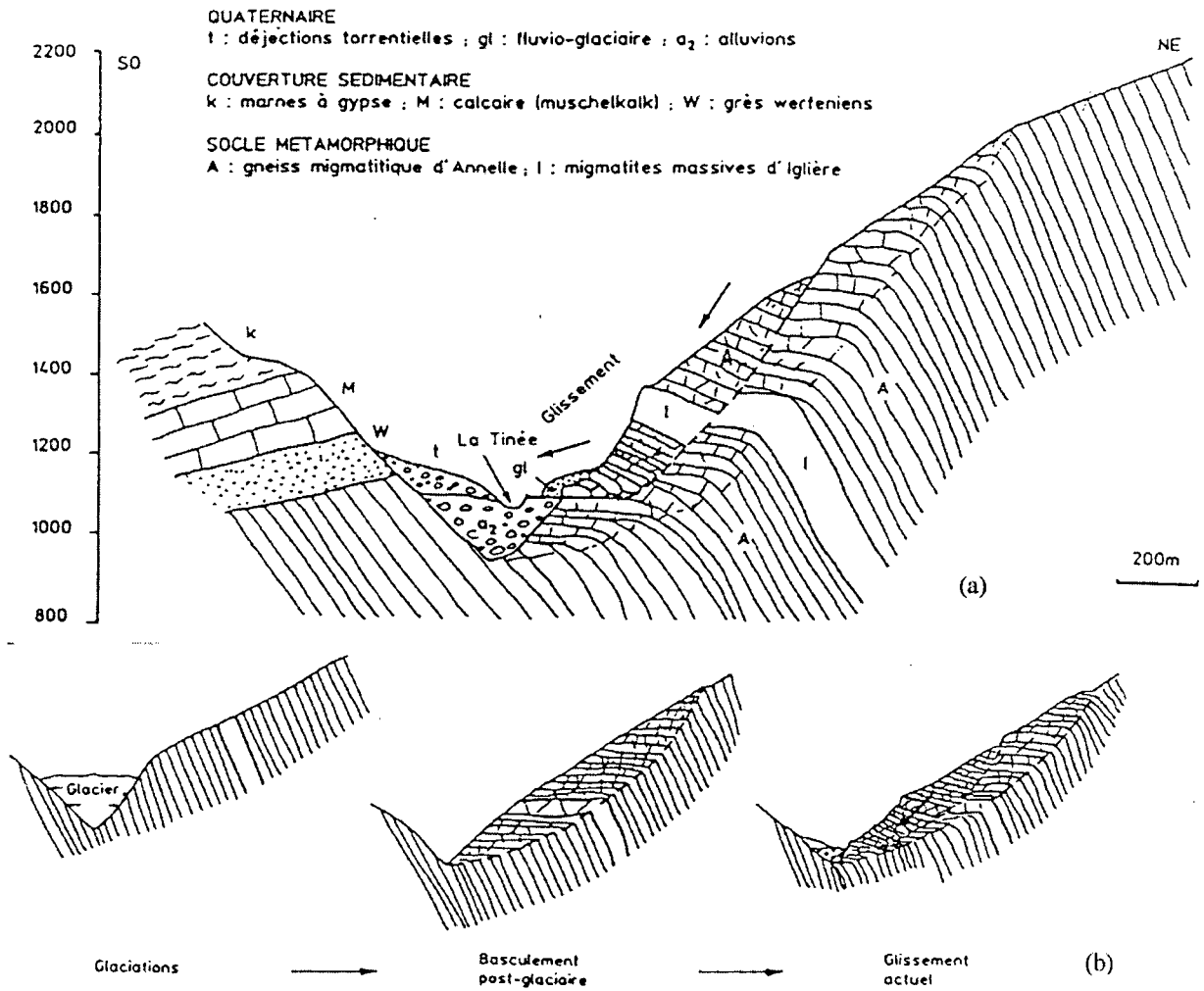


Figure 4-3: Failure mechanism of La Clapière: (a) cross-section; (b) stages of failure development (Anon., 1992 after Follacci, 1987).

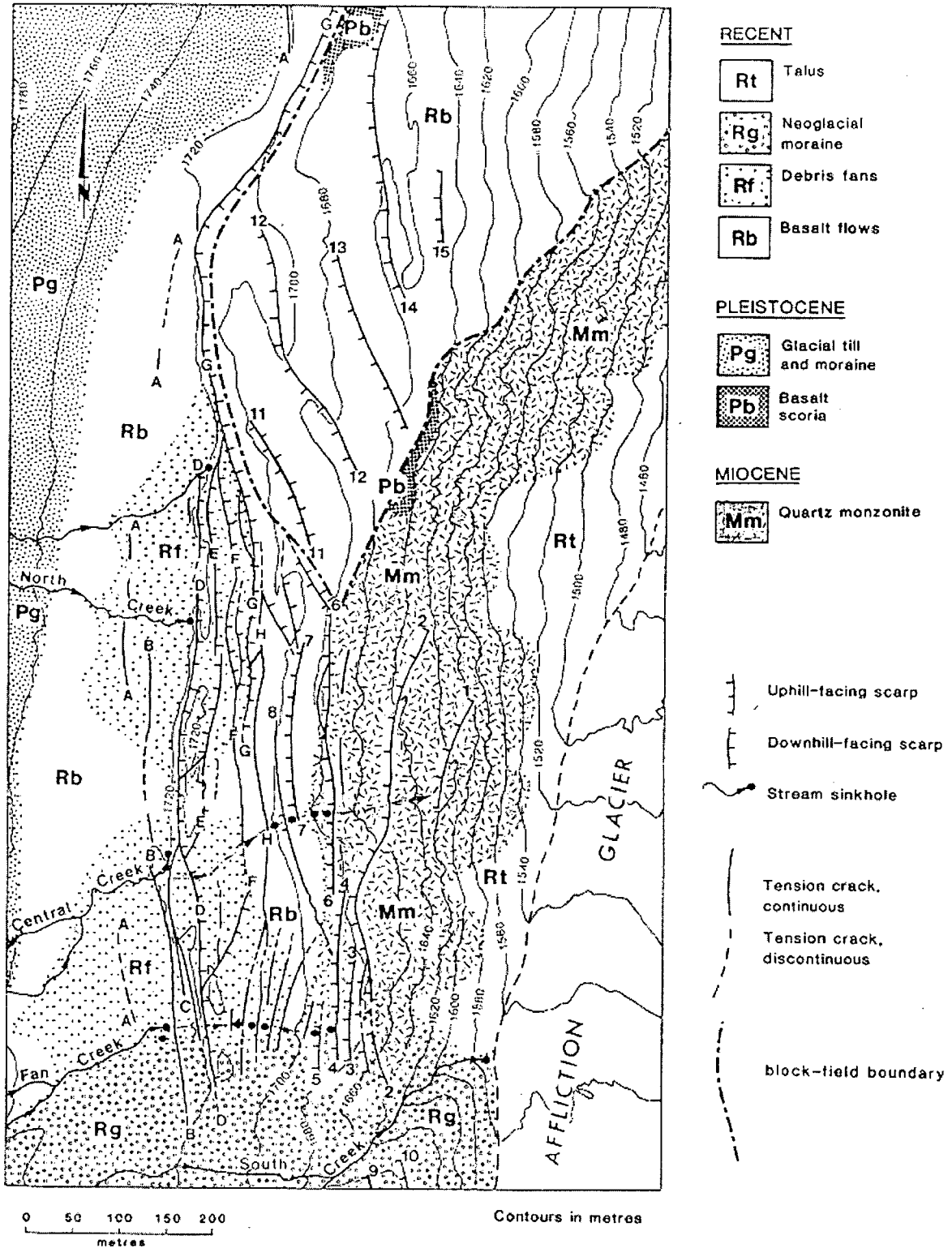
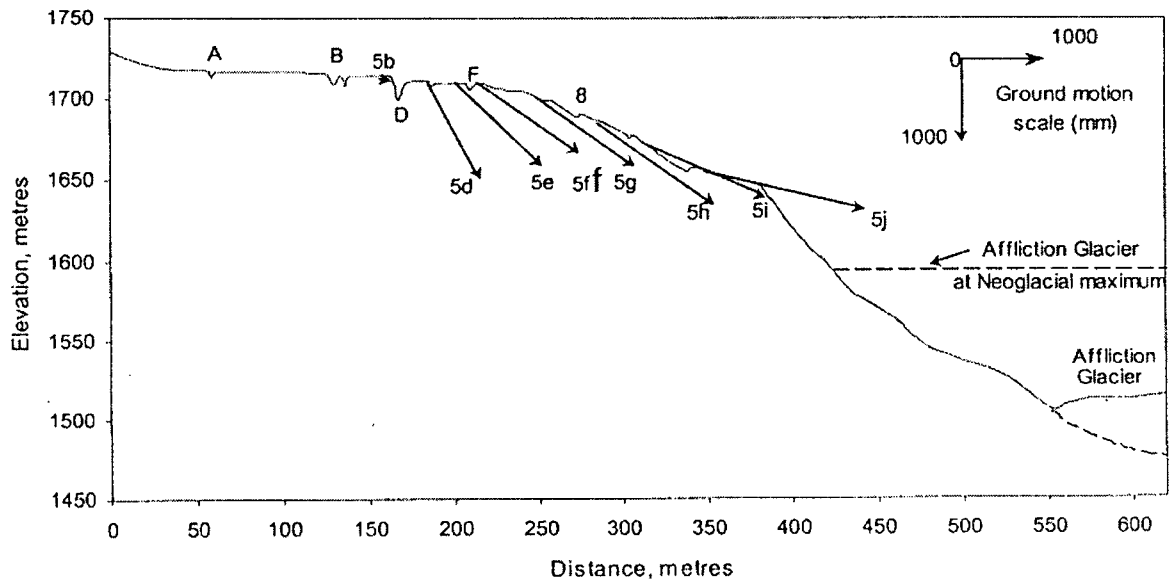
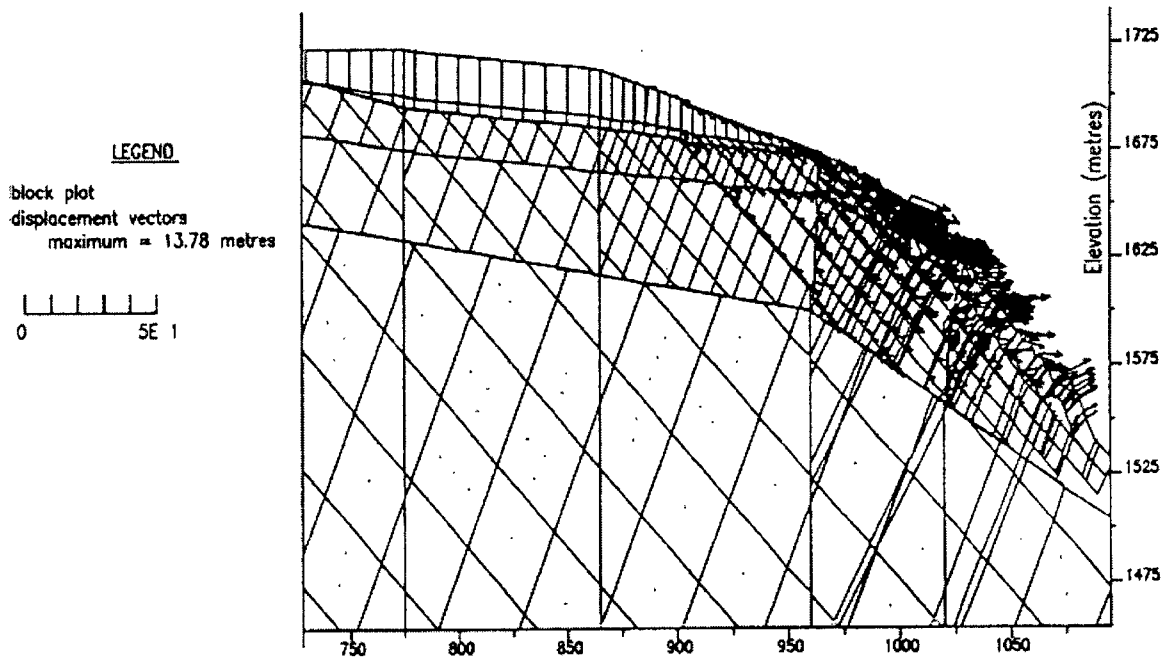


Figure 4-4: Geology and slope-movement features of the Affliction Creek study area (Bovis, 1990).



(a)



(b)

Figure 4-5: Affliction Creek (a) ground-motion vectors; (b) modelled displacements (Bovis and Stewart, 1998).

Figure 4-6:  
North-south section  
through Glen Pean slide  
(De Freitas and Watters,  
1973).

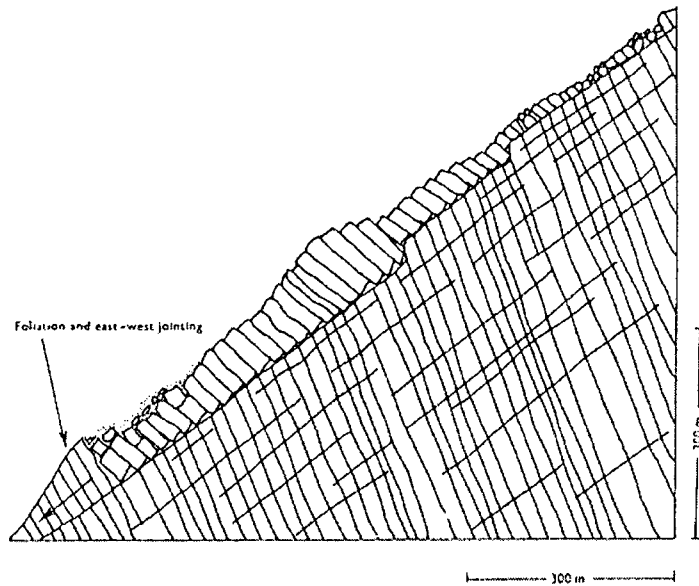
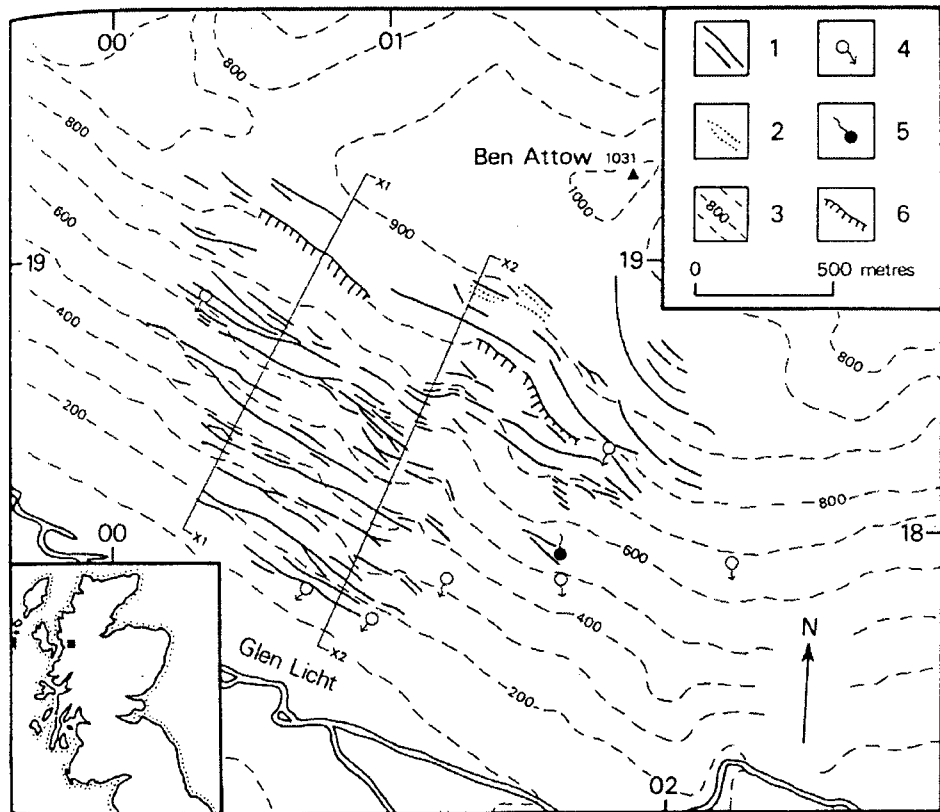


Figure 4-7:  
Geomorphological map of the  
southwest slope of  
Ben Attow.  
1: obsequent  
scarplets;  
2: linear  
depressions;  
3: contours (100-m  
intervals);  
4: springs;  
5: sink holes;  
6: failure scarp  
(Holmes and  
Jarvis, 1985).



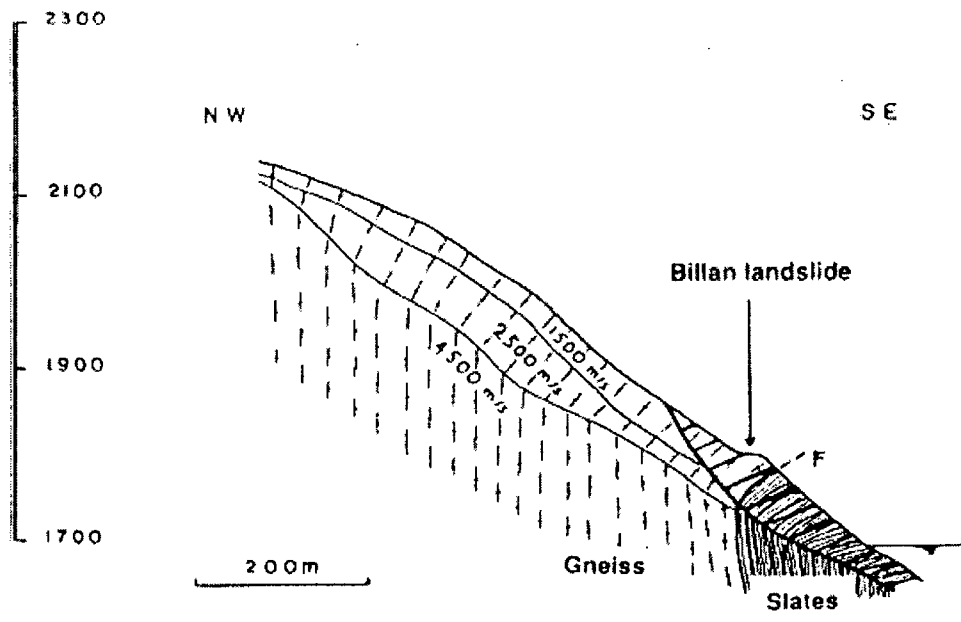


Figure 4-8: General slope profile of the Billan landslide (Giraud et al., 1990).

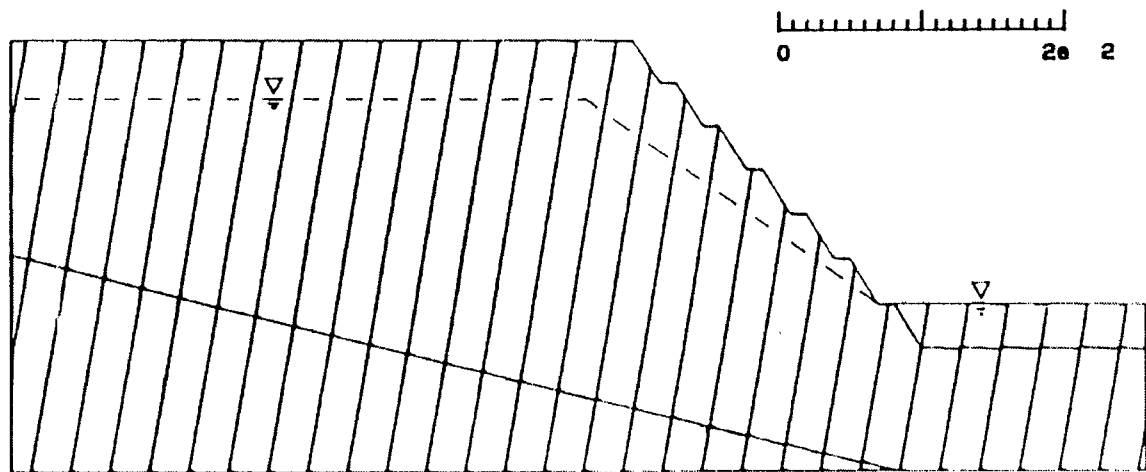
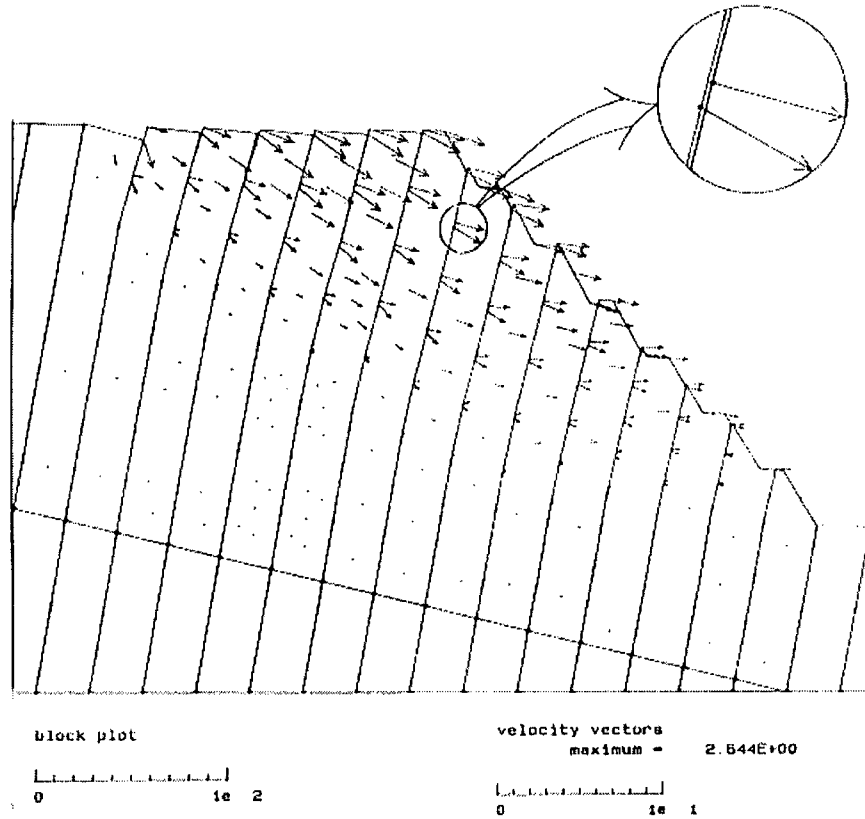


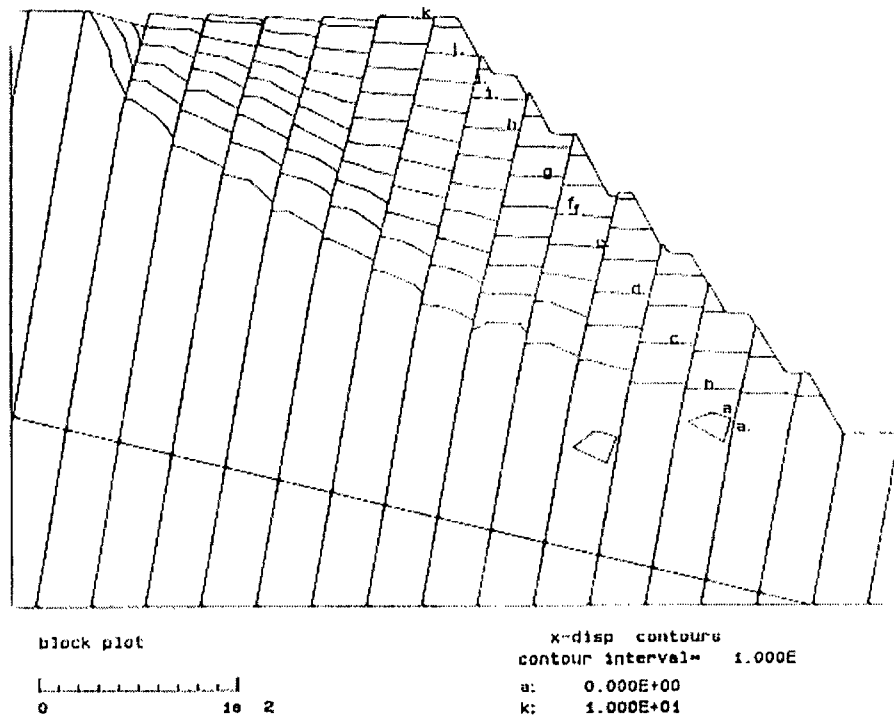
Figure 4-9: Block geometry and assumed water table for UDEC modelling of Brenda Mine (after Pritchard, 1989, Fig. 4.6b).

Figure 4-10:  
 Pure flexural  
 toppling  
 deformation at  
 Brenda Mine:  
 (a) with grid  
 point velocities  
 (dry slope);  
 (b) horizontal  
 displacement  
 contours (after  
 Pritchard, 1989,  
 Figs. 4.7a, b).

(a)



(b)



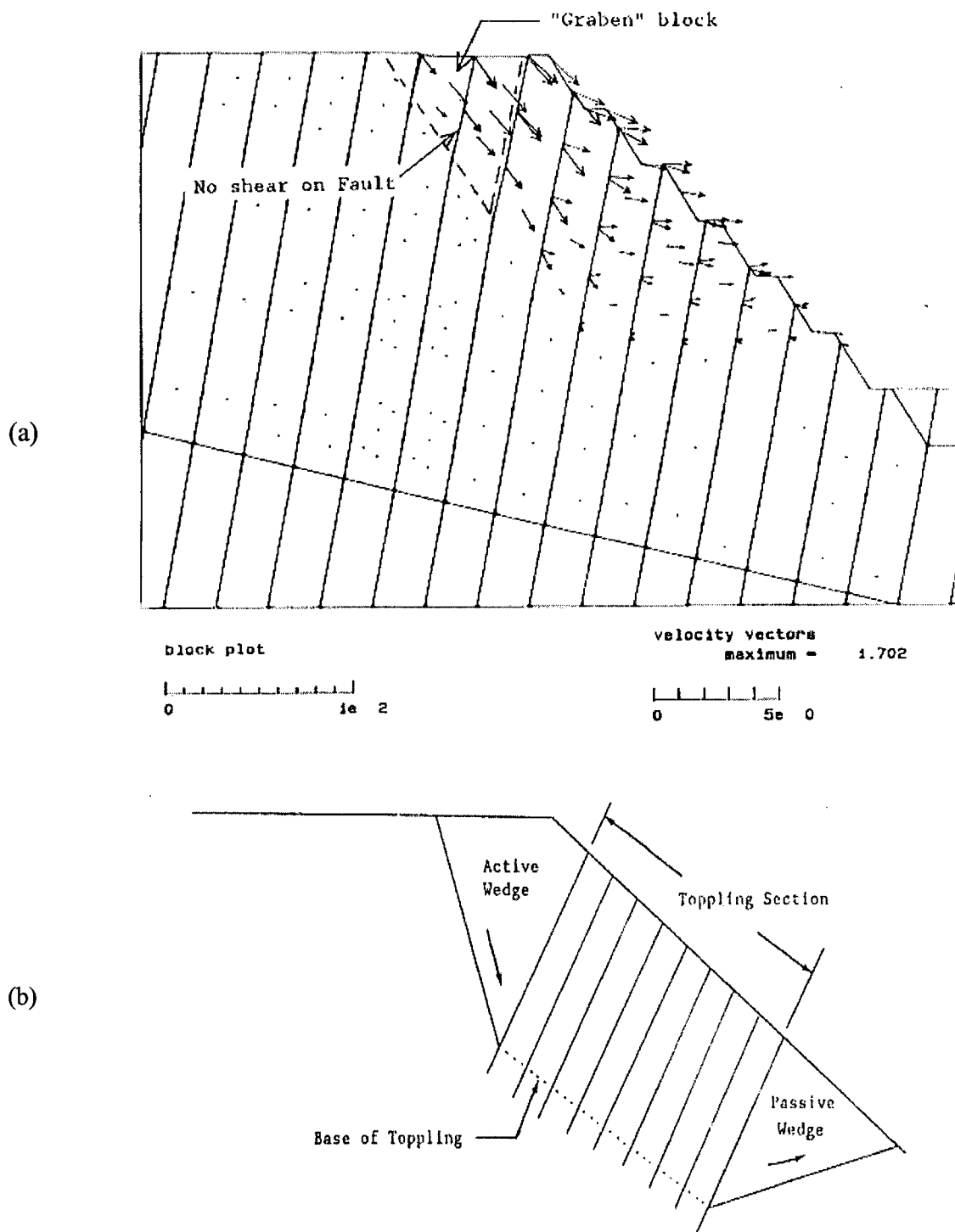


Figure 4-11: "Graben" toppling deformation at Brenda Mine: (a) with grid point velocities (dry slope) (after Pritchard, 1989, Fig. 4.8); (b) moment driven deformation with active and passive wedges (Pritchard, 1989, Fig. 4.9a, after Nieto, 1987).

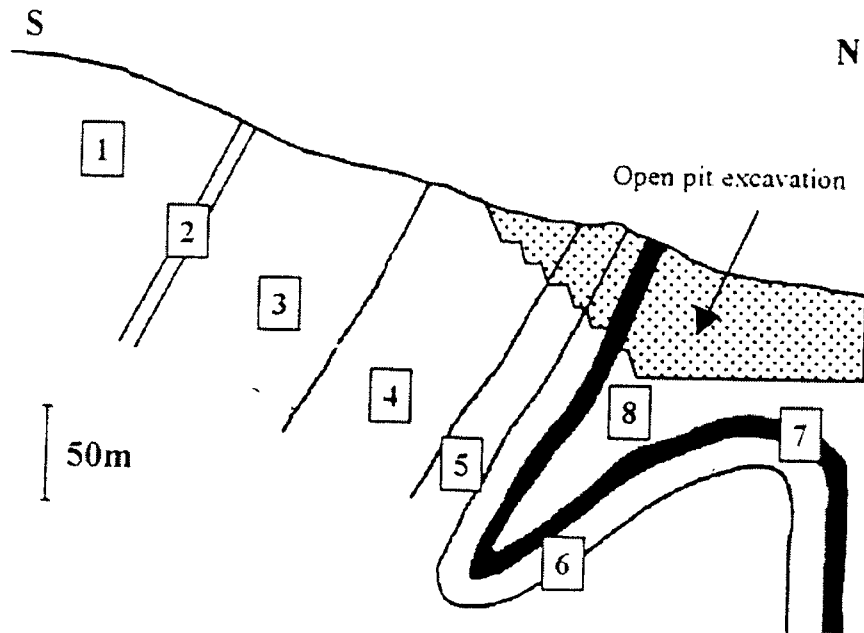


Figure 4-12: Geological structure in Luscar pit: [1] Nikanassin Formation – thin-bedded shales and siltstones; [2] Cadomin – conglomerate; [3] Luscar Formation, Gladstone Member – thinly interbedded siltstones and shales; [4] Luscar Formation, Moosebar Member – marine shales; [5] Luscar Formation, Torrens Member – sandstone; [6] Luscar Formation, Torrens Member – interbedded siltstones and sandstones; [7] Luscar Formation, Member D – Jewel coal seam; [8] Luscar Formation, Member D – massive siltstones and sandstones with minor shale and coal.

## 5.0 NUMERICAL MODELLING STUDY – METHODOLOGY

When conducting a study, it is common to start with the simplest conditions and gradually increase the complexity of the problem. This allows improved interpretation of results and understanding of the impact of the various input parameters. In numerical modelling, there are a significant number of variables, making for myriad combinations, and starting off with simple conditions makes it much easier to understand the role of each variable. In general, nature is so complex that it is next to impossible to realistically model every detail, particularly when there is often little information about subsurface conditions. Simplifying assumptions allow only those variables of interest to be considered. It should be remembered that modelling is merely another tool for analyzing problems, and is not a substitute for real observations.

Two failure mechanisms associated with toppling are examined in this study: flexural toppling and block toppling, as described in Chapter 2. Both mechanisms have been studied in the past, usually through the detailed examination of a specific slope (e.g., the cases given in Chapter 4). Using a systematic examination of key parameters, this study attempts to identify the influence of each parameter on the failure mechanism. As well, this study aims to demonstrate that the two mechanisms have significantly different stress distributions resulting in fundamentally different behaviour, in other words, that flexural toppling is a ductile process occurring in relatively weak rock having few cross-joints, while block toppling occurs in relatively strong rock with significant cross-jointing and is a brittle process.

## 5.1 *General Modelling Procedure*

The standard procedure for modelling in UDEC is first to set up the problem geometry, including discontinuities. This divides the problem area into blocks. The blocks and discontinuities are then assigned parameters. The parameters assigned to the blocks depend on whether or not the blocks are deemed to be deformable. It is not uncommon for intact blocks to be considered rigid (i.e., not deformable) for numerical simplicity or because intact rock is considerably stiffer than the rock mass as a whole. However, even strong rock is somewhat deformable, and over a large slope this deformation may have a significant influence on the overall behaviour (see, for example, Sjöberg (1999) or Benko and Stead (1999)). Thus, for this study, the intact rock was considered to be deformable.

The parameters of interest in this study were: rock strength; discontinuity orientation, spacing and persistence; and conditions at the toe of the slope. The rock strength parameters required by UDEC depend on the type of constitutive model used (models are described in Chapter 3). This study used the Mohr-Coulomb plasticity model, which is commonly used to model stress-strain relationships in rock and is relatively simple to interpret. The parameters required by UDEC for the Mohr-Coulomb model are: bulk modulus, shear modulus, internal friction angle, dilation angle, cohesion and tensile strength.

There are five constitutive models for discontinuity strength available in UDEC: (1) point contact – Coulomb slip, (2) joint area contact – Coulomb slip, (3) joint area contact – Coulomb slip with residual strength, (4) continuously yielding, and (5) Barton-Bandis. This

study used model (2) (which is a simpler version of model (3)), with the following input parameters: joint normal stiffness, shear stiffness, friction angle, dilation angle, cohesive strength and tensile strength. Other parameters, such as joint permeability and joint aperture, may also be specified with this model, but in order to keep the model simple, these parameters were not included. This is discussed further in Chapter 9.

Discontinuity orientations, spacing and persistence are input with the initial geometry. Once the geometry is defined, the blocks are zoned, a process that divides deformable blocks into triangular regions for the purposes of finite difference calculations. For reasonable solution accuracy, the aspect ratio of the zones must be less than about 1:10 (UDEC Manual, p. 2-36). Parameters are then assigned to the zones and to the discontinuities, and initial in situ stress, boundary and groundwater conditions are defined. The behaviour of the model may be monitored by setting up a number of “history points” to track such things as unbalanced forces in the model, x- and y-displacements or x- and y-velocities at points in and along the slope as the model runs. After all initial conditions have been defined, gravity is turned on, and the model is run until equilibrium is achieved. Equilibrium is defined as the state at which the unbalanced forces in the model are reduced to nearly zero and deformation due to gravity has essentially stopped.

Initial in situ stress conditions were identical for all models, and were based on a horizontal to vertical stress ratio ( $k$ ) of 0.5. Plane-strain conditions were assumed. This and other assumptions are discussed further in Chapter 9.

Artificial boundary conditions were specified for all sides of the model except the ground surface. The right and left sides were assigned zero x-velocity, and the bottom assigned zero y-velocity. Work by Sjöberg (1999) showed that, for accurate analysis when modelling open pit mines, the model should be roughly 3 to 4 times the pit width and 2 to 3 times the pit depth, in order to limit the effects of boundary conditions on the area of interest. The size of the model in the current study, with a slope 350 m wide and 350 m high, is 1500 m wide and 850 m high (making the model perhaps slightly wider than necessary). In order to improve computing times, the model was divided into three regions, with the inner area parameters varied while the parameters in the outer two regions were held constant (Figure 5-1).

Arguably the most serious simplifying assumption made in this parametric analysis was not to include the effects of groundwater. All models were run under dry conditions.

The initial model was set up as shown in Figure 5-1. History points were set up as illustrated in Table 5-1, with data collected every 50 cycles. After coming to equilibrium under gravity, the three overburden layers were removed one by one, to simulate the formation of the valley. The model was cycled between the first and second layers, and between the second and third layers, to allow time for equilibration. All of the models in this study used the same outer slope geometry after overburden removal, with a slope angle of  $45^\circ$ , as shown in Figure 5-2. After excavation of the third overburden layer, the model was run until equilibrium was achieved, or until it was considered that catastrophic failure was in progress based on displacement and velocity histories, at which point the model was stopped.

## 5.2 *Parametric Modelling*

The parameters varied in the study were: intact rock strength; cross-joint orientation, spacing and persistence; and conditions at the toe of the slope. To improve computational time, only the parameters in the inner slope region were varied (Figure 5-2). All models had one main joint set dipping 80° into the slope, with joints spaced 3 m apart. The friction angle, dilation angle, cohesion and tensile strength of the main joint set were held constant at 30°, 0°, 0 and 0, respectively. These values, which imply that the joints are all at residual strength, were selected so that the influence of the varied parameters could be better identified. Joint normal stiffness and joint shear stiffness were varied in proportion to the variation of the bulk and shear moduli, discussed below. It should be noted that the models did not appear to be overly sensitive to the values used for normal and shear stiffness.

### 5.2.1 Intact Rock Strength

Two extremes of intact rock strength were first examined. The “strong” case used an unconfined compressive strength (UCS) of 100 MPa, which is defined as strong to very strong (ISRM grade R4 to R5), while the “weak” case used a UCS of 10 MPa (weak rock, ISRM grade R2) (Hoek et al., 1995). The UCS was increased to 20, 40, 60 and 80 MPa to map behaviour between the two extremes. Note that the parameters were not changed with depth. This will be discussed further in Chapter 9.

The information required by UDEC using the Mohr-Coulomb model are: bulk modulus, shear modulus, internal friction angle, dilation angle, cohesion and tensile strength. The values for these parameters are given in Table 5-2. The values were determined using Hoek and Brown's (1997) practical estimates for rock mass strength, as shown in Table 5-3. Input values for  $m_i$ , GSI, Poisson's Ratio ( $\nu$ ) and  $\sigma_{nt}$  were held constant at 12.5, 62, 0.25 and 0.7, respectively (based on "good" rock, after Hoek et al., 1995, Table 8.4, reproduced in the Appendix). The calculated instantaneous value was used for friction angle, and 3/4 of the calculated instantaneous cohesion was used (this is standard practice: Rose, N., personal comm.). Tensile strength was estimated to be approximately 1/5 of the cohesion value used (Ripley, B., personal comm.).

### 5.2.2 Cross-Jointing

The effect of cross-joints, i.e., a set of joints roughly orthogonal to the main sub-vertical joint set, was examined by varying the persistence, spacing and orientation of the cross-joints. "Strong" intact rock was used in order for the majority of the deformation to occur along the discontinuities (i.e., UCS = 100 MPa – see Table 5-2 for parameters). It was not feasible to examine every possible combination; rather, the extreme conditions and some conditions in between were modelled.

The friction angle, dilation angle, cohesion and tensile strength of the cross-joints were held constant at 30°, 0°, 0 and 0, respectively. These values, which imply that the joints are all at residual strength, were selected so that the influence of the varied parameters could be better

identified. Joint normal stiffness and joint shear stiffness were set at 10 GPa/m and 5 GPa/m, respectively. Benko and Stead (1999) examined the sensitivity of their models to different values for  $j_{kn}$  and  $j_{ks}$  (they used  $j_{ks}=1/10 j_{kn}$ ), and found that there were larger movements with lower stiffness values, but the overall behaviour of the slope was unchanged.

#### 5.2.2.1 Persistence

Joint sets are generated in UDEC by inputting the mean and standard deviation (for uniform probability distribution) of the following parameters: the angle of the cross-joint track relative to the positive x-axis; the trace length of the cross-joint segment; the gap length between cross-joint segments; and spacing normal to cross-joint tracks. Joint persistence was varied by adjusting the mean and standard deviation of the trace length and gap length of the cross-joints. Five cases were compared, with persistence ranging from zero (no cross-joints) to almost fully continuous (idealized). Input parameters for the four cases with cross-joints are given in Table 5-4. Note that all joint angles have a standard deviation equal to zero. Four cases are illustrated in Figure 5-3 (case with zero cross-joints not shown).

#### 5.2.2.2 Spacing

Spacing normal to the cross-joints was modelled at 20 m and 50 m with continuous cross-joints. Additionally, a single cross-joint dipping out of the slope at 25° and daylighting near the toe of the slope was modelled. Finally, Test 2 from Section 5.2.2.1 was re-run using the same parameters but with a normal spacing of 25,5 (mean, standard deviation).

### 5.2.2.3 Orientation

Two orientations of cross-joints were compared: at 0° and at 25°, with spacing normal to the cross-joints at 50 m. The UCS for both orientations was 100 MPa (see Table 5-2).

### 5.2.3 Toe Conditions

A valley slope undercut by a glacier may remain stable while the glacier is present. However, if the glacier melts away relatively rapidly, as occurred at the end of the last ice age, stresses in the slope may result in landslides as the oversteepened slope returns to a stable state. The effect of oversteepening of the toe of the slope was investigated by excavating portions of the toe after the slope had been formed as described in Section 5.1. While this does not exactly reproduce glacial conditions (i.e., modelling did not take into account ice in the valley instead of rock), it does give some indication of how the slope behaves due to rapid unloading at the toe. In order to keep the study simple, it was not attempted to have different material types in the slope, e.g., more deformable material at the base of the slope such as exists at the Chuquicamata mine in Chile (Board et al., 1996).

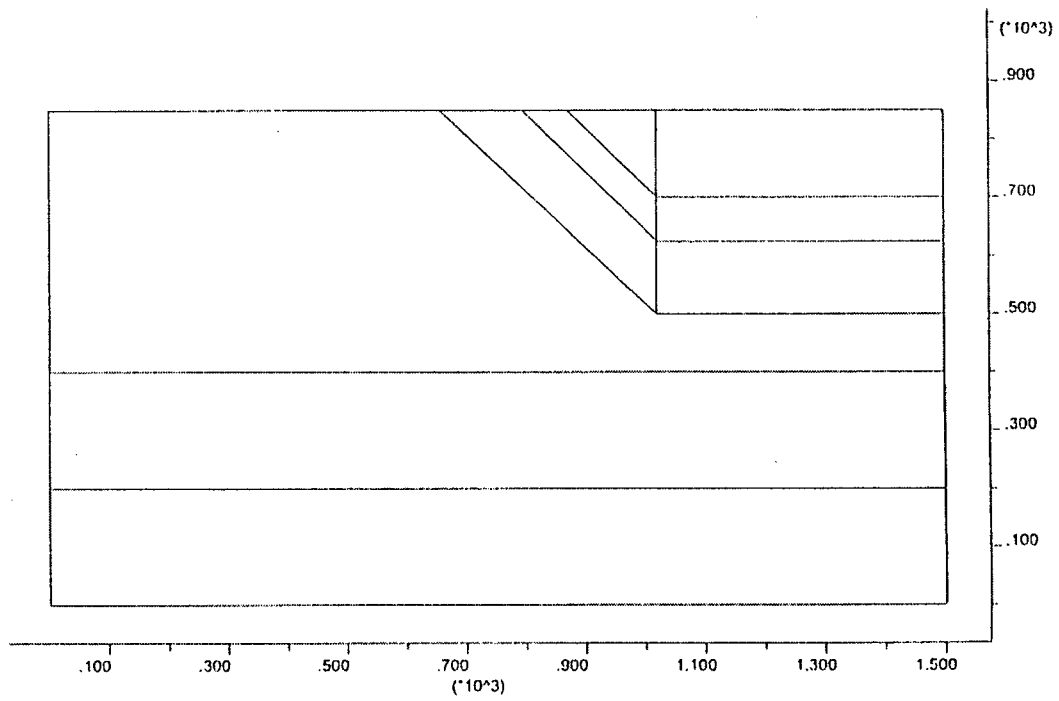


Figure 5-1: Initial Model Set Up for Parametric Study

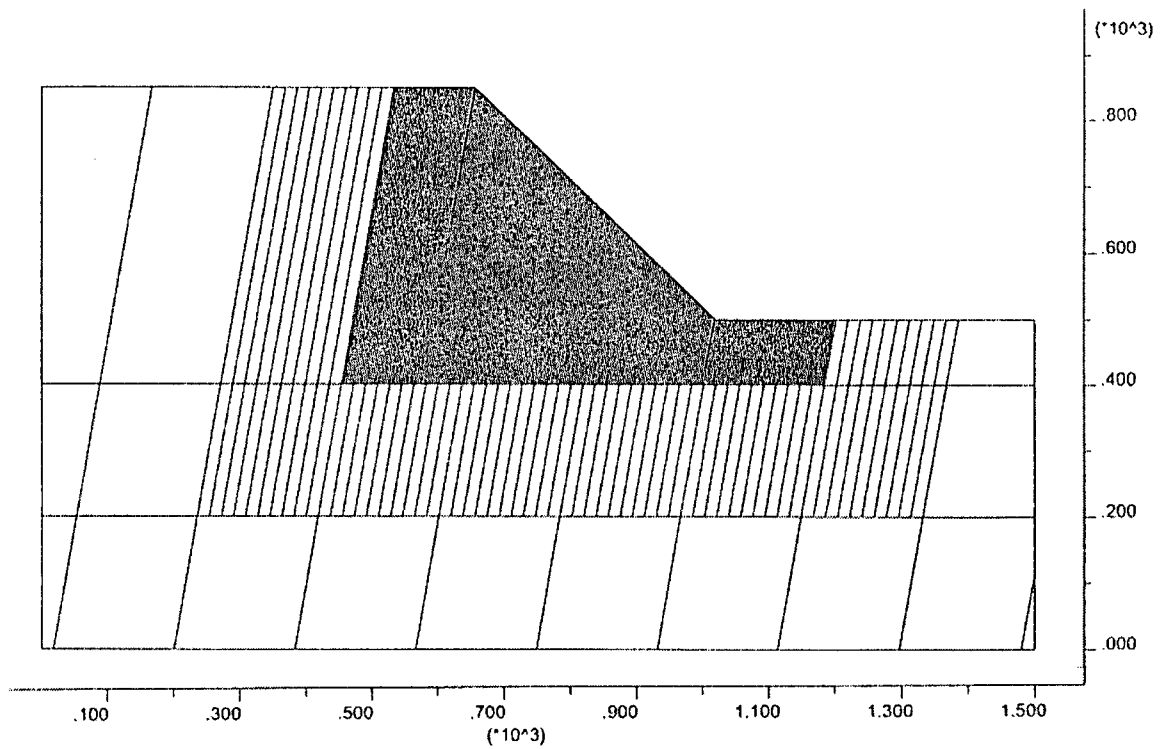
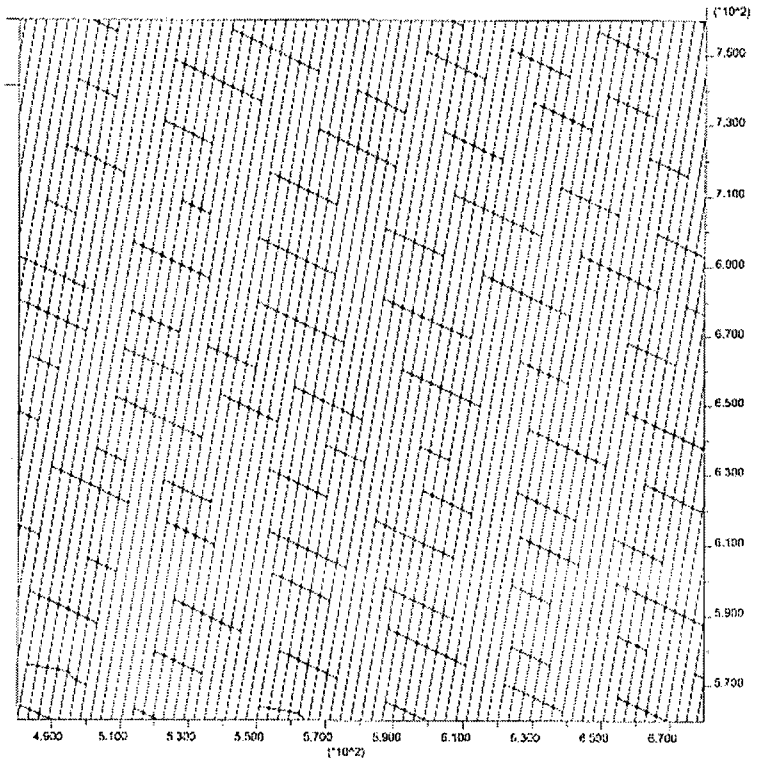


Figure 5-2: Outer Slope Geometry for Parametric Study. Three zones with different joint spacing shown: outer zone, 180 m; middle zone, 18 m; inner zone, 3 m.

(a) Test 0;



(b) Test 1;

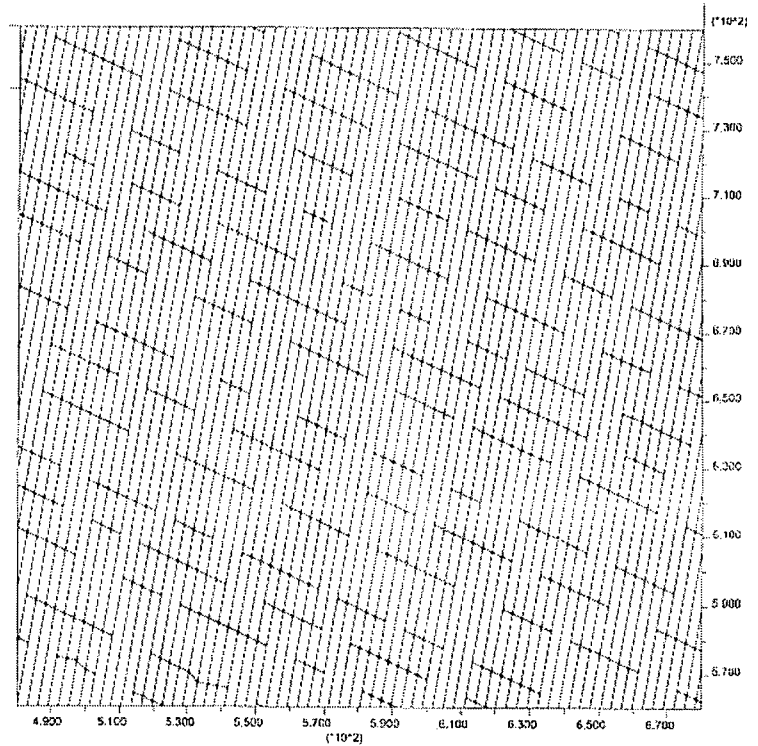
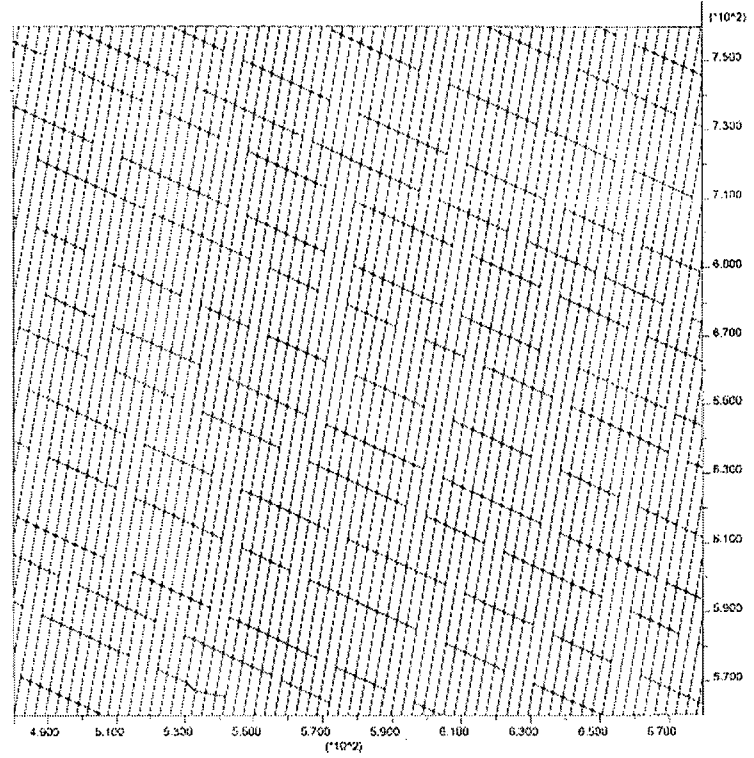


Figure 5-3: Four Cases of Variation in Cross-Joint Persistence (see Table 5-4).

(c) Test 2;



(d) idealized cross-joints.

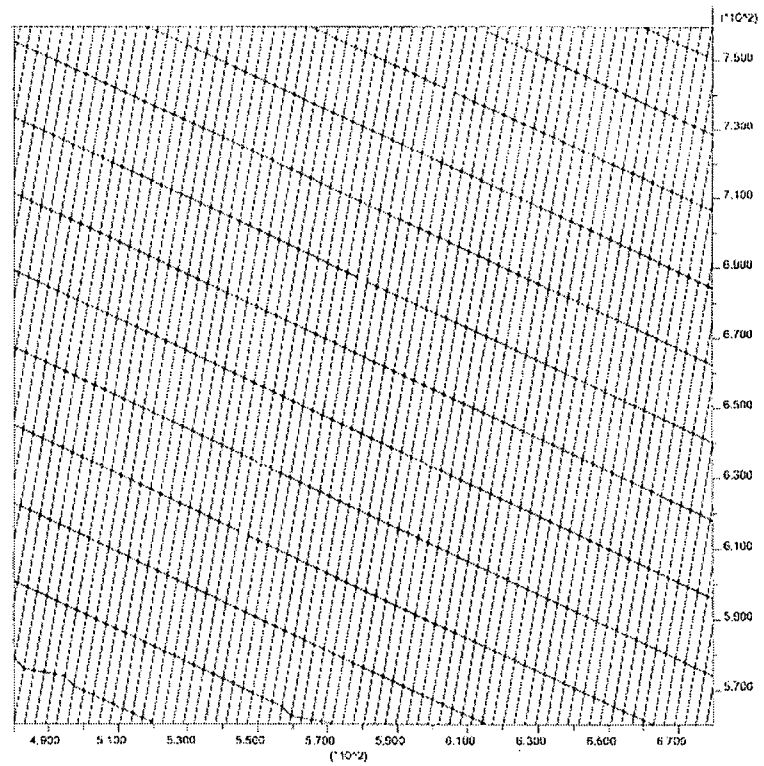


Figure 5-3 (cont'd): Four Cases of Variation in Cross-Joint Persistence (see Table 5-4).

Table 5-1: Monitoring Points

<u>History #</u>	<u>Monitored Information</u>	<u>Location on Slope (x,y)</u>
1	unbalanced forces	N/A
2, 3	x-displacement, y-displacement	1000, 515
4, 5	x-displacement, y-displacement	950, 560
6, 7	x-displacement, y-displacement	867, 636
8, 9	x-displacement, y-displacement	847, 656
10, 11	x-displacement, y-displacement	827, 676
12, 13	x-displacement, y-displacement	807, 696
14, 15	x-displacement, y-displacement	787, 716
16, 17	x-displacement, y-displacement	767, 736
18, 19	x-displacement, y-displacement	727, 756
20, 21	x-displacement, y-displacement	707, 776
22, 23	x-displacement, y-displacement	687, 796
24, 25	x-displacement, y-displacement	667, 816
26, 27	x-displacement, y-displacement	627, 836
28, 29	x-displacement, y-displacement	658, 845
30, 31	x-velocity, y-velocity	867, 636
32, 33	x-velocity, y-velocity	747, 756
34, 35	x-velocity, y-velocity	658, 845

Table 5-2: Rock Mass Strength Parameters Used in UDEC Modelling

	<u>UCS=10</u>	<u>UCS=20</u>	<u>UCS=40</u>	<u>UCS=60</u>	<u>UCS=80</u>	<u>UCS=100</u>
Density (kg/m <sup>3</sup> )	2700	2700	2700	2700	2700	2700
Bulk Modulus (MPa)	4200	5900	8400	10 300	11 900	13 000
Shear Modulus (MPa)	2500	3600	5000	6200	7100	8000
Friction Angle (°)	33	38	44	47	49	51
Dilation Angle (°)	2	2	2	2	2	2
Cohesion (MPa)	0.170	0.230	0.330	0.420	0.500	0.590
Tensile Strength (MPa)	0.030	0.040	0.060	0.80	0.100	0.120

Table 5-3:  
Spreadsheet  
for  
Calculation  
of Hoek-  
Brown and  
Mohr-  
Coulomb  
Parameters

INPUT	Intact Rock Strength or UCS (sigci)	Material Constant	GSI	Poisson's Ratio
Unit	sigci= 10 Mpa	mi= 12.5 mi	GSI= 62	0.25
OUTPUT	mb = 0.83 sigtm = -0.02 k = 2.53 sigcm = 1.06 Mpa	s = 0.001776 A = 0.41 phi = 25.7° E = 6309.6 Mpa	a = 0.5 B = 0.68 coh = 0.33 Mpa	Bulk Mod= 4206 MPa Shear Mod= 2524 MPa
TANGENT (INSTANTANEOUS VALUES)	signt = 0.7 Mpa	phit = 32.8 Mpa	coht = 0.23 Mpa 3/4 coht= 0.171199	
Calculations:				
sig3	1E-10	1.07	2.14	10
sig1	4E-01	4E+00	6E+00	34
ds1ds3	10.83	2.38	1.98	27
sign	0.04	1.96	3.56	17
tau	0.12	1.37	2.00	11
x	-2.24	-0.70	-0.45	-7
y	-1.93	-0.86	-0.70	-8
xy	4.33	1.24	0.31	8
xsq	5.04	1.22	0.20	8
sig3sig1	0.00	0.76	13.66	56
sig3sq	0.00	0.13	4.59	18

Cell Formulae:

$mi/mb = EXP((GSI-100)/14)$   
 $mb = mi * EXP((GSI-100)/14)$   
 $E = IF(sigci > 100, 1000 * 10^{(GSI-10)/40}, SQRT(sigci/100) * 1000 * 10^{(GSI-10)/40})$   
 $sig3 = sigci / 2^n$  where n starts at 10 and decreases by 1 for each subsequent cell  
 $sig1 = sig3 + sigci * ((mb * sig3) / sigci + s)^a$   
 $ds1ds3 = IF(GSI > 25 THEN 1 + mb * sigci / (2 * (sig1 - sig3)) ELSE 1 + (a * mb^a) * (sig3 / sigci)^{(a-1)})$   
 $sign = sig3 + (sig1 - sig3) / (1 + ds1ds3)$   
 $tau = (sign - sig3) * SQRT(ds1ds3)$   
 $k = (sumsig3sig1 - (sumsig3 * sumsig1) / 8) / (sumsig3sq - (sumsig3^2) / 8)$   
 $sigtm = sumsig1 / 8 - k * sumsig3 / 8$   
 $sigcm = 0.5 * sigci * (mb - SQRT(mb^2 + 4 * s))$   
 $phi = ASIN((k-1) / (k+1)) * 180 / PI()$   
 $coh = (sigcm * (1 - SIN(phi * PI() / 180))) / (2 * COS(phi * PI() / 180))$   
 $Bulk Mod = E / (3 * (1 - 2 * Poisson))$   
 $s = IF(GSI > 25, EXP((GSI-100)/6), E/6)$   
 $a = IF(GSI > 25, 0.5, (0.65 - GSI / 200))$   
 $x = LOG((sign - sigtm) / sigci)$   
 $y = LOG(tau / sigci)$   
 $A = 10^{(sumy / 8 - B * sumx / 8)}$   
 $B = (sumxy - (sumx * sumy) / 8) / (sumxsq - (sumx^2) / 8)$   
 $phit = (ATAN(A * B * ((sigtm - sigtm) / sigci)^{(B-1)})) * 180 / PI()$   
 $coht = A * sigci * ((sigtm - sigtm) / sigci)^B - sign * TAN(phit * PI() / 180)$   
 $Shear Mod = E / (2 * (1 + Poisson))$

Table 5-4: Parameters for Variation of Cross-Joint Persistence  
(mean, standard deviation)

	Joint Angle	Trace Length	Gap Length	Normal Spacing
Test 0	25,0	20,10	15,5	15,5
Test 1	25,0	20,10	10,5	15,5
Test 2	25,0	25,10	6,3	15,5
Idealized cross-joints	25,0	300,0	0	20

## 6.0 NUMERICAL MODELLING STUDY – RESULTS

It should be remembered that UDEC modelling is simply a tool to analyze behaviour under certain input conditions. Results should be considered generally, with displacements and velocities determined by the program considered in terms of order of magnitude and not as exact values. By examining results in this manner, general predictions of behaviour in actual (vs. modelled) rock slopes may be possible.

### 6.1 *Variations in Intact Rock Strength*

With a single sub-vertical joint set and with rock mass quality held constant, toppling motion decreased as the unconfined compressive strength (UCS) of the intact rock increased. This is illustrated in the block plots shown in Figure 6-1 (see Table 5-2 for UDEC input parameters). Where the UCS is low, a hinge zone develops, as shorter columns at the base of the slope bend slightly, allowing more movement to occur upslope in the longer columns. Figure 6-1 shows the models at approximately the same run time (about 20 seconds). Note that Figures 6-1(e) and (f) (UCS = 80 and 100 MPa, respectively) are essentially identical, showing very little deformation.

Displacement due to overburden removal occurs at the base of the slope. Toppling motion begins approximately two thirds of the way up the slope. In all six cases, movement is concentrated near the top of the slope; however, the amount of movement decreases significantly once the UCS is greater than about 60 MPa.

The area of movement concentration moves upslope as the UCS increases, i.e., there is less movement at the toe of the slope. For UCS greater than 60 MPa, the slope shows little deformation compared to the scale of the slope (Figures 6-1(e) and (f)). Displacement vectors for UCS = 10 MPa and UCS = 80 MPa, showing an order of magnitude difference in displacement, are provided for comparison in Figure 6-2. Shearing takes place along the sub-vertical joints, resulting in small up-slope facing scarps where the UCS is less than about 60 MPa (Figures 6-1(a), 6-2(a)).

The principal stresses are parallel to the slope surface in the upper 100 m or so (i.e., the first 100 m or so below the ground surface) for all six cases, even after the slope has undergone some deformation. Below 100 m depth, the principal stresses rotate towards vertical (Figure 6-3).

Allowing the models to run further, it was found that deformation ultimately stopped (where the UCS was less than 60 MPa, the model had to be run for a longer period of time before movement ceased). This result is due to a number of factors. Firstly, flexural toppling is a self-stabilizing mechanism. Under the criteria of Goodman and Bray (1980) (Equation 2, Chapter 2), as the columns bend and the dip of the discontinuities becomes less steep, the potential for flexural toppling is substantially reduced. The models stabilized at a dip value roughly corresponding to the Goodman-Bray criterion. Secondly, the damping process used in UDEC for static analysis works to bring the model into equilibrium (this is discussed further in Chapter 9). Finally, UDEC cannot create joints, so the slopes, by their defined geometry, cannot fail catastrophically. Note that the model with UCS = 20 MPa was re-run

with the tensile strength of the intact rock set to zero, and the behaviour of the slope was not significantly altered.

These models illustrate the formation of a hinge zone where the rock has a UCS less than 60 MPa. In reality, the existence of cross-joints, the presence of groundwater, as well as failure in tension of the weak columns could lead to catastrophic failure at the hinge zone. This is discussed further in Chapter 9.

## 6.2 *Cross-Joints*

The existence and persistence of cross-joints has perhaps the most significant effect on the overall behaviour of the slope. Refer to Section 5.2.2 for input parameters.

### 6.2.1 Variation of Persistence

Variation of the persistence of cross-joints altered overall slope behaviour. Block plots for the five cases (Table 5-4) are shown at approximately the same model run time (~18 seconds) in Figure 6-4. All cases have a UCS = 100 MPa (Table 5-2). Very little movement occurs without cross-joints, as discussed in Section 6.1, but as cross-joint persistence increases, the amount of movement increases. This is not a surprising result, as higher persistence gives more release surfaces and allows blocks to move more freely. The two extremes may be considered highly idealized; however, they provide simple starting points of reference.

With no cross-joints, deformation occurs due to bending of the columns and shearing along the sub-vertical joints. The majority of the deformation occurs at the crest of the slope, with some movement occurring at the bottom of the slope due to continuing rebound from removal of the overburden. The principal stresses remain essentially parallel to the slope and are not sufficiently high to cause failure of the intact rock (Figures 6-1(f) and 6-3(f)).

In Test 0, deformation is also concentrated at the top of the slope, but the x-displacement has increased by roughly an order of magnitude in the positive direction. Y-displacement has increased only marginally, showing downward motion at the top of the slope. The amount of movement is very small when compared to the scale of the slope. Velocities are low and movement ultimately stops. Again, it should be pointed out that UDEC cannot create joints, so the persistence as given by this set of randomly-generated joints is ultimately stable. Stresses in the longer columns holding back the slope are not sufficiently high to cause failure of the intact rock and are oriented sub-parallel to the slope surface (Figure 6-5). This might not be the case if there was groundwater in the slope. As well, it is possible that the geometry given by another set of randomly-generated joints with the same parameters as given in Table 5-4 for Test 0 (i.e., the same theoretical persistence) might not be stable. This is discussed further in Chapter 9. These results are almost identical to those for Test 1, with low velocities and only a small increase in movement, but the slope takes a bit longer to stabilize.

Deformation in Test 2 is also concentrated in the upper section, but involves a much larger portion of the slope. X-displacement has increased in the positive direction by about two

orders of magnitude and y-displacement in the negative direction (downward) by about one order of magnitude over Tests 0 and 1. Gaps have opened up between blocks. Figure 6-6 illustrates that the slope is failing: histories 30, 32 and 34 show x-velocity and histories 31, 33 and 35 show y-velocity (refer to Table 5-1 for exact location of history points on the slope). The maximum velocities are roughly 4 m/s and 2 m/s in the x and y directions, respectively, and while these values cannot be considered exact, they are sufficiently high that they cannot realistically be stopped by natural damping. The sudden drop at about 37000 cycles is due to the effect of damping in UDEC, which is discussed further in Chapter 9.

With idealized joints (essentially fully continuous) the slope fails catastrophically. Movement is not concentrated at the top of the slope; rather, a kink band develops as the toe of the slope kicks out. Shearing along the sub-vertical joints first begins at the toe of the slope and is gradually concentrated in the kink band (Figure 6-7). The upper section of the slope rotates backward as the section below rotates forward (Figure 6-4(e)).

### 6.2.2 Variation of Spacing

Increasing the spacing perpendicular to the fully continuous cross-joints from 20 m to 50 m does not significantly change the behaviour of the slope. Movement still begins at the toe of the slope and a kink band develops. The slope fails catastrophically. Block plots for the two cases are shown at approximately the same run time in Figure 6-8. The kink band is roughly the same width in both cases (~60 m for 20 m spacing and 50 m for 50 m spacing).

One model was run with only a single continuous cross-joint dipping  $25^\circ$  and daylighting near the toe of the slope. This slope also failed catastrophically, with movement beginning at the toe of the slope (Figure 6-9). As the smaller columns at the toe rotate outwards, the larger columns upslope begin to rotate and the entire slope is quickly unstable. This mechanism is characteristic of block toppling rather than flexural toppling.

Test 3 had the same input parameters as Test 2, described above, except that the spacing normal to the cross-joints was set at 25,5 instead of 15,5 (mean, standard deviation). Movement is concentrated at the top of the slope (Figure 6-10), as with Test 2. The slope becomes unstable, with high velocities and stresses.

### 6.2.3 Variation of Orientation

For  $UCS = 100$  MPa and with spacing normal to cross-joints = 50 m, changing the orientation of the cross-joints from  $25^\circ$  to horizontal altered the behaviour of the slope. A kink band did not develop with horizontal joints as it did for joints at  $25^\circ$  (Figure 6-8(b)); rather, movement was concentrated in the top portion of the slope and a hinge zone developed (Figure 6-11), much the same as when there were no cross-joints.

There is very little movement on the horizontal joints except near the base of the failure zone (Figures 6-11(b) and 6-12). Shearing occurs on the sub-vertical joints, and upslope-facing scarps are formed as the columns topple. Columns near the hinge zone are seen to bend,

while columns near the slope face remain essentially straight. Movement increases at such a rate that the slope cannot self-stabilize and fails catastrophically.

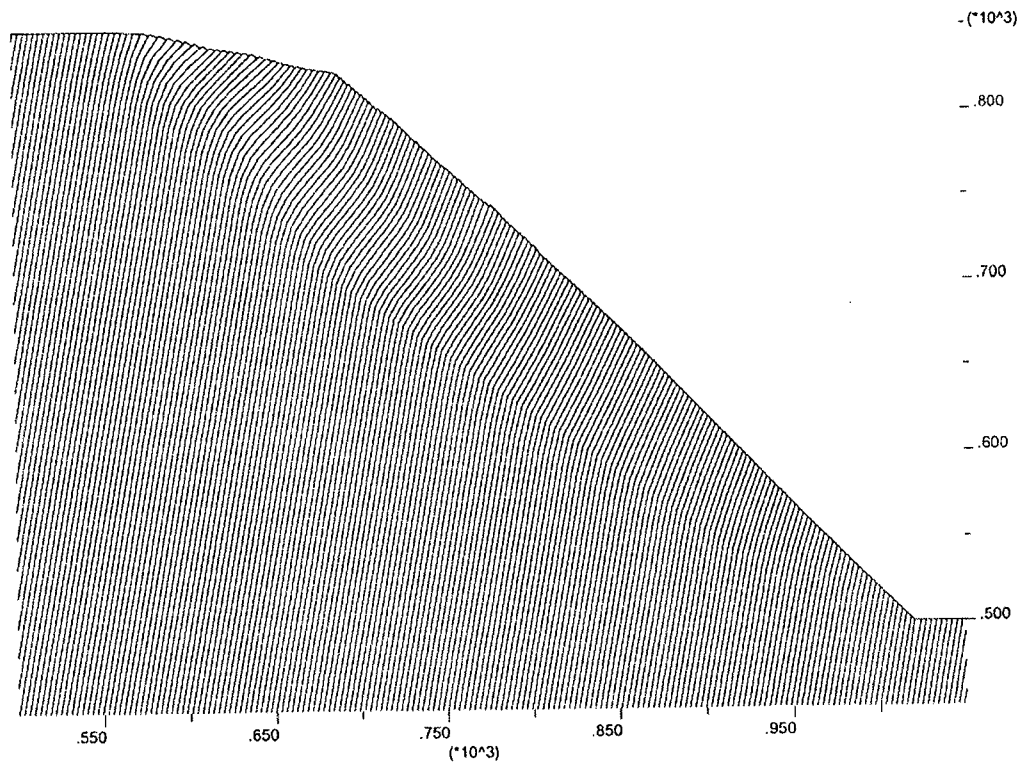
### 6.3 *Variation of Toe Conditions*

The effect of oversteepening of the toe was investigated by removing a portion of the toe immediately after the third overburden layer had been removed for fully continuous cross-joints in rock having UCS = 100 MPa (see Tables 5-2 and 5-4). When a small portion is removed, leaving a near vertical cliff at the toe, a kink band develops as it did when the entire slope was at 45° (compare Figure 6-13 with Figure 6-4(e)). Removal of a larger portion of the slope gives the same results (Figure 6-14). Movement is concentrated at the toe of the slope, and there is little movement initially along the cross-joints. The base of the kink band jumps where there is a single longer column in Figure 6-14(b). In both cases the slope fails catastrophically.

Another variation in toe condition was examined during the process of determining the lower bound for “weak” rock (Section 6.1). It was found that for rock mass quality constants of GSI = 48 and  $m_i = 2.5$ , with UCS = 10 MPa (Table 5-3), the slope failure mode was more like slumping rather than toppling (Figure 6-15). A large amount of movement occurred at the toe as opposed to at the crest of the slope, as shown in Figure 6-16. The deformability of the rock means that it essentially gets squeezed up at the toe, making room for the rest of the slope to sag. This process is similar to that occurring at the Chuquicamata mine (Chapter 4). A detailed discussion of these results is given in Chapter 9.

Figure 6-1:  
Block plots  
for  
variations of  
intact rock  
strength  
after approx.  
20 s run  
time.

(a) UCS =  
10 MPa



(b) UCS =  
20 MPa

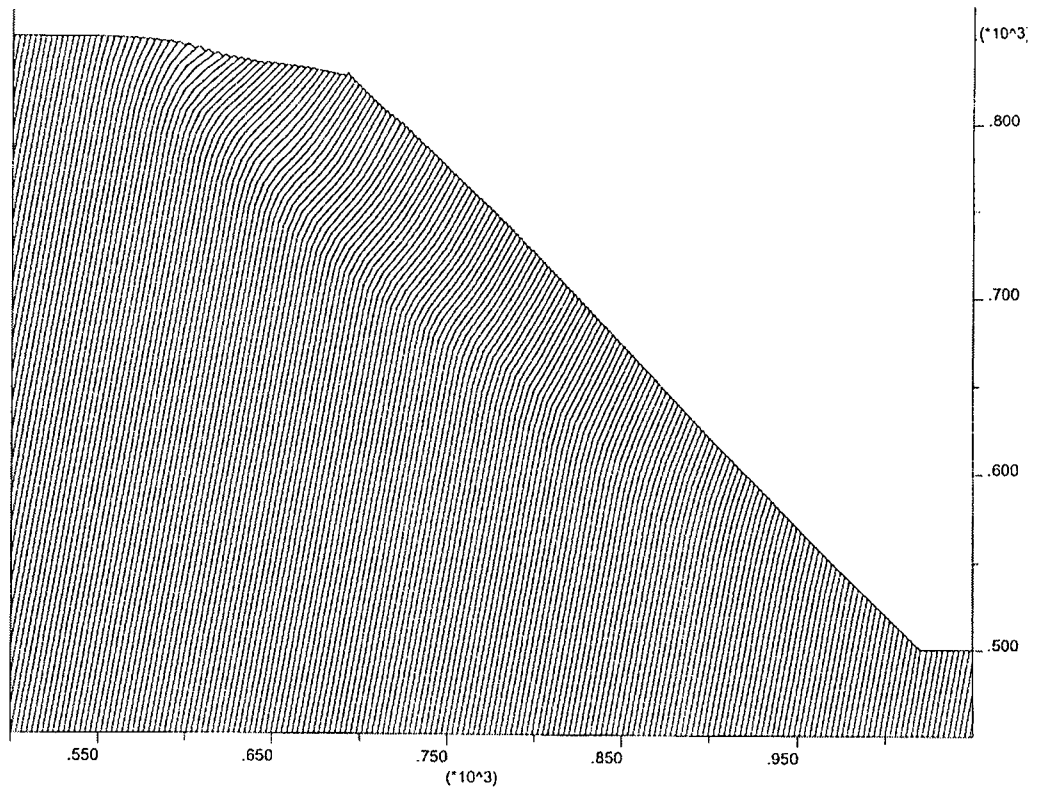
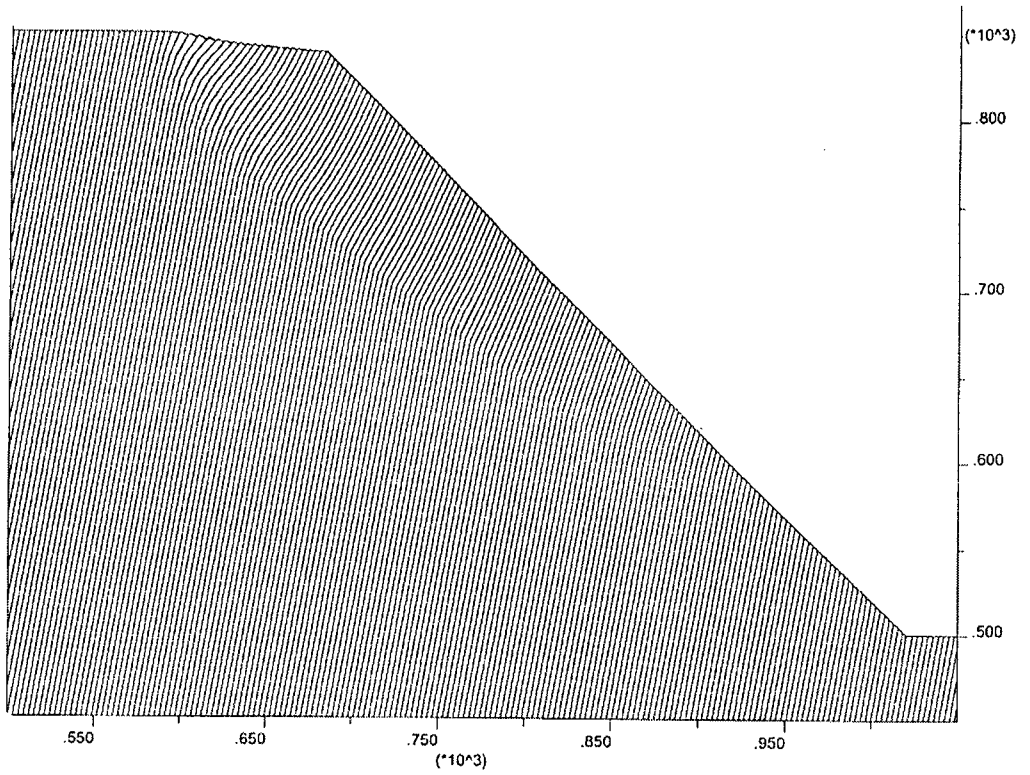


Figure 6-1  
(cont'd):  
Block plots  
for  
variations of  
intact rock  
strength  
after approx.  
20 s run  
time.

(c) UCS =  
40 MPa



(d) UCS =  
60 MPa

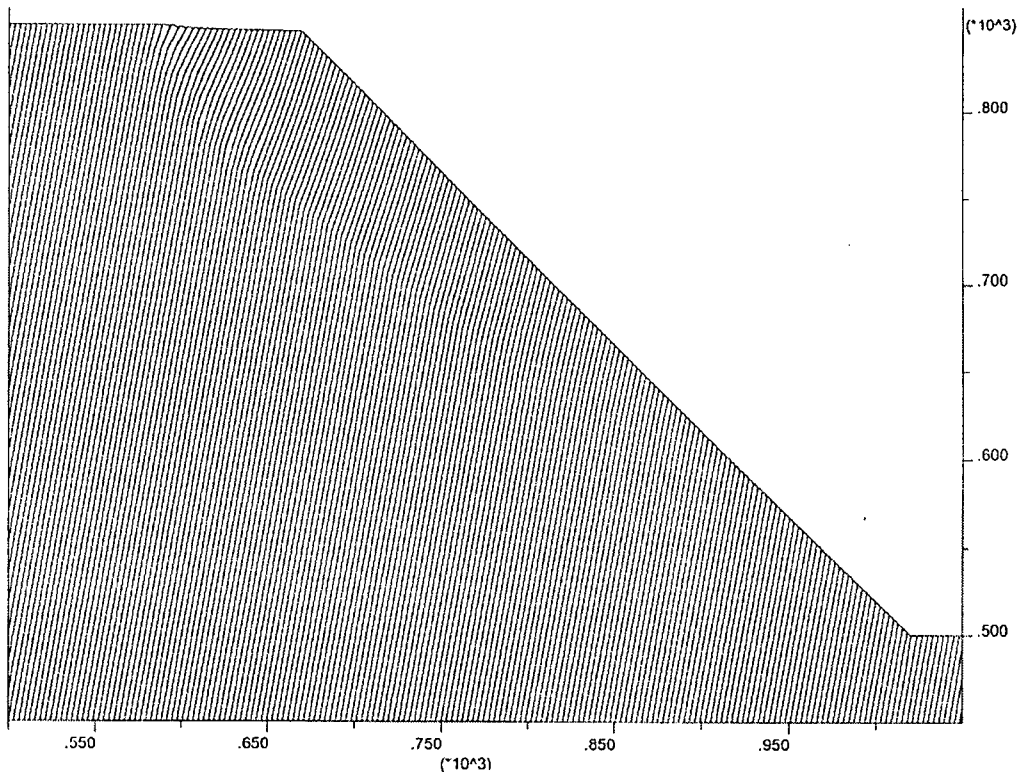
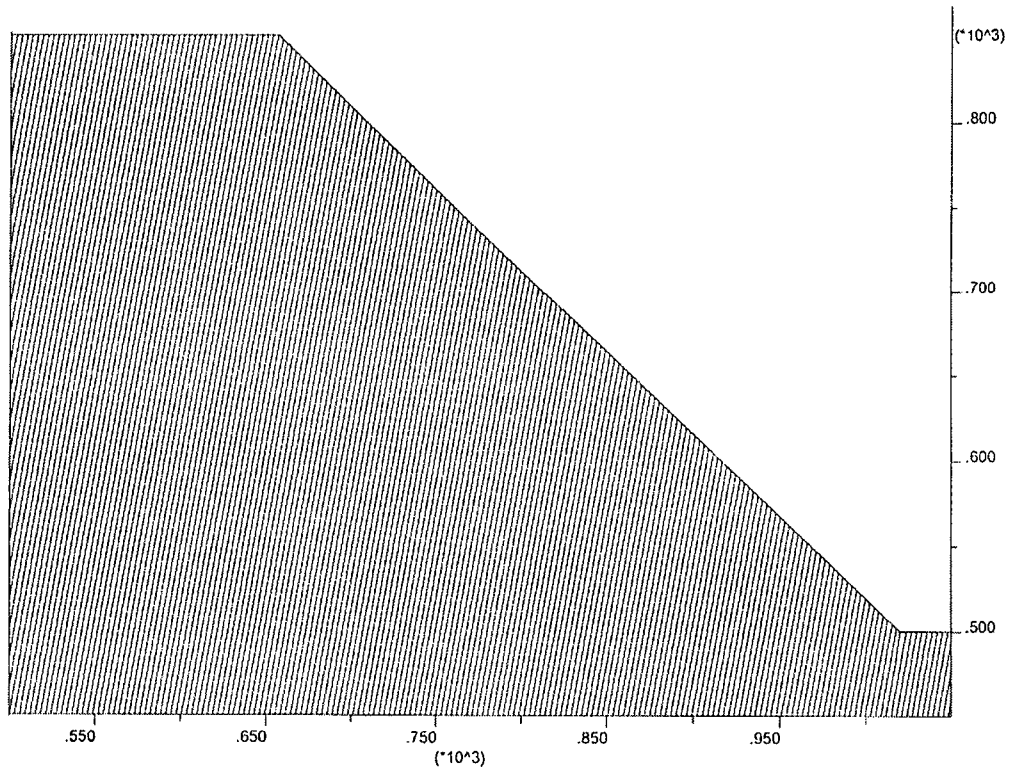


Figure 6-1  
(cont'd):  
Block plots  
for  
variations of  
intact rock  
strength  
after approx.  
20 s run  
time.

(e) UCS =  
80 MPa



(f) UCS =  
100 MPa

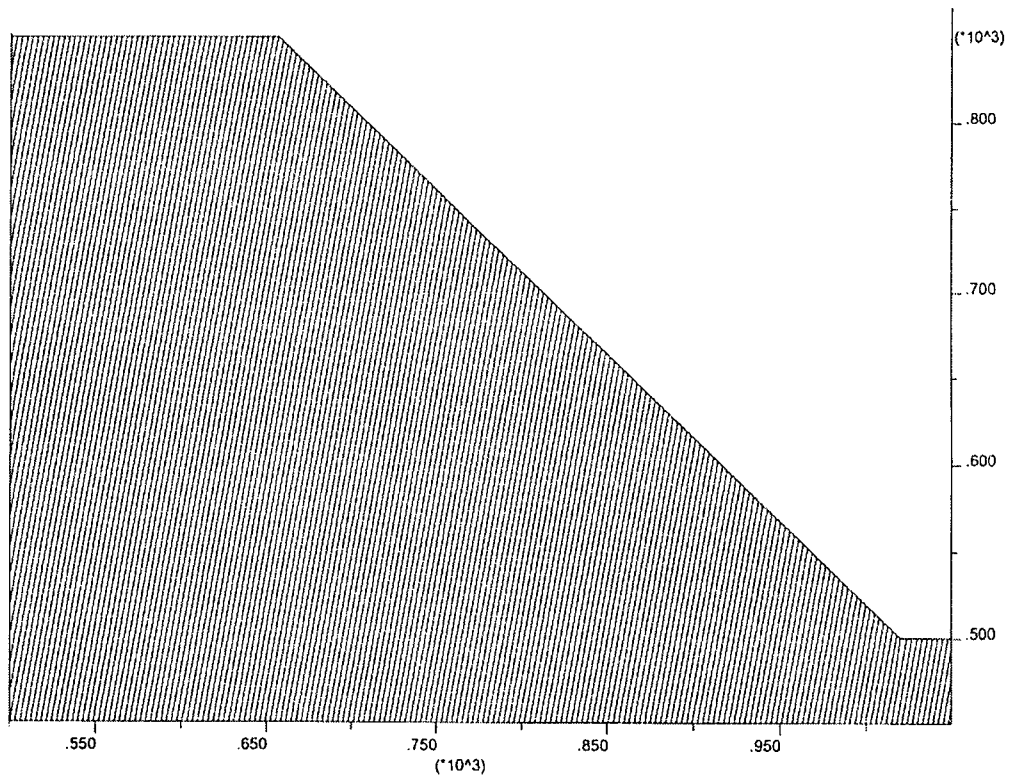
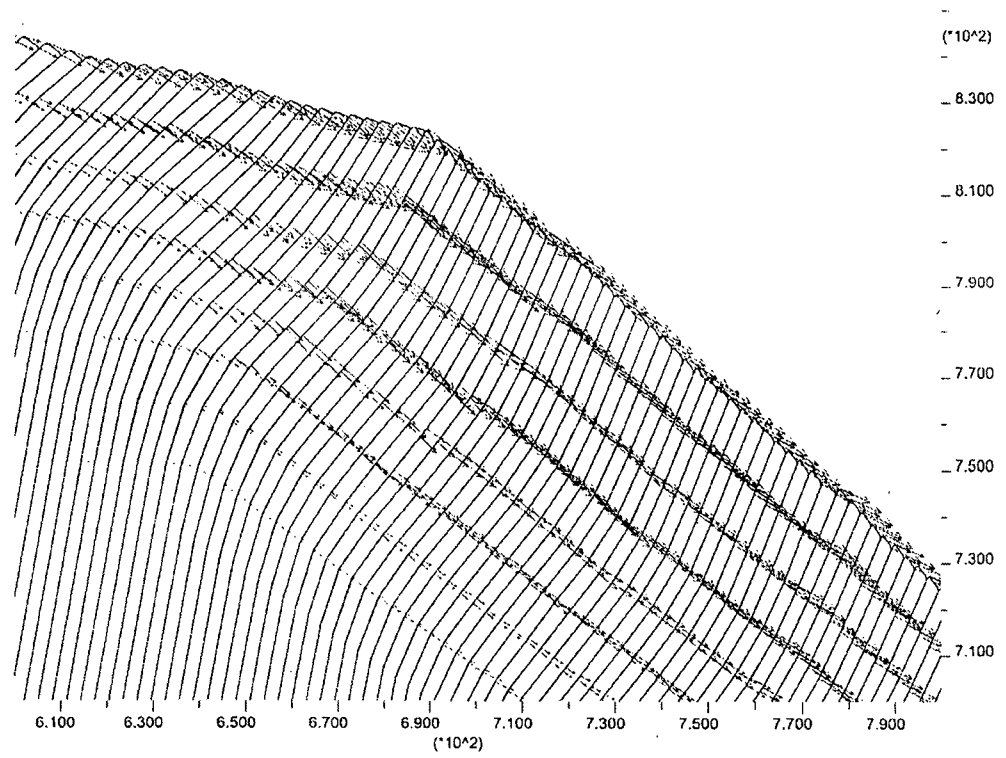


Figure 6-2:  
Detail of  
displacement  
vectors for  
variations of  
intact rock  
strength after  
approx. 20 s  
run time.

(a) UCS =  
10 MPa



(b) UCS = 80  
MPa

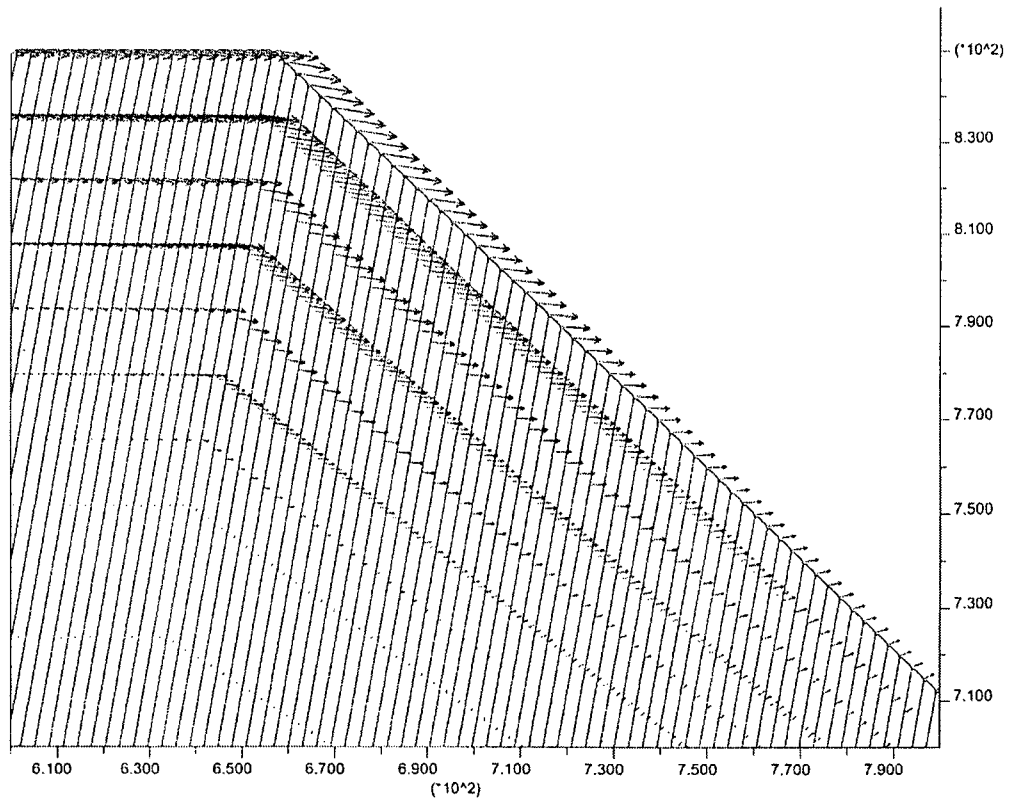
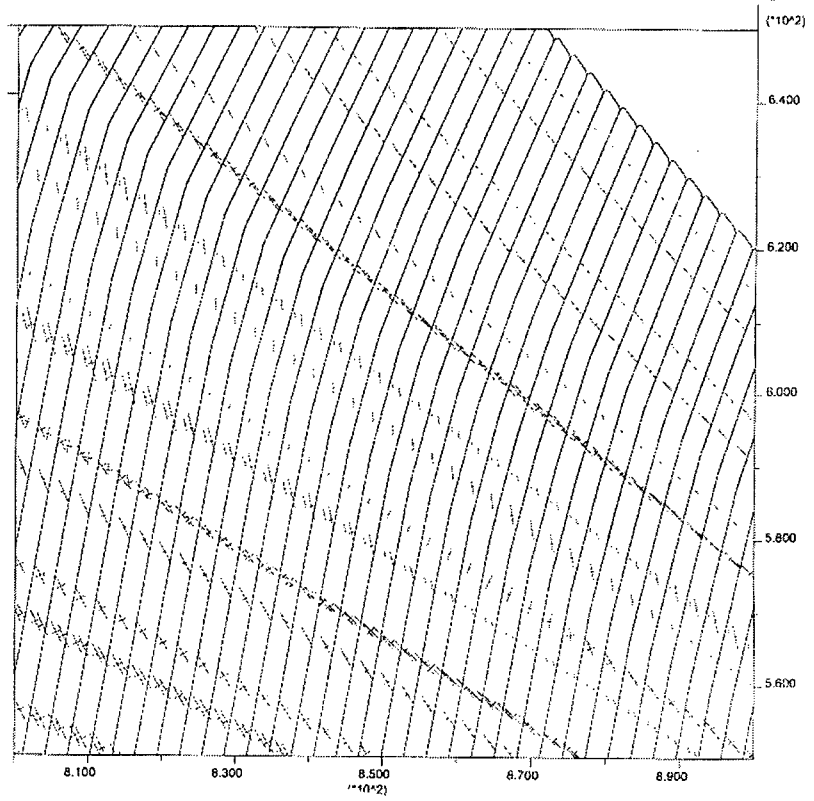


Figure 6-3:  
Detail of principal stresses for variations of intact rock strength after approx. 20 s run time.

(a) UCS = 20 MPa



(b) UCS = 80 MPa

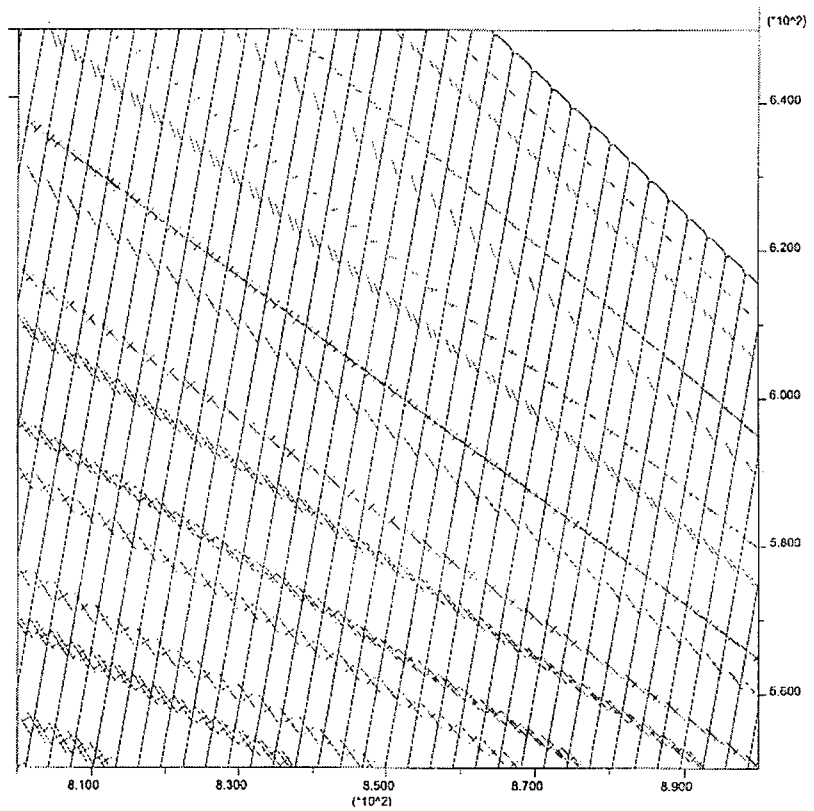
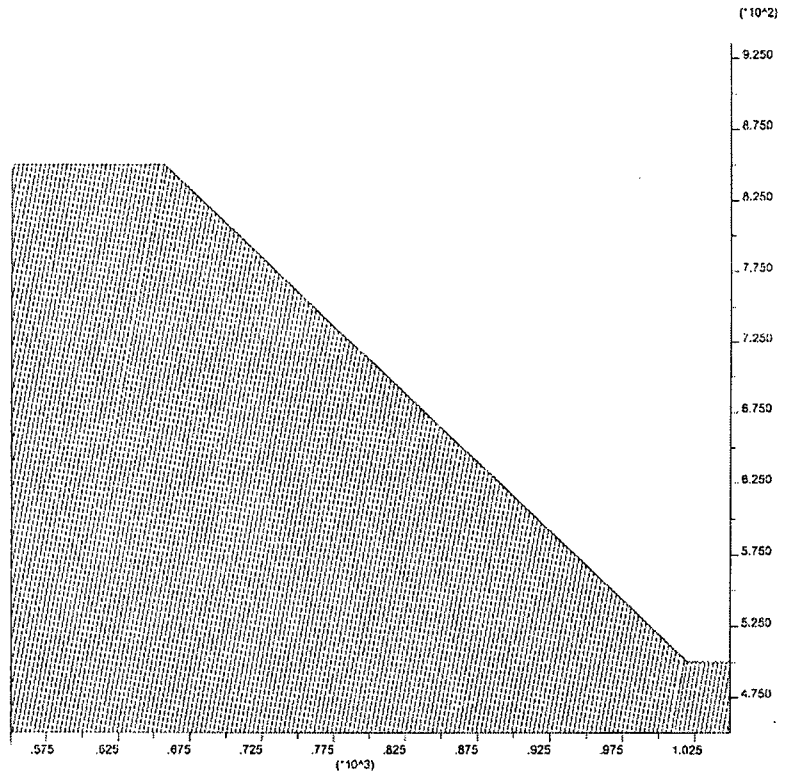


Figure 6-4:  
Block plots for variation in cross-  
joint persistence after approx. 18 s  
run time (refer to Table 5-4,  
Figure 5-3).

(a) No cross-joints



(b) Test 0

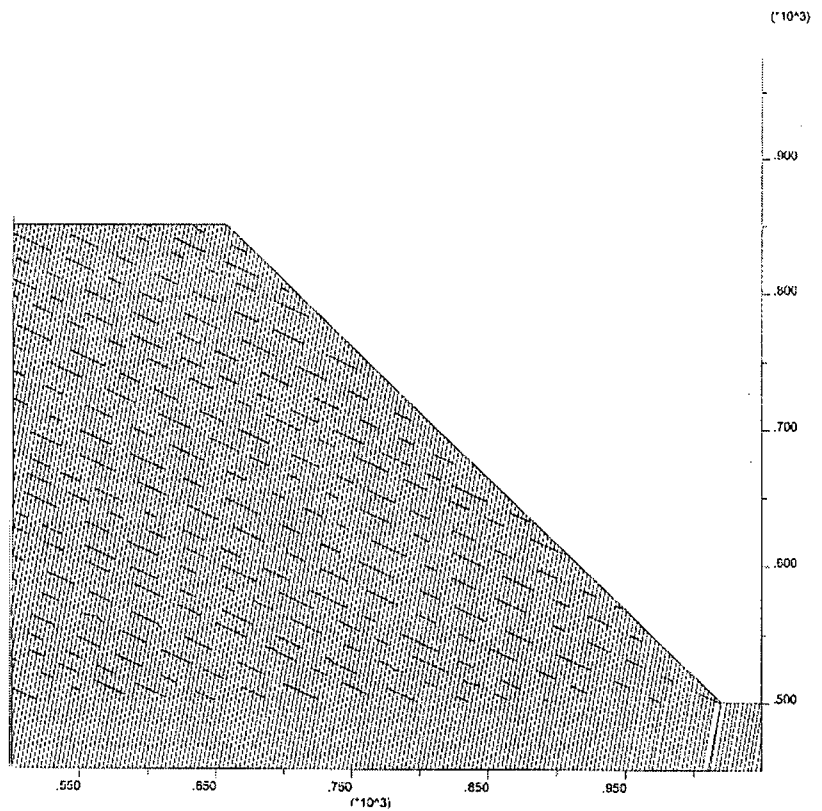
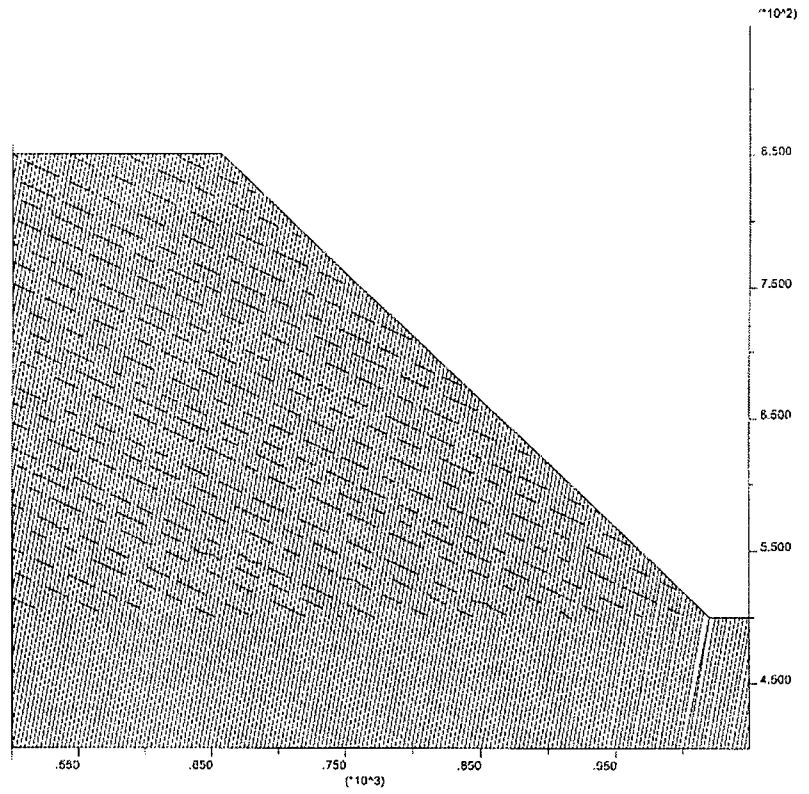


Figure 6-4 (cont'd):  
Block plots for variation in cross-  
joint persistence after approx. 18 s  
run time (refer to Table 5-4,  
Figure 5-3).

(c) Test 1



(d) Test 2

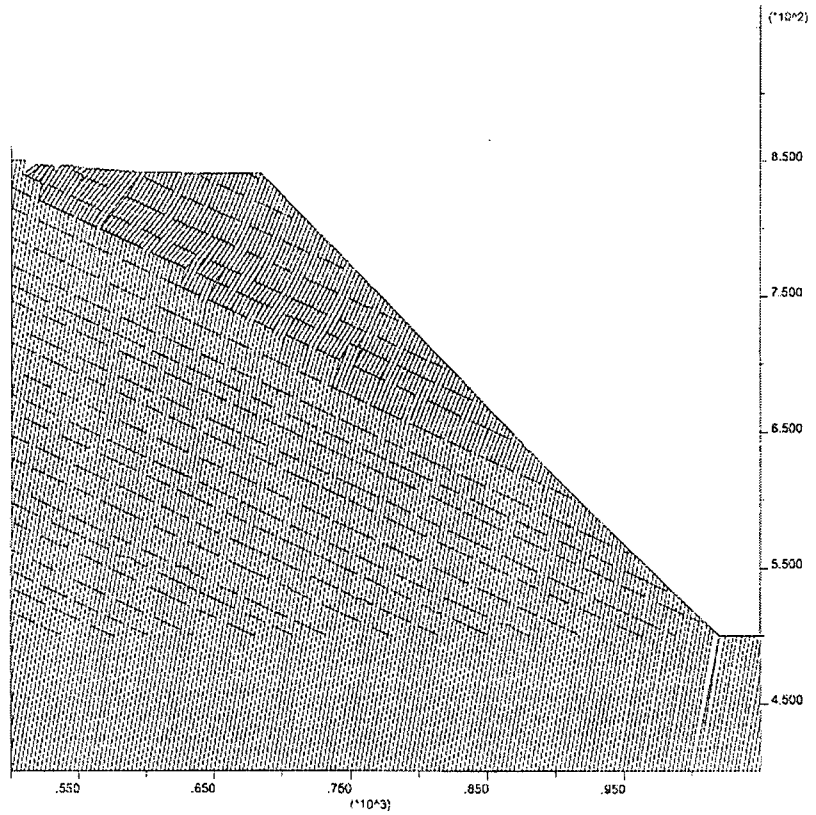
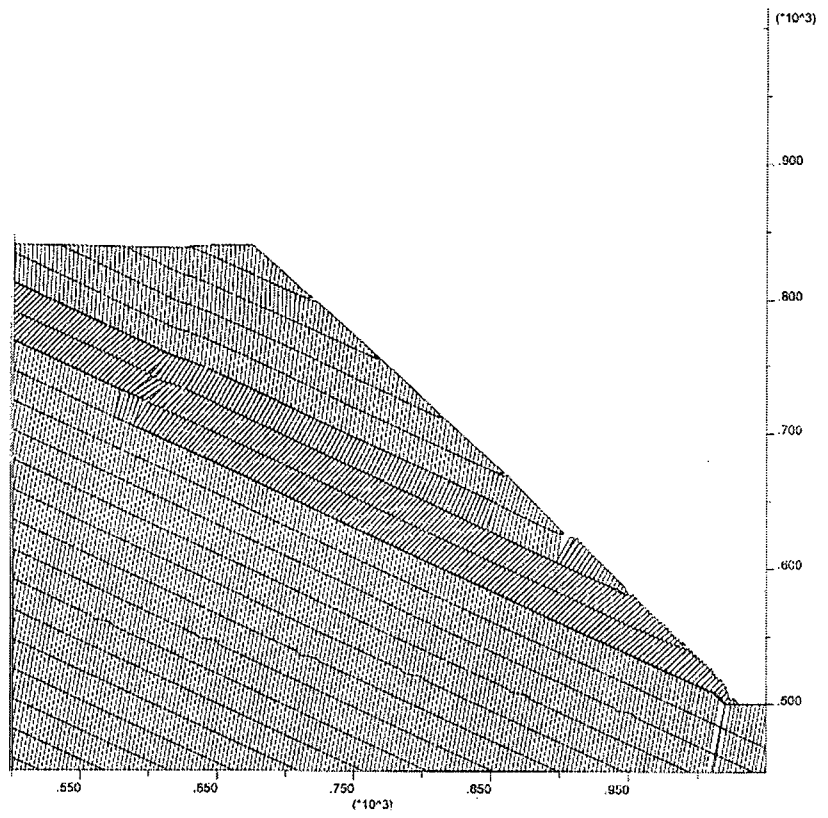


Figure 6-4 (cont'd):  
Block plots for variation in  
cross-joint persistence after  
approx. 18 s run time (refer to  
Table 5-4, Figure 5-3).

(e) idealized cross-joints



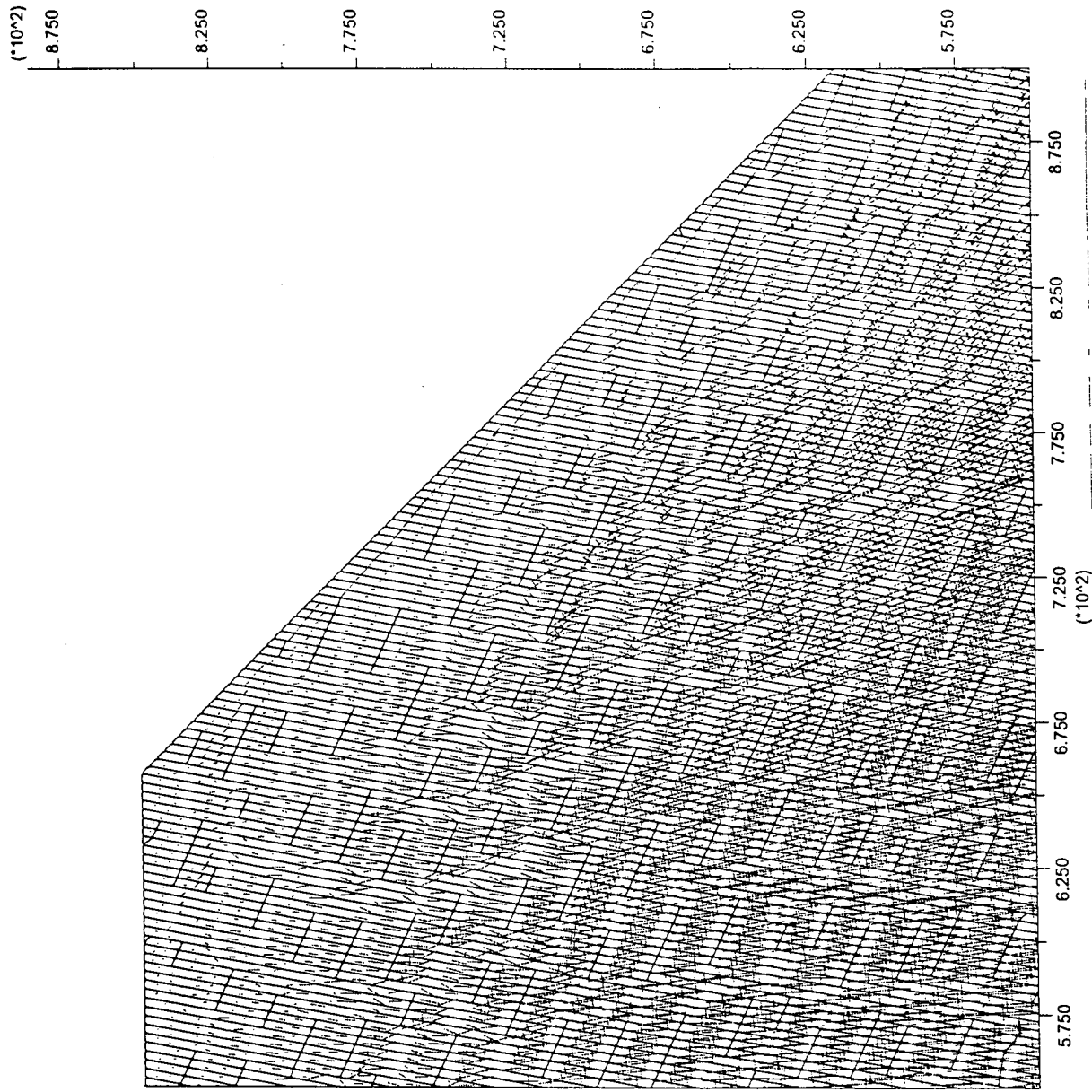


Figure 6-5:  
Stresses in the Slope for Test 0  
(refer to Table 5-4, Figure 5-3).

UDEC (Version 3.00)

LEGEND

15-Sep-99 17:04  
cycle 55003  
time 2.568E+01 sec

historyplot

- 4.16E-02 < hist30 > 1.25E+00
- 5.18E-01 < hist31 > 2.62E-01
- 2.62E-02 < hist32 > 3.27E+00
- 1.33E+00 < hist33 > 1.63E-01
- 5.62E-02 < hist34 > 4.24E+00
- 1.85E+00 < hist35 > 2.85E-02

Vs.

0.00E+00 < cycle > 5.50E+04

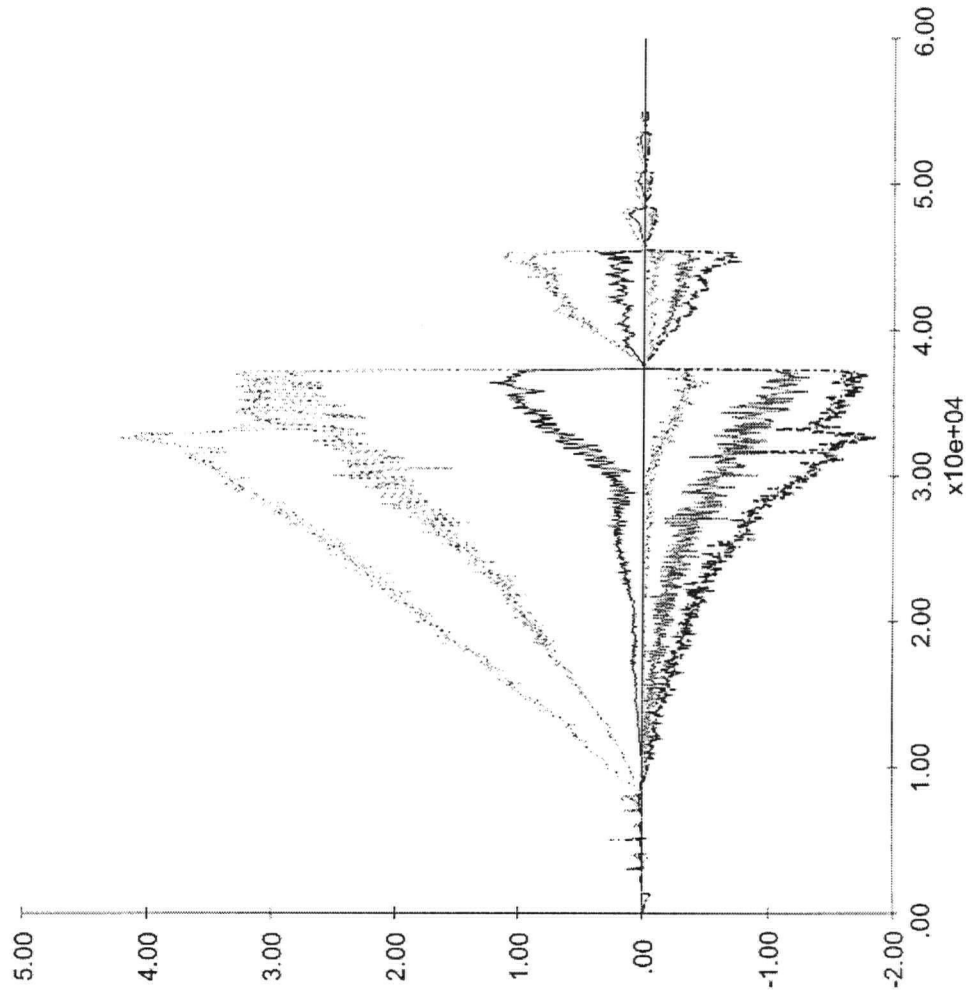
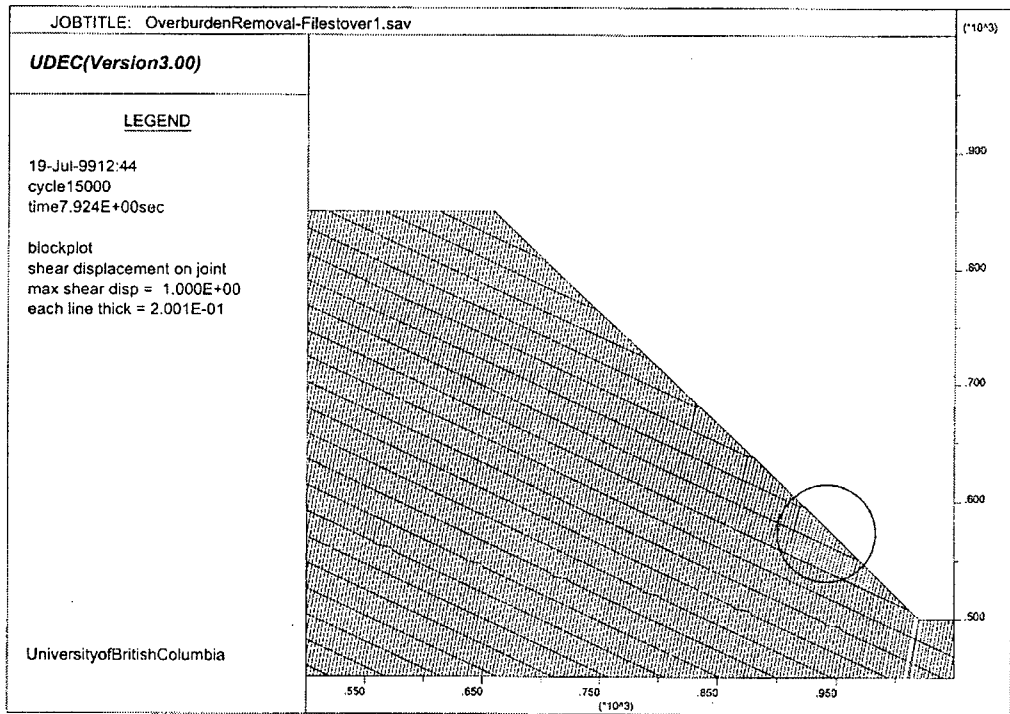


Figure 6-6: Velocity History for Test 2; see text for detailed discussion (refer to Table 5-1 for locations on the slope).

Figure 6-7:  
Shear  
Displacement  
for Idealized  
Cross-Joints.

(a) after  
15000 cycles  
(shear shown  
in circled  
area)



(b) after  
40000 cycles

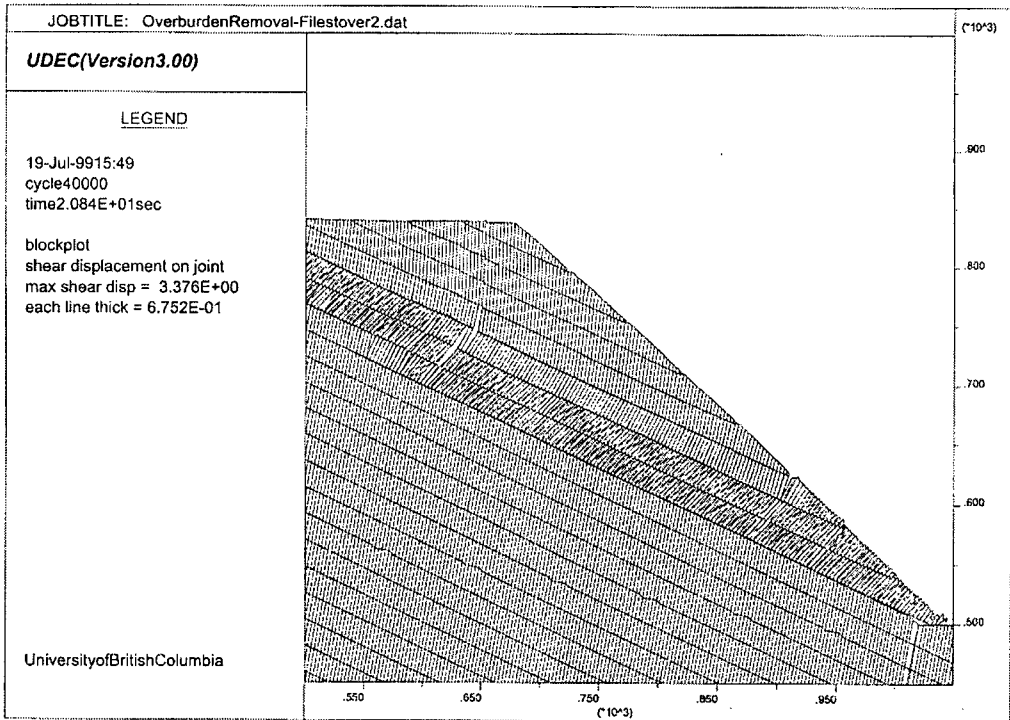
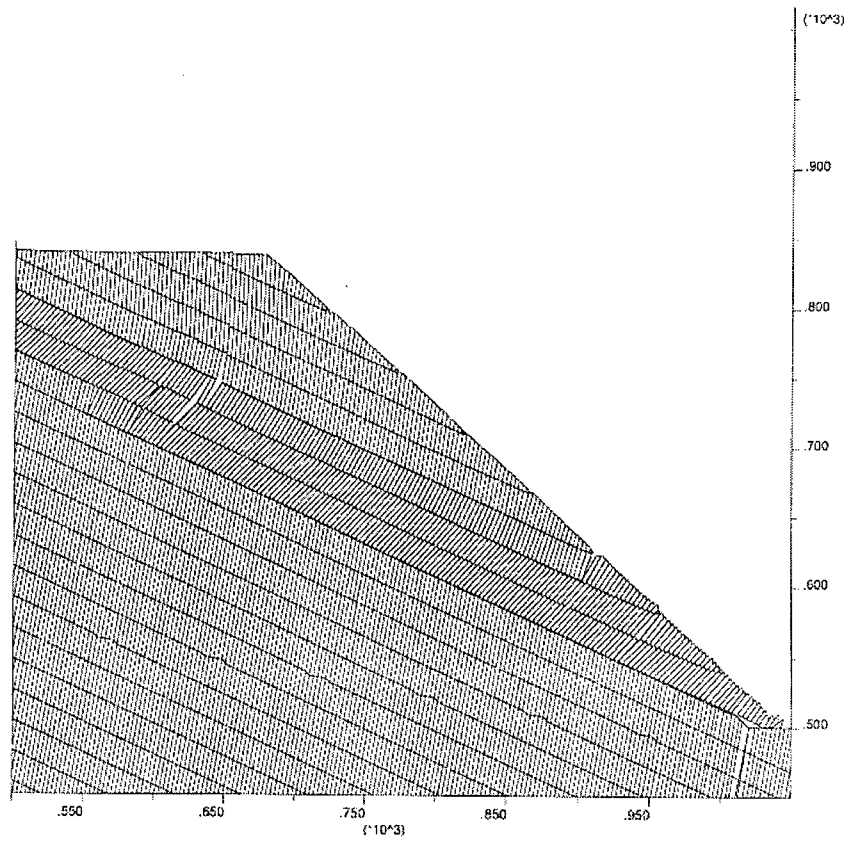


Figure 6-8:  
Block plots for variation in  
spacing normal to cross-  
joints after approx. 20  
seconds run time.

(a) spacing 20 m



(b) spacing 50 m

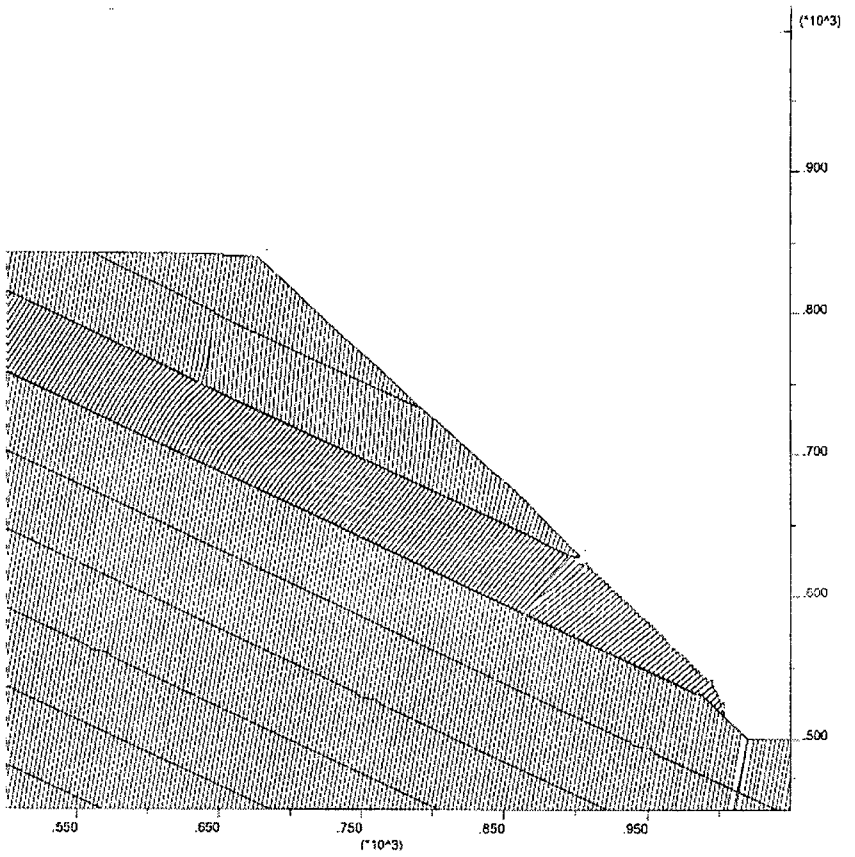
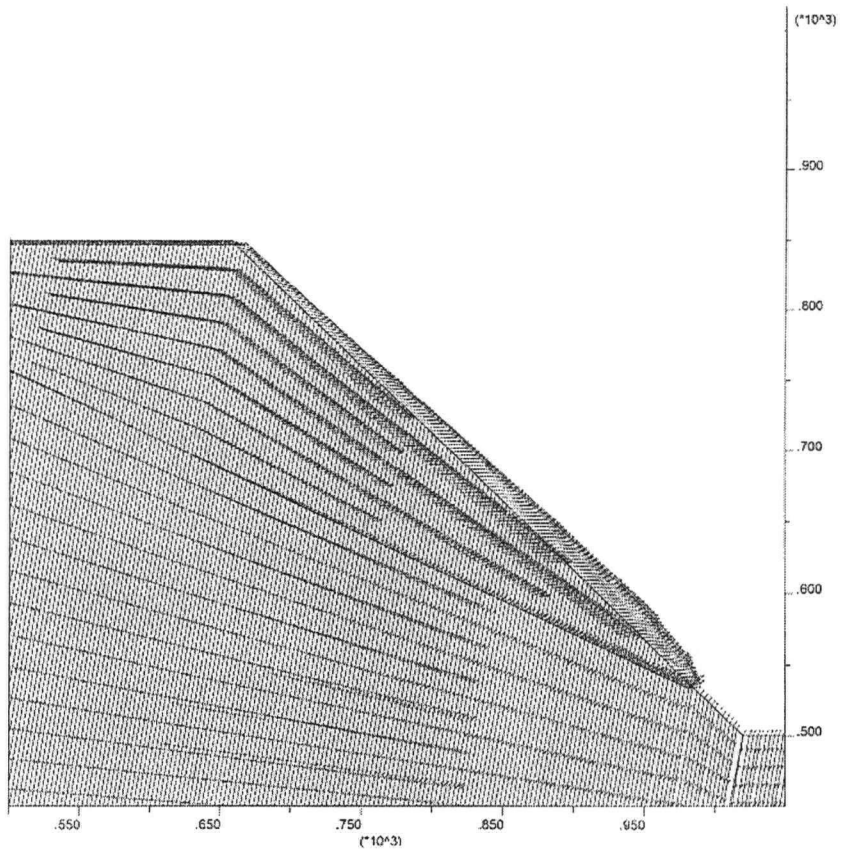


Figure 6-9:  
Displacement Vectors for a  
Single Cross-Joint.

(a) after 20000 cycles



(b) after 75000 cycles

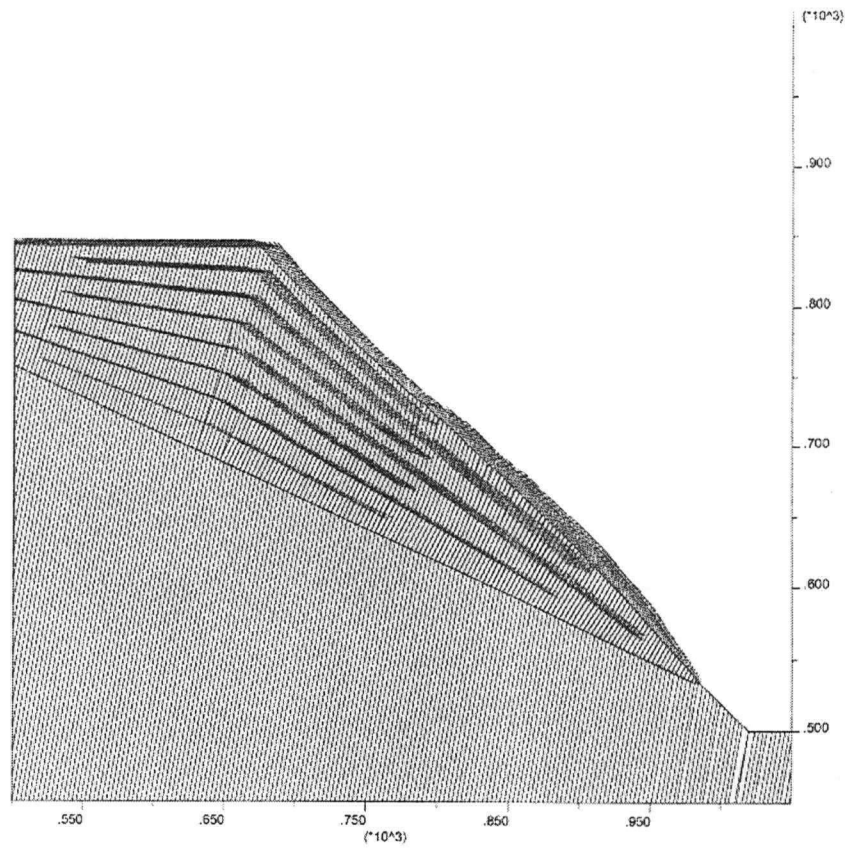
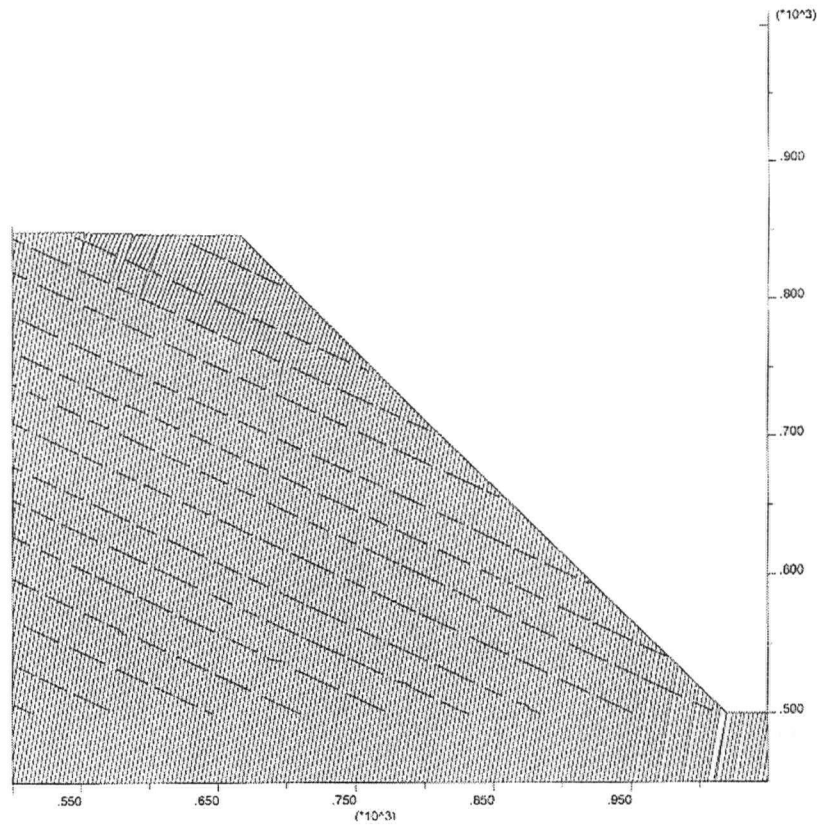


Figure 6-10:  
Test 3 after approx. 20 s  
run time.

(a) block plot



(b) shear

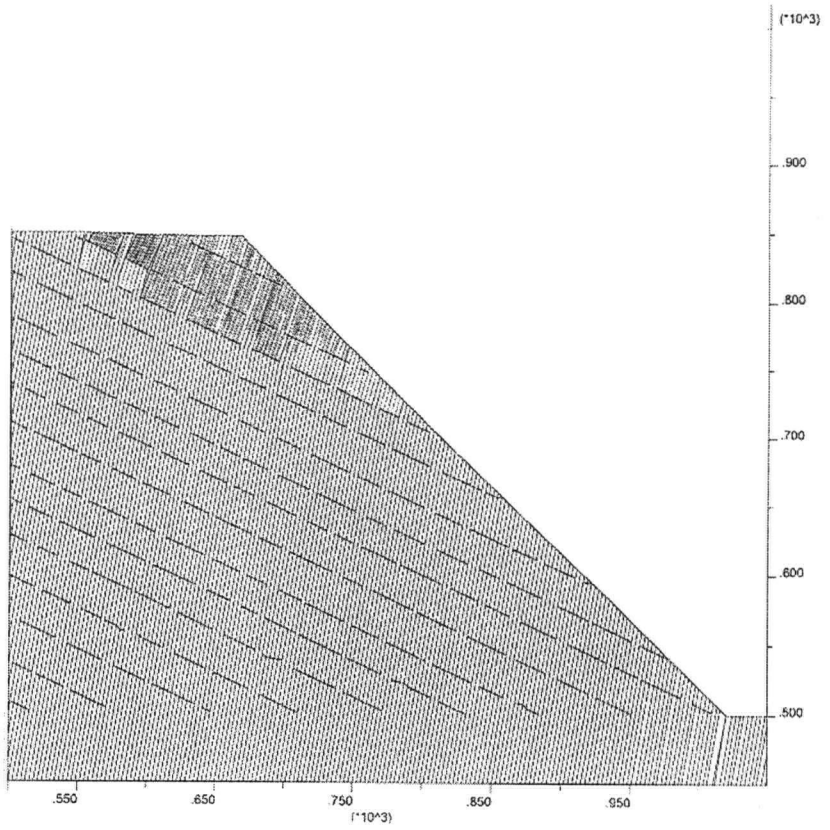
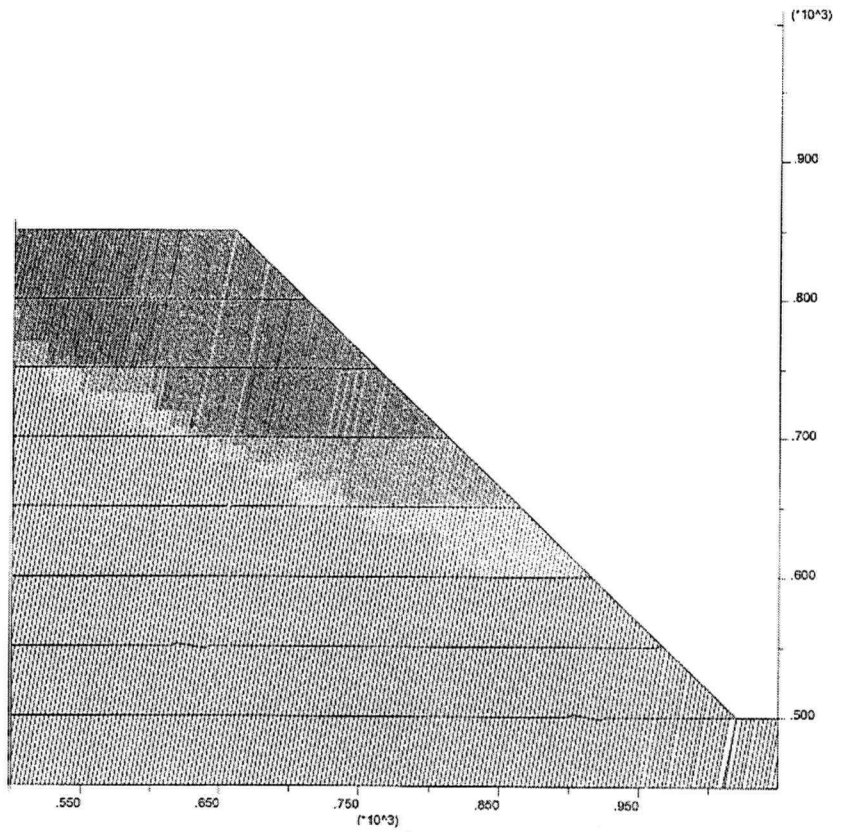


Figure 6-11:  
Shear plots for horizontal  
cross-joints (normal  
spacing 50 m).

(a) after 20000 cycles



(b) after 70000 cycles

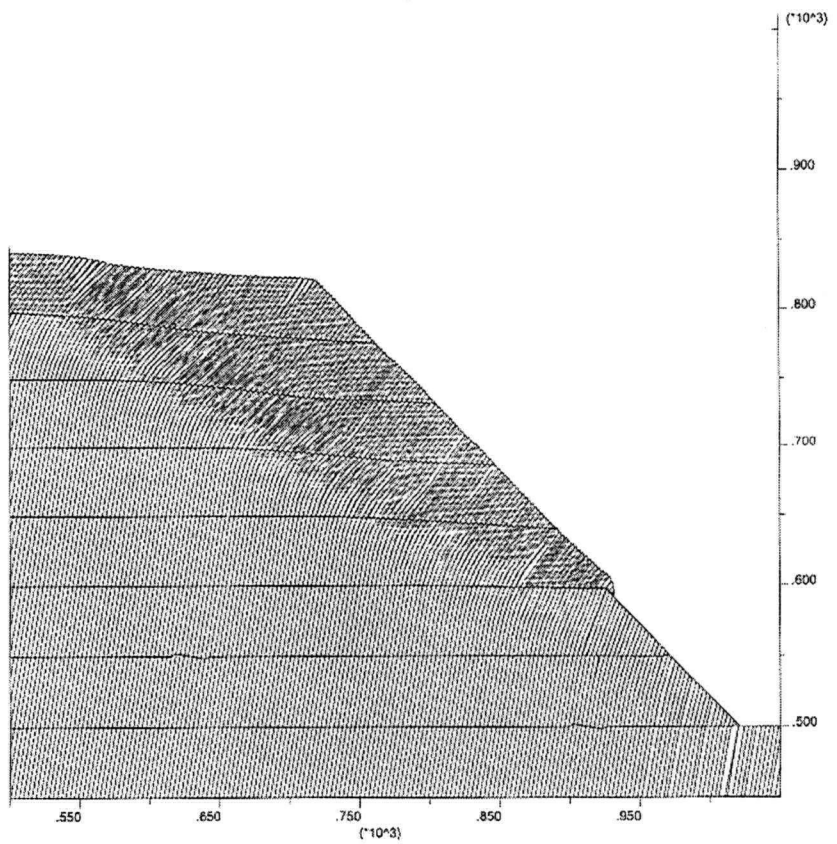


Figure 6-12:  
Detail of Horizontal  
Cross-Joints After  
70000 cycles

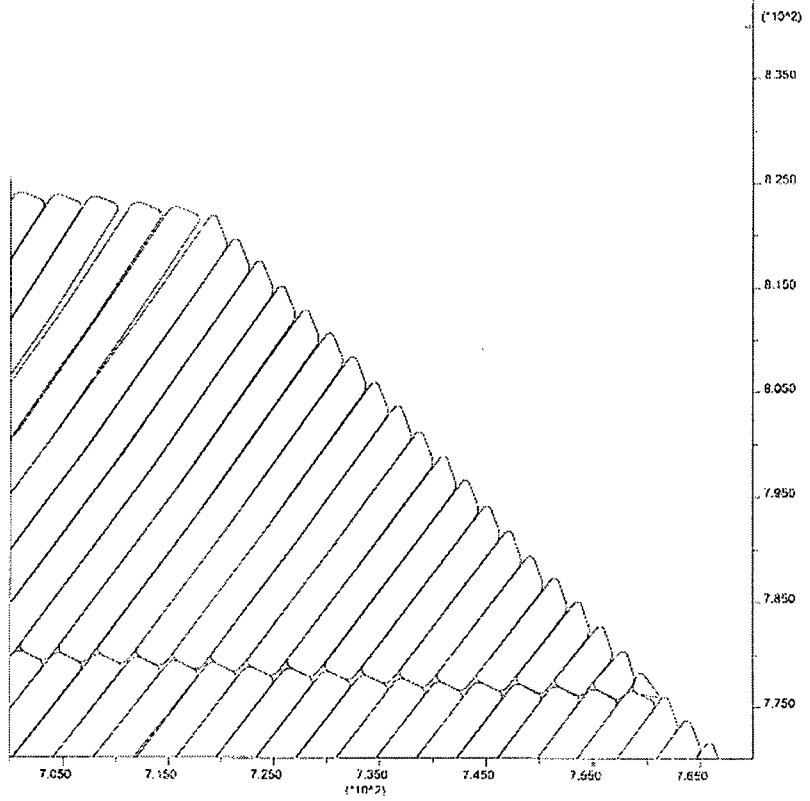


Figure 6-13:  
Block Plot of  
Oversteepened  
Slope #1 After  
40000 Cycles  
(compare with  
Figure 6-4(e)).

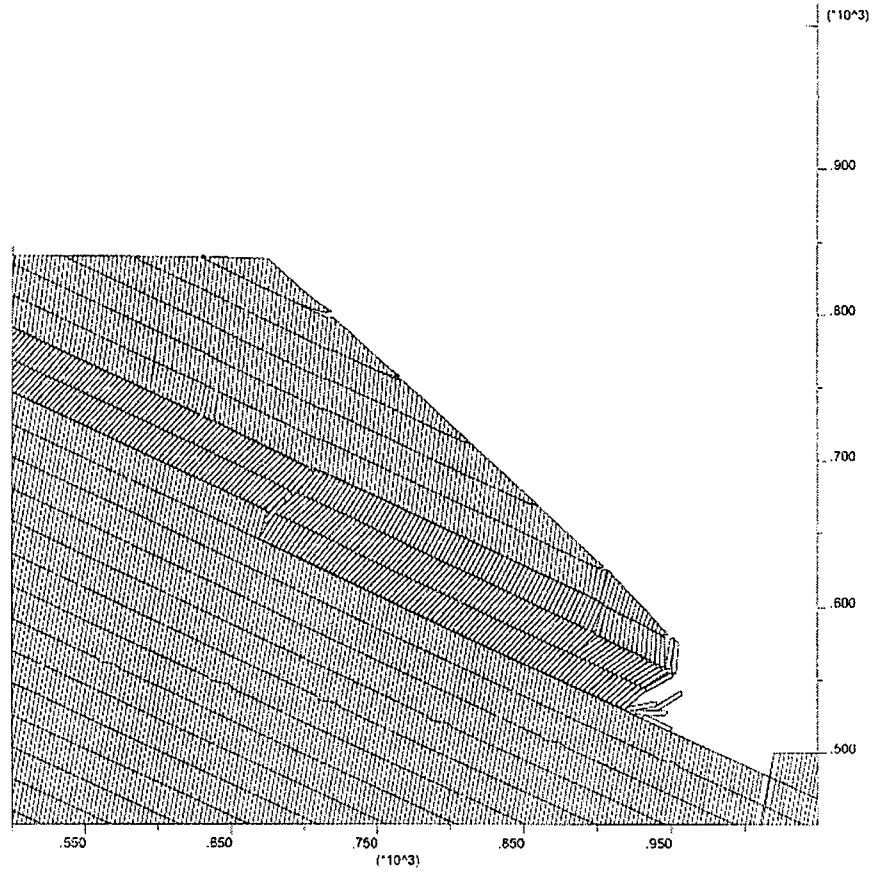
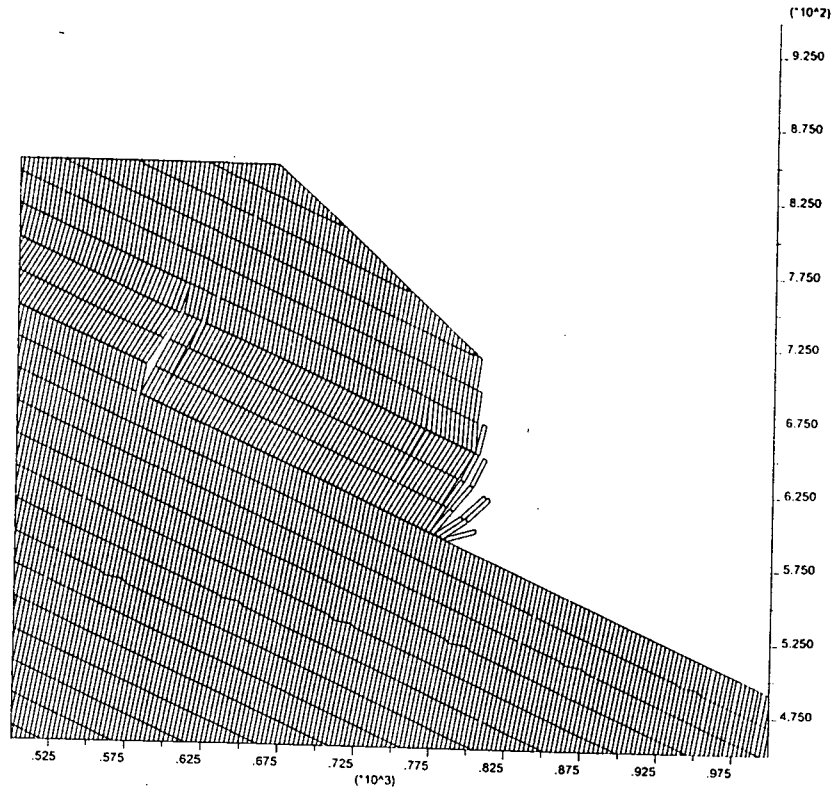
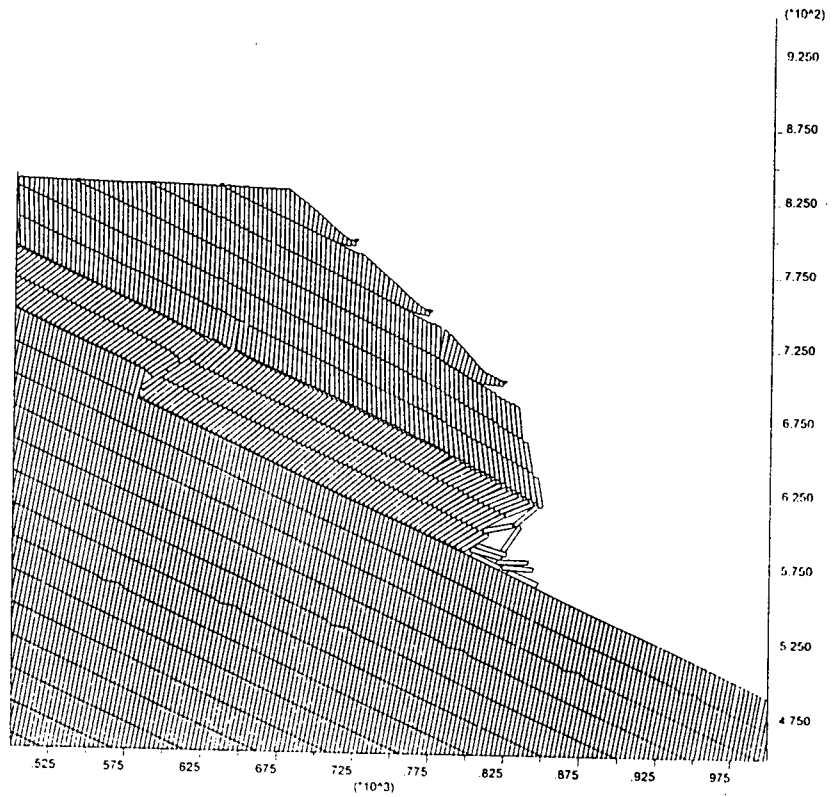


Figure 6-14:  
Block Plots for  
Oversteepened  
Slope #2.

(a) 20000 cycles



(b) 40000 cycles



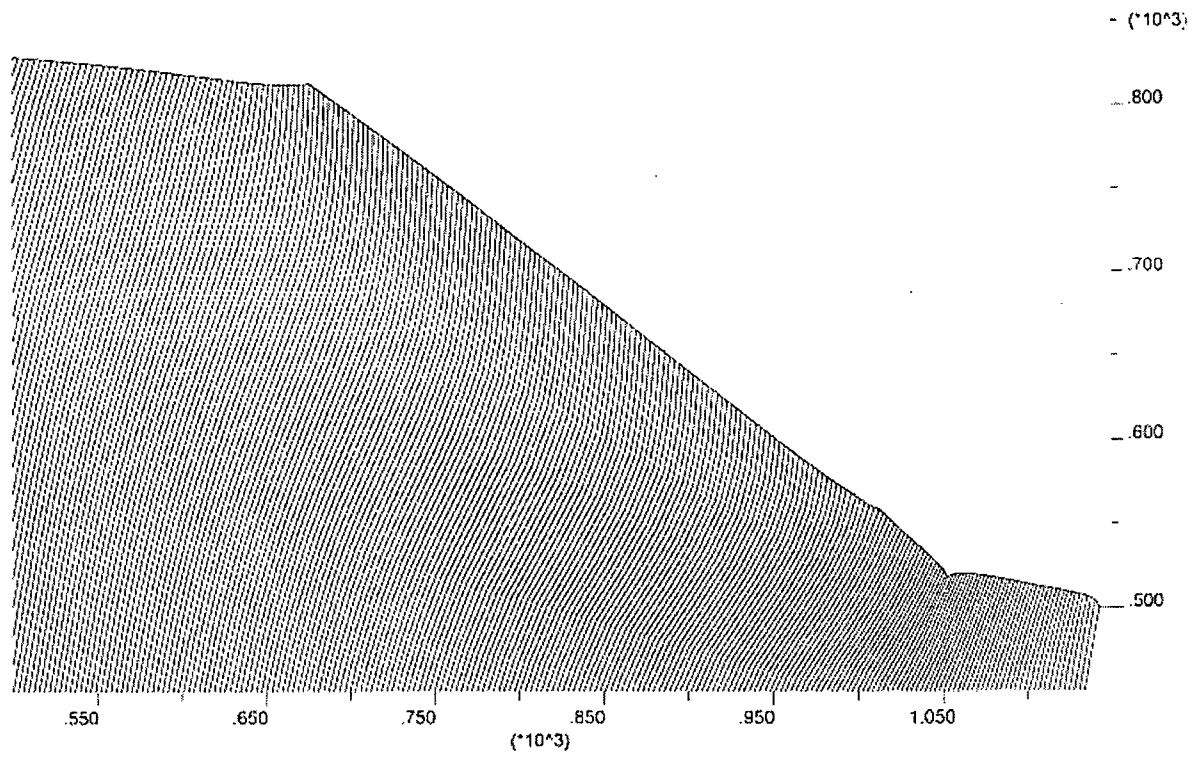
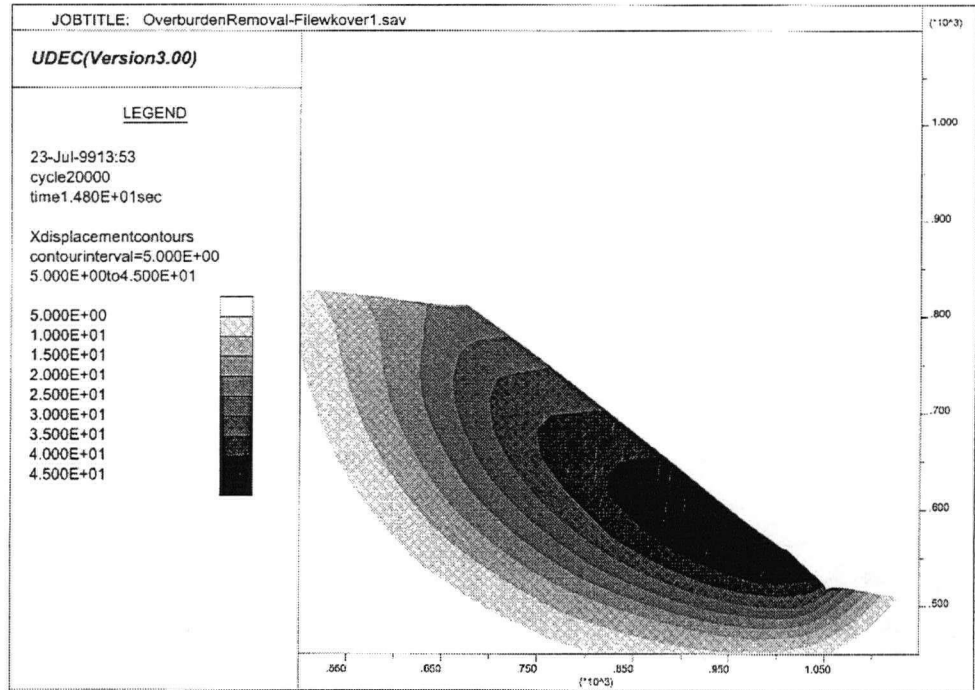


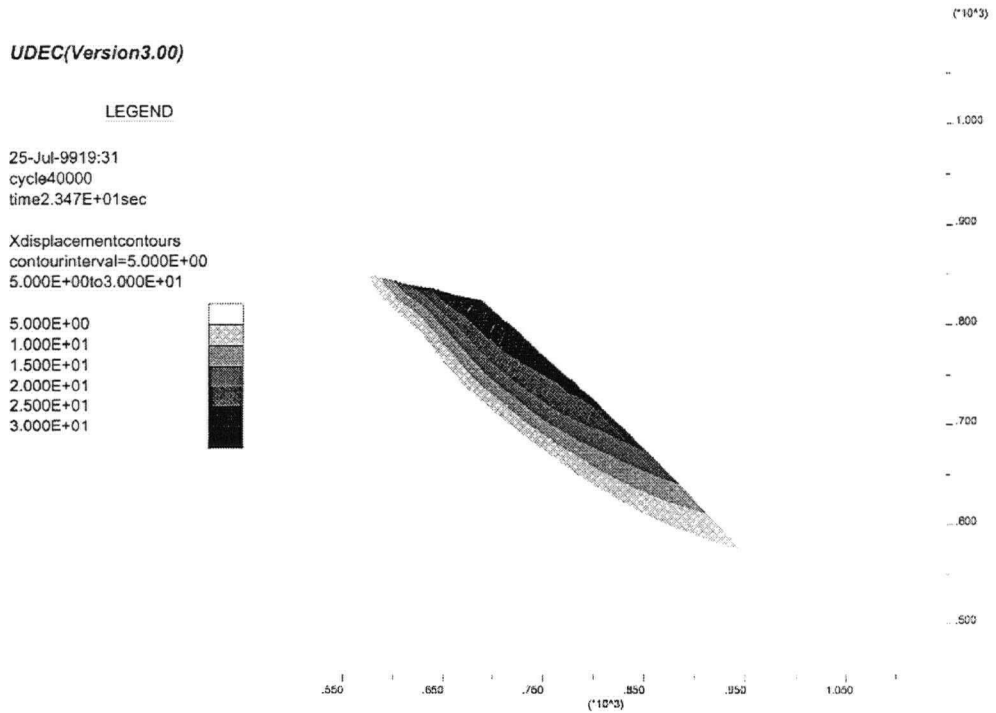
Figure 6-15: Block Plot with GSI = 48,  $m_i = 2.5$ , UCS = 10 MPa

Figure 6-16:  
X-Displacement  
Contours

(a) GSI = 48,  
mi = 2.5,  
UCS = 10 MPa



(b) GSI = 62,  
mi = 12,  
UCS = 10 MPa



## 7.0 MYSTERY CREEK CASE STUDY

### 7.1 *Background Information*

The Mystery Creek rock avalanche is a large prehistoric landslide on the east side of the Green River valley approximately 20 km north of Whistler, British Columbia (Number 19 in Figure 7-1). The landslide was first described by Eisbacher (1983), who estimated the volume of debris at  $40 \times 10^6 \text{ m}^3$ . The failure occurred in foliated hard intrusive rock of the Pemberton Dioritic Complex. After failure, the rock disintegrated and descended about 1000 m to the toe of the slope and crossed the Green River (approx. 400 m a.s.l.), with the front of the debris climbing roughly 140 m up a bedrock ridge in the centre of the valley, overtopping its crest and coming to rest at the present location of Highway 99 and a B.C. Hydro main transmission line. Blocks up to 15 m in diameter are found in a 30-m levee that formed along the southern edge as the mass climbed the ridge (Eisbacher, 1983). The debris covers an area of about  $1.2 \text{ km}^2$  in the bottom of the valley (Figures 7-2 and 7-3) (Evans and Savigny, 1994).

The landslide was estimated by Eisbacher (1983) to be at least 400 years old, based on large Douglas firs and cedars on the floodplain upstream of the avalanche debris. Later radiocarbon dating of charcoal dug out from beneath a large boulder in the debris showed an age of  $880 \pm 100 \text{ BP}$  (Evans and Savigny, 1994).

Evans (1992) describes the failure as detachment on a joint surface dipping out of the slope preceded by toppling toward the valley involving flexural slip on steep foliation surfaces dipping into the slope. Antislope scarps formed by toppling are present in the rock mass along the southern edge of the scar (Figure 7-4). Evans states that the basal surface is dipping at about  $18^\circ$ , but field evidence suggests that this angle may be somewhat steeper ( $25^\circ$  to  $30^\circ$ ), which is supported by Eisbacher (1983).

A preliminary site investigation was made in June 1998, with a detailed investigation made in July 1998. Structural data collected are summarized in Figure 7-5. Figure 7-5 also shows data collected by Evans (1987) for nearby Mount Currie (Figure 7-1). The Mystery Creek data show three sets of discontinuities: Set A, striking between 345 and 355 dipping east  $57^\circ$  to  $72^\circ$  (compare to D1 in Figure 7-5(b)); Set B, dipping  $30^\circ$  towards 288 (compare to D3); and Set C, striking about 017 and nearly vertical (compare to D2). Average spacing of Set A is about 5 m. It is interesting to note that the orientations of the Mystery Creek data are almost identical to those of Mount Currie rotated clockwise approximately  $45^\circ$ . As well, while D1 of the Mount Currie data is essentially vertical, Set A of the Mystery Creek data is at somewhat shallower dips. This is explained by the fact that the Mystery Creek data were collected in an area that had already experienced some toppling deformation in a westward direction. It is believed that the Mystery Creek discontinuities were originally near vertical as well, and while this was not confirmed in the field, it has been evidenced in unpublished data collected by S.G. Evans.

Eisbacher (1983) noted that the crown fracture of the Mystery Creek avalanche is on trend with a fault scarp running along the northeastern summit ridge of Mount Currie. As a result, Eisbacher tentatively suggested that the landslide was triggered by the earthquake that also created the Mount Currie fault scarp. The predominant near-vertical cliff has a similar trend to the crown fracture.

## 7.2 *UDEC Modelling*

All analyses were carried out using the input parameters shown in Table 7-1, which are derived from estimated rock mass properties of  $GSI = 62$ ,  $m_i = 12.5$ , and  $UCS = 150$  MPa (Table 5-3). The simplified input geometry, based on a profile of the existing slope through the failure with an estimated overall slope angle of  $30^\circ$ , is shown in Figure 7-6. The model was initially run without cross-joints to see how much movement would take place. Cross-joints were then added, with continuity gradually increased to 100% (i.e., fully continuous). This study of Mystery Creek is somewhat simplistic (e.g., groundwater was not included), mainly due to the lack of detailed information about subsurface conditions which results in a large number of possible models and parameters.

Block displacement without cross-joints is illustrated in Figure 7-7 (shear is shown also). The joints dip  $85^\circ$  into the slope and are spaced at 15 m; maximum displacement is in the order of 80 m. The stresses in the slope near the surface are roughly parallel to the ground surface. Shear is concentrated in the upper portion of the slope and does not form a distinct hinge region. It should be noted that the majority of this displacement occurs above the actual

failed region of the slope, which is roughly between El. 1200 and El. 1600. Antislope scarps develop, though not quite to the same extent as observed in the field.

The next stage involved adding cross-joints. The cross-joints were given the same properties as the sub-vertical joints (Table 7-1) and dipped out of the slope at 25°. The continuity of the cross-joints was varied, while the spacing perpendicular to the cross-joints was held constant at 40 m (with standard deviation of 5 m). ["Constant" may not be entirely accurate, as UDEC generates a slightly different geometry each time for spacing equal to 40 m and standard deviation equal to 5 m.]

The model with fully continuous cross-joints gives the most interesting results. Flexural toppling of the columns occurs, with antislope scarps forming. The cross-joints initially rotate with the columns (i.e., there is no sliding on the cross-joints), because the angle of friction is set at 30°. In the upper portion of the slope, the columns rotate enough that the cross-joints no longer form continuous planes (Figure 7-8). Though they are now dipping more steeply than the angle of friction, they are not free to slide. In the lower part of the slope, the columns have not rotated to the same extent. The cross-joints remain essentially as continuous planes, and the overturning of the columns up slope results in sliding along the cross-joints.

These models, while interesting, did not adequately reproduce the existing observed conditions on the slope, i.e., a distinct failure surface in the vicinity of the existing scar did not develop. A second input geometry having a cliff similar to the one existing to the south of

the landslide scar, pictured in Figure 7-4, was then tested (Figure 7-9). The input geometry of the slope was generated by projecting the existing cliff upslope. The parameters used are identical to those used in the previous Mystery Creek models (Table 7-1). Cross-joints were generated using a mean spacing of 40 m and standard deviation of 5 m, but were not generated throughout the entire slope. Groundwater was not considered in the model.

Maximum displacement at the run time shown in Figure 7-9 is on the order of 60 m, with most of the movement taking place in the upper portion of the slope. The columns undergo flexural toppling, much more so upslope from the cliff than downslope of it. Anti-slope scarps develop and gaps open between the columns, in particular at  $\sim 1150, 1700$  (x,y). The gap here may be influenced by a discontinuity in the cross-joint sets in this region, inadvertently created when inputting the joint generation geometry. As in the Mystery Creek model with continuous cross-joints (Figure 7-8), the columns rotate so that the cross-joints no longer form continuous planes in the upper portion of the slope and are not free to slide. In the lower part of the slope, the columns have not rotated to the same extent. This is perhaps significant at the toe of the cliff, where one of the cross-joints daylights.

Allowing the model to run, further flexure of the columns occurs, with block toppling of blocks at the cliff (Figure 7-10). X- and y-displacement plots show that the deformation of the slope is controlled by the cross-joints, and that there is a significant amount of movement between El. 1200 and El. 1800, the location of the actual failure surface. Velocities indicate catastrophic failure.

While the actual failure surface was not recreated, these results are encouraging. It was beyond the scope of the current project to model the Mystery Creek landslide in greater detail; a more in-depth study involving research into subsurface conditions, joint and rock mass parameters and extensive modelling of the slope, particularly with respect to groundwater, would provide valuable information on the failure mechanism.

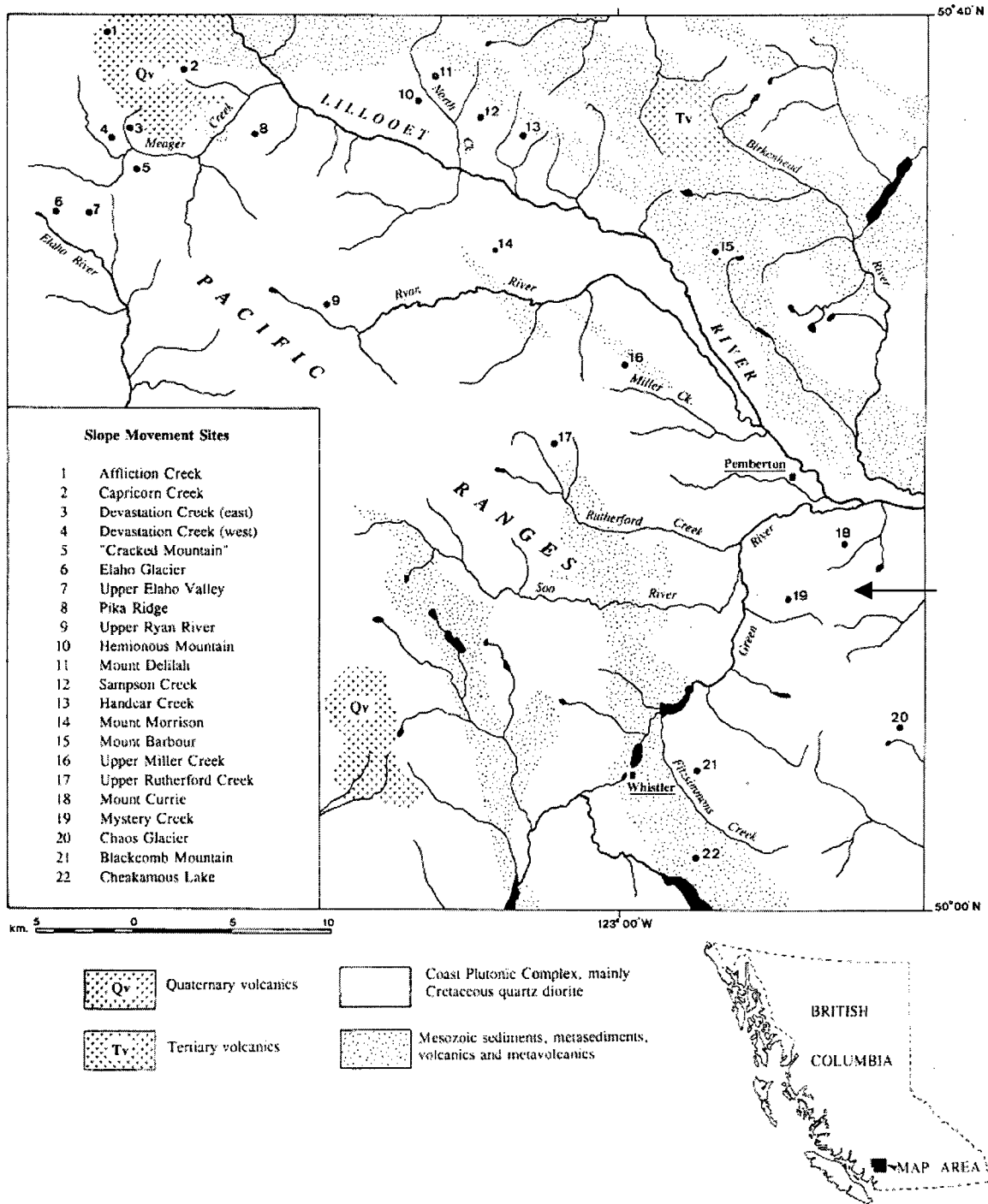


Figure 7-1: Location of the Mystery Creek rock avalanche – see arrow (Bovis and Evans, 1996, Fig. 1).

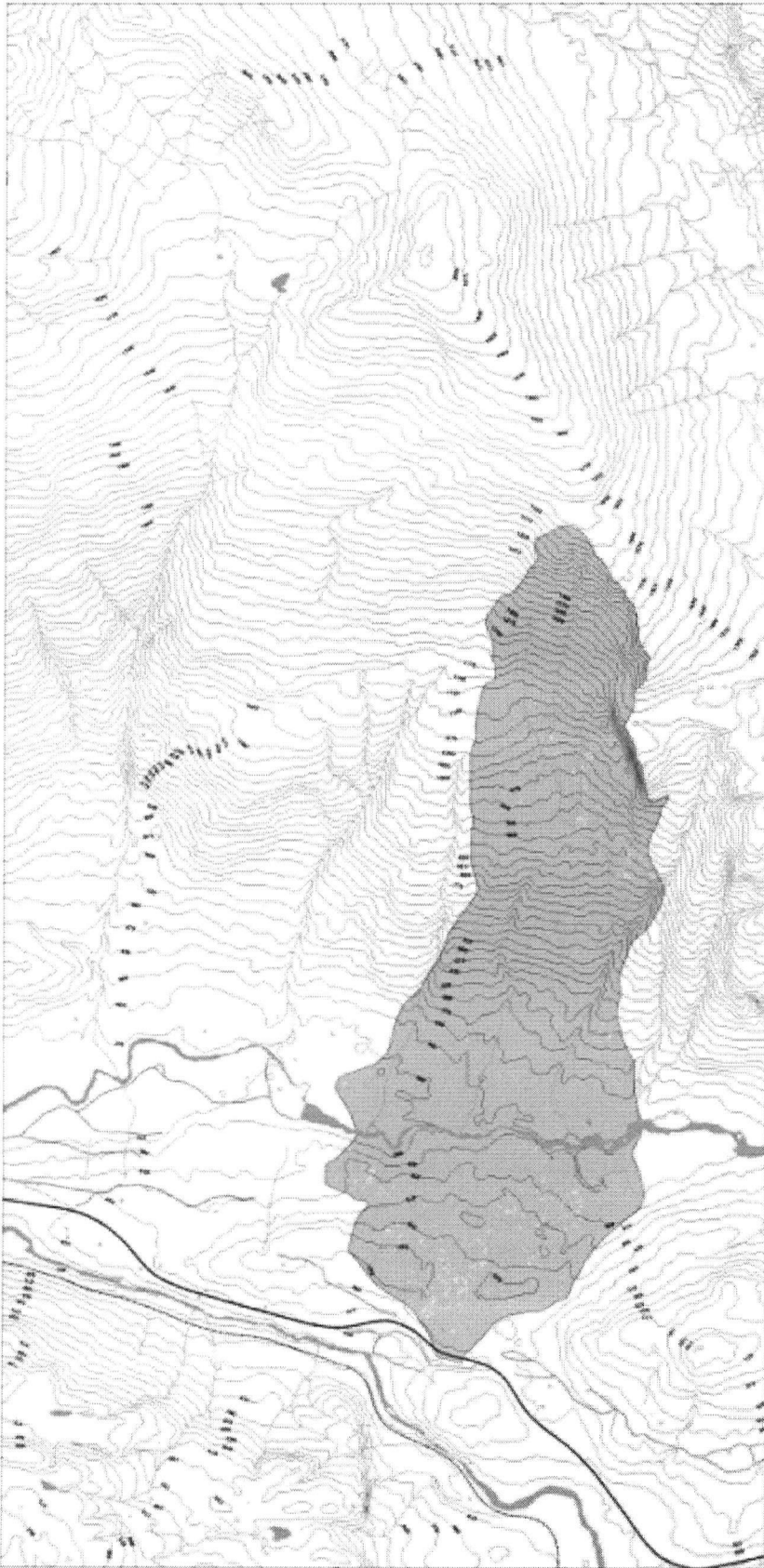


Figure 7-2:  
Overview of the  
Mystery Creek  
rock avalanche;  
north is to the left;  
contour interval 25 m;  
top of slide area is at  
El. 1650 m; scale is  
approx. 1:40,000  
(GSC data, processed by  
GeoSolutions Consulting,  
Nepean, Ontario).

Figure 7-3:  
Photo of the Mystery Creek  
rock avalanche  
(photo by Dr. S.G. Evans,  
Geologic Survey of Canada).



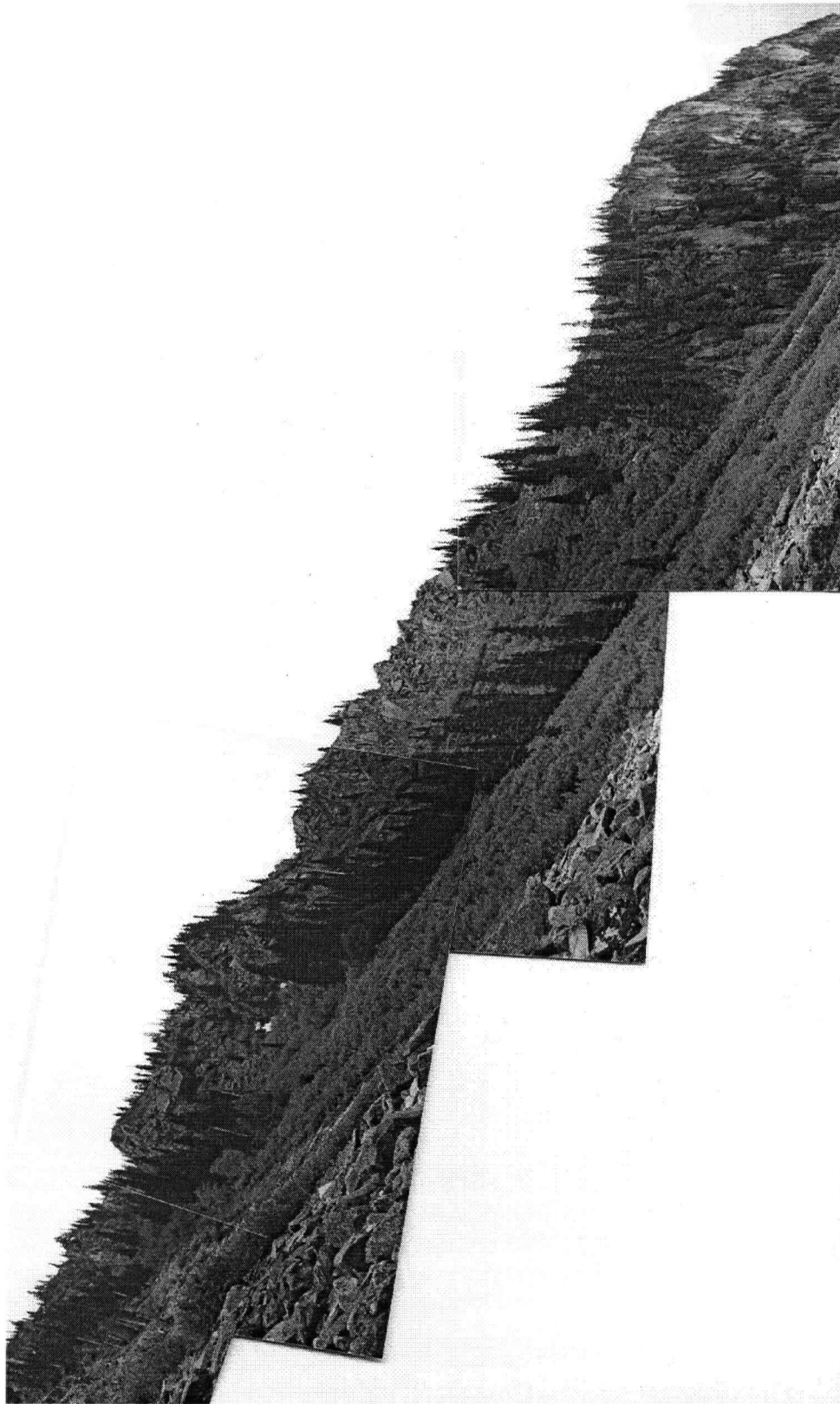
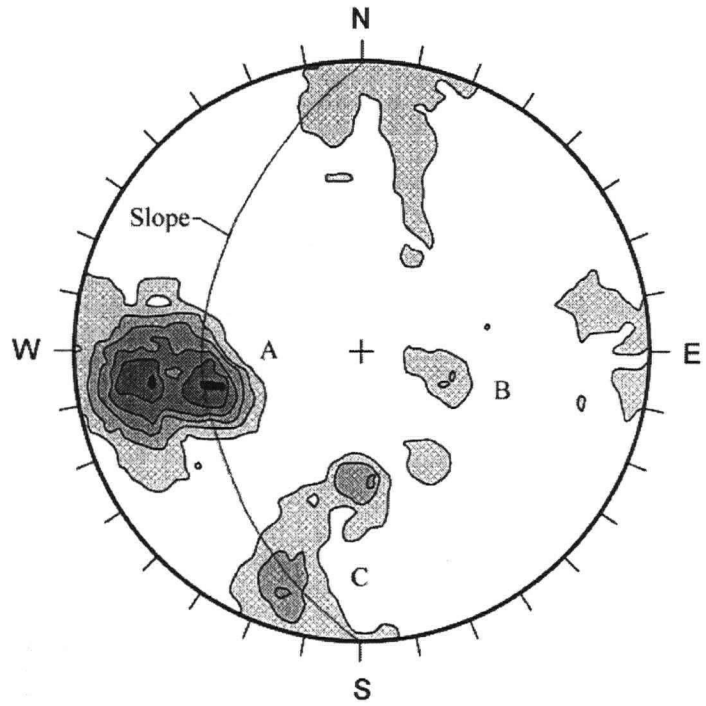
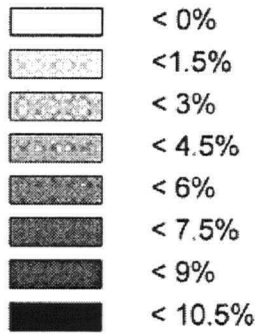


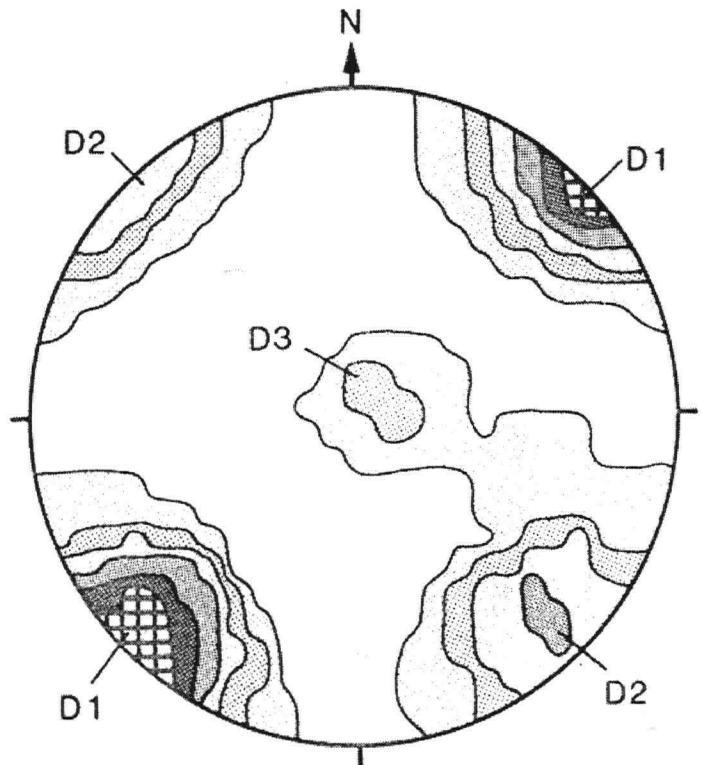
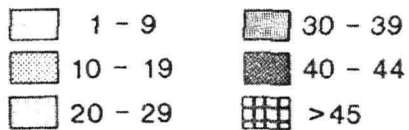
Figure 7-4: Photographs of toppling in rock mass on southern edge of scar – note sub-vertical cliff at right  
(4-photo series taken by the author).

% of 178 points per 1% area



(a)

percentage of 39 points in 5%  
of area of hemisphere



(b)

Figure 7-5: Structural data: (a) poles to discontinuities, Mystery Creek (by the author);  
(b) poles to discontinuities, Mt. Currie (Evans, 1987).

Figure 7-6:  
Input geometry for  
UDEEC modelling of  
Mystery Creek.

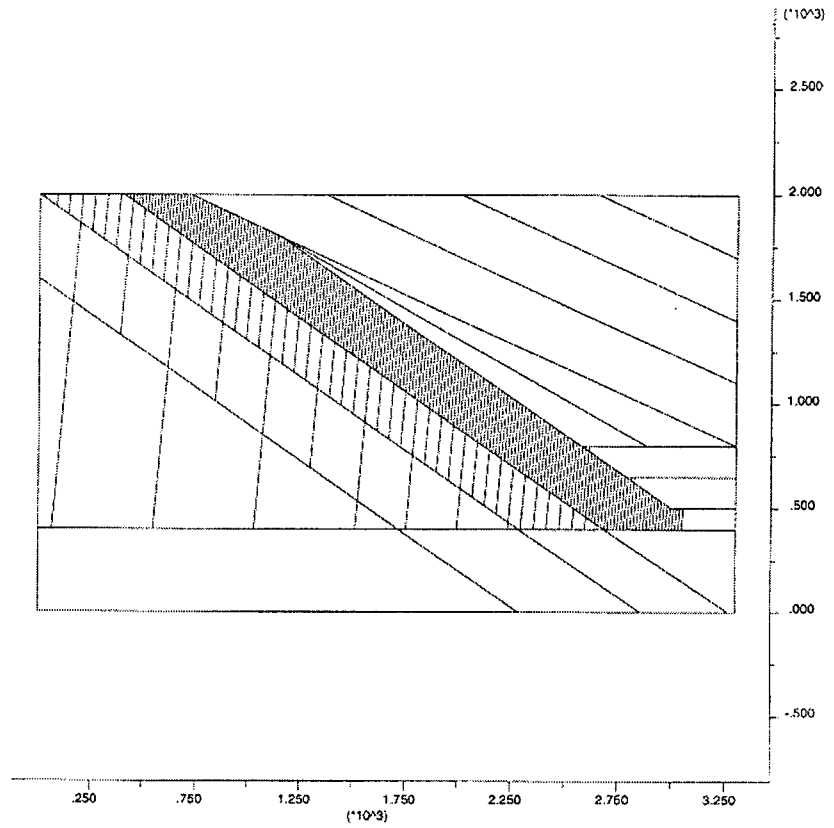


Figure 7-7:  
Displacement and shear  
without cross-joints in  
Mystery Creek model.

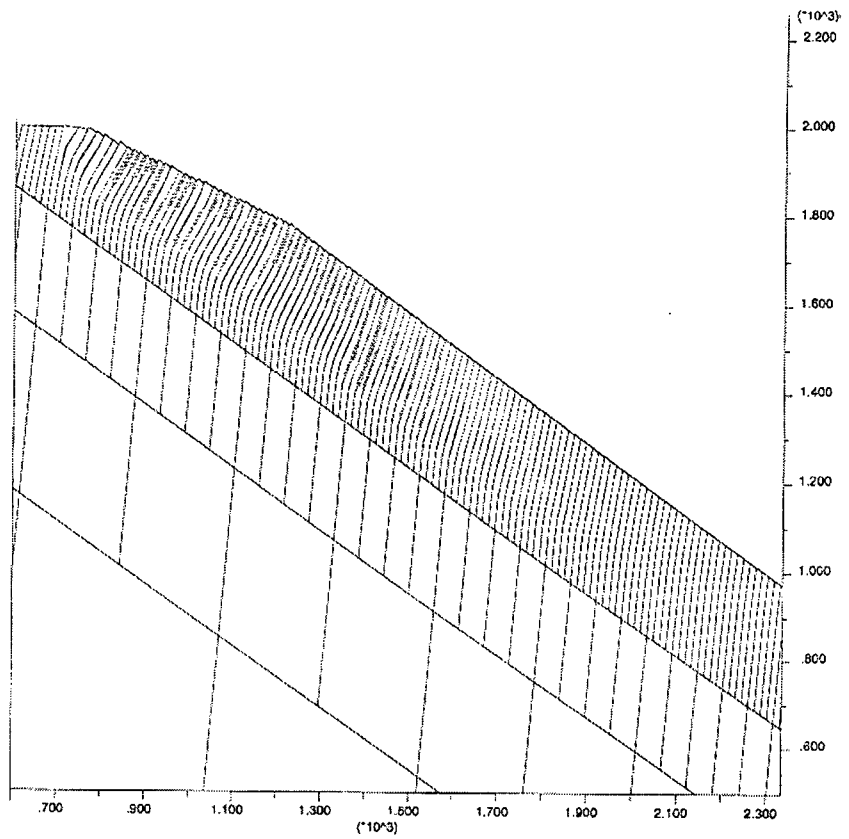


Figure 7-8:  
Block plot of fully  
continuous cross-joints  
after 50 000 cycles.

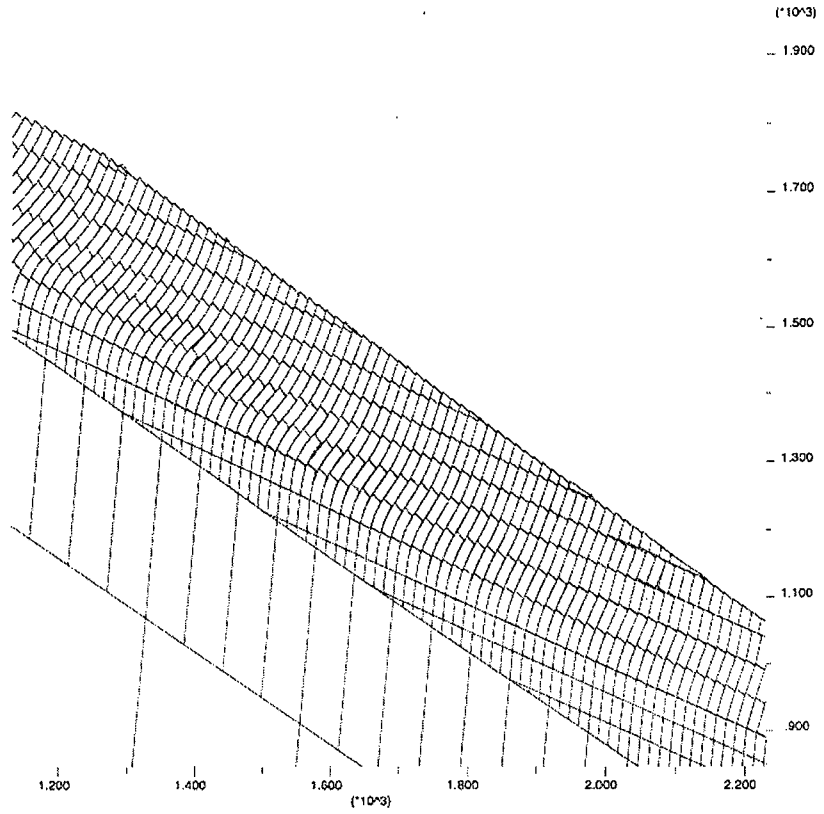


Figure 7-9:  
Block plot of cliff in  
Mystery Creek model  
after 30000 cycles.

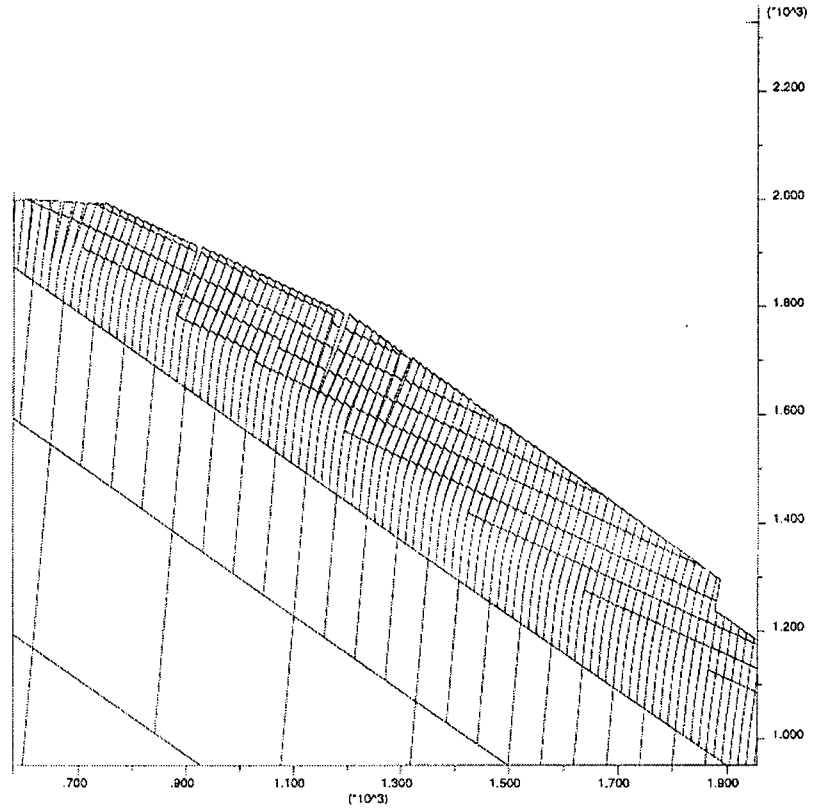


Figure 7-10:  
Block plot of cliff  
in Mystery Creek  
model after 49000  
cycles.

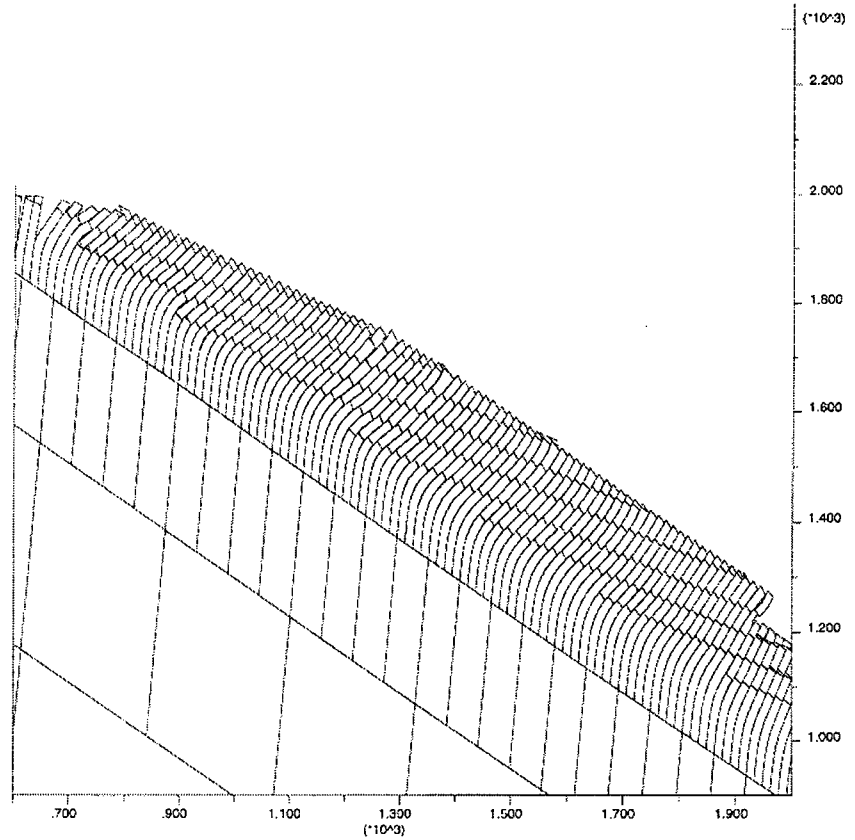


Table 7-1: Input parameters for UDEC modelling of Mystery Creek.

Rock Properties		Joint Properties	
Density	2700 kg/m <sup>3</sup>	Joint Normal Stiffness	10 GPa/m
Bulk Modulus	13 GPa	Joint Shear Stiffness	5 GPa/m
Shear Modulus	8 GPa	Friction Angle	30°
Friction Angle	51°	Dilation Angle	0°
Dilation Angle	2°	Cohesive Strength	0
Cohesive Strength	900 kPa	Tensile Strength	0
Tensile Strength	180 kPa		

## 8.0 MOUNT BREAKENRIDGE CASE STUDY

A highly disturbed area on the east side of Harrison Lake, approximately 43 km north of the town of Harrison Hot Springs, was identified in 1989 by Dr. S.G. Evans of the GSC. Due to the proximity of Harrison Hot Springs and other small communities on the lake, the consequences of failure of the slope and a landslide-induced wave could be quite severe. Preliminary site investigation was carried out by Thurber Consultants Ltd. (Thurber) at the request of the Regional District of Fraser-Cheam (under the B.C. Provincial Emergency Program), followed by a second, more detailed study (Phase 2). The following information on the unstable area is taken from the Phase 2 report produced by Thurber (Anon., 1990).

### 8.1 *Background Information*

Harrison Lake is located in a north-northwest trending valley approximately 100 km east of Vancouver (Figure 8-1). The east valley slope rises from the lake at El. 10 m a.s.l. to the summit of Mount Breakenridge at El. 2403 m. The unstable area is located on a promontory having a slope angle of  $41.4^\circ$  up to a ridge at El. 1000 m, with lower angles on the flanks and crest of the ridge above this elevation (Figure 8-2). Adjacent to the site the lake bottom is featureless and roughly U-shaped in cross-section, typical of formerly glaciated valleys, and has a maximum depth of 250 m.

Metamorphic rocks of Jurassic age called Slollicum Schist (Monger, 1986) make up the entire slope, extending as a band parallel and adjacent to the eastern shoreline of Harrison

Lake (Figure 8-3). The western boundary is the Harrison Lake Shear Zone, a group of major strike-slip faults extending beneath the lake, while the eastern boundary is a possible thrust fault separating the lower metamorphic grade Slollicum rocks from the higher grade Mount Breckenridge Gneiss to the east. The Oligocene Doctors Point Pluton, consisting of coarse grained, non-foliated granodiorite with an estimated age of 24.6 million years, interrupts the northwest trend of the lithologic and structural boundaries, crossing the lake immediately northwest of the unstable area.

The Slollicum Schist consists of meta-sedimentary rocks (quartz-chlorite granulite schist, phyllite and talc schist) and massive meta-volcanics (amphibole granulite and schist). The rock mass is divided into four geotechnical units, each having reasonably uniform physical characteristics (from Anon., 1990, Table 2):

- (1) Massive Granulite. Dark grey, fine-grained, very strong (UCS > 100 MPa), faintly banded but non-fissile, unweathered, and contains three joints sets which break the rock mass into cubic blocks having an average side length of 3 metres. All joints are unweathered, unfilled and tight.
- (2) Quartz Schist. Grey, fine-grained, very strong (UCS > 50 MPa), moderately to highly anisotropic, foliated and slightly fissile, with interbeds of fissile schist 20 cm thick spaced at 2 m intervals. The rock mass is unweathered to slightly weathered, with three joints sets and random joints, and is dilated with some open joints. Blocks are tabular to platy in shape with modal size of 1 metre, and joints are unfilled and unweathered. Foliation and schistosity dip into the slope at 24°.

- (3) Mica Schist. Silvery grey, fine grained, of medium strength, highly anisotropic, strongly fissile and unweathered. It contains two joint sets, with platy-shaped blocks having a modal size of 30 cm. Joints are unweathered and unfilled, with some dilation. Schistosity dips into the slope at roughly 20°, with some variation.
- (4) Altered Schist. Moderately weathered mica schist with quartz schist interbeds. It is white to orange, fine to coarse grained, very weak, highly fissile and crumbly (block size a few cm). Schistosity makes up the lone joint set dipping 30° to 50° into the slope, with joints infilled with silty gouge containing talc (residual friction angle of approximately 14°).

The granulites and schists are interbedded in a complex manner in all parts of the slope, usually with gradational contacts between the various lithologies. Roughly 90% of exposures are formed by the granulites and quartz schists, with micaceous schist (10%) occurring primarily in thin units exposed along the foot of each of the three main slope scarps. The massive metavolcanics occur mainly in two thick zones below the second and third scarps (El. 1200 m). The altered schist forms a single thin band that roughly follows the contours near El. 800 m; however, its thickness cannot be precisely determined due to poor exposures.

Large-scale structures mapped in the area are the Harrison Lake Shear Zone faults and the thrust fault running parallel to the ridge. These trend northwest-southeast, are probably steeply dipping, and are truncated by the Doctors Point Pluton, which suggests that there has been no active movement on these faults for over 20 million years. There is no reported active fault within at least a 100 km radius of the site. Mapping carried out during the

Thurber study revealed no minor structures of obvious tectonic origin. Features on the slope, predominantly lineaments trending northwest parallel with slope contours, are interpreted to be the result of gravitational disturbance. All structural data for the area are shown in Figure 8-4. Foliation and schistosity dip consistently towards the northeast at intermediate to steep angles, thought to be the result of tight isoclinal folding (Anon., 1990). There is a widely distributed and nonsystematic series of joints that dip toward the valley. These are interpreted as possible longitudinal joints related to folding. Other joints occurring sub-parallel to the slope surface are attributed to stress relief. There are two major north-south trending lineaments that form partial segments of the slope disturbance boundaries.

Attention is drawn to the difference between structural attitudes within the unstable area and those outside the area, as illustrated in Figure 8-5. Foliation in the undisturbed area dips 50° on average, compared to 30° in the unstable area, suggesting toppling of the beds.

Two large talus cones buttress the lower reaches of the slope. Based on airphotos spanning the last 40 years, the Thurber report considers the northern cone appears more active than the southern cone, one possible explanation being the amount of loose rock present at mid-levels of the slope above the apex of each cone. Debris flows occur on both cones. An accumulation of boulders near the front part of the first bench is thought to be of glacial origin.

The main features on the slope are three scarps separated by back-tilted benches in the upper part of the slope, steep gullies frequented by rockfall on mid-slopes, and large talus deposits on the benches and at the foot of the slope. Severe cracking and deformation has occurred on

the top of the ridge over a distance of 800 m, with the largest amount of cracking occurring in the southeast segment (approximately 500 m wide by 300 m long). The features include tension cracks (both individual and in groups), trenches and some reverse scarps. The tension crack openings range from a few centimetres to 4 m, while the trenches and scarps have several metres of relief. The dilation in this area is estimated to be greater than 5%. The northwest segment is about 300 m wide and 300 m long, and is roughly 25 m higher than the southeast segment. This area also contains extensive tension features, though the overall dilation is considered to be less than 5% (Anon., 1990). The northeast boundary of the cracked portion of the ridge is formed by a distinct hinge zone. To the northeast of the hinge zone the rock mass is apparently undisturbed, with tight discontinuities dipping at 50° to 55°. The lower slopes of the mountain (below El. 800 m) show no apparent signs of disturbance; however, some signs may be obscured by the talus cones and heavy forest cover.

Desloges and Gilbert (1991) used geophysical studies to map the sedimentary record of Harrison Lake. Their results indicate that there has not been a large scale slope failure into the lake at the site of the current unstable slope nor elsewhere around the lake.

## 8.2 *UDEC Modelling*

Section b-b of Figure 4 of the Thurber report was used as a starting point for the UDEC model (Figure 8-6). The initial input geometry is shown in Figure 8-7. Three rock types were included in the model: quartz schist, mica schist and granulite. For purposes of simplification, the altered schist unit identified as a thin band at El. 800 m was modelled as

mica schist. Quartz schist was interpreted to exist in zones 3 and 7, due to the relatively shallow slope angles and the interbedded nature of the sequence. Granulite was assumed for zone 10, due to a slope angle similar to zone 9 and lack of a visible mica schist layer at the downslope margin of zone 9. Vegetation covering the slope in these areas and lower down the slope prevented identification of the rock types over the entire profile. From Section b-b (Figure 8-6), the slope face was estimated at 45° prior to deformation.

Sub-vertical joints were added to the quartz schist and mica schist units; initially, no joints were added in the granulite. Based on structural data from undisturbed areas near the unstable slope, the steeply dipping joint set is oriented at 55° into the slope. However, in order to meet the Goodman and Bray (1976) criteria for flexural toppling ( $\beta \geq \phi + (90 - \psi)$ ), friction along the joints would have to be 10° or less. This friction angle may not be unrealistic based on results in the Thurber report; however, in the models the sub-vertical joints were input slightly steeper at 60° with maximum friction for flexural slip then 15°. This value may still be considered somewhat low; however, if groundwater had been considered in the model, friction along the joints may have been reduced to this level.

Properties were first assigned based on the description of the rock masses in Table 2 of the Thurber report as described above (Table 8-1). The artificial overburden joints were given high values for friction angle (60°), cohesive strength (1 MPa) and tensile strength (1 MPa) to prevent any movement. Joint spacing in the quartz schist was set at 10 m and in the mica schist at 3 m. These spacings are 10 times the actual spacings (1 m and 30 cm, respectively), for simplification but mainly to have somewhat reasonable model run times. Ideally, the mica

schist and quartz schist units would have been modelled using the ubiquitous joint model (they are described as highly anisotropic, and moderately to highly anisotropic, respectively); however, for simplicity all units were modelled using the Mohr-Coulomb plasticity model. Further study of this slope using the ubiquitous joint model would no doubt provide further insight into the deformation mechanism.

Some toppling deformation occurred (on the order of 10 m), with shearing taking place along the mica schist joints, but in general, the model did not reproduce the kind of deformation observed in the field, specifically the flattening of the joints. It was considered that the model was "too strong". Sub-vertical joints were then added in the granulite at a spacing of 20 m (actual spacing is 3 m), with the input parameters kept the same, in order to see the effect of the new joints. Again, the model did not produce the observed deformation. Cross-joints at 20 m spacing were added in the granulite dipping 30° out of the slope with a friction angle of 30° to just prevent sliding (Figure 8-8). Parameters were gradually lowered (i.e., the strength of the rock masses were gradually reduced). Results are presented for the parameters given in Table 8-2.

Maximum displacement in this model is on the order of 100 m (Figure 8-9). Shearing has occurred along the joints in the granulite, forming anti-slope scarps. There is some shearing in the schists, though not nearly to the same extent. The shearing in the upper quartz schist (zones 1 and 3) occurs at the base of the columns where a slight kink band has developed (Figure 8-10). The deforming area has a circular boundary surface. Part of the reason for this may be that the input parameters do not change with depth; the weak characteristics of the

quartz schist at depth in the slope are perhaps not realistic. This is also indicated by sagging at the crest and bulging at the toe (compare to Chiquicamata, s. 4.11), although the bulging may also be due in part to the input geometry in the toe area (Figure 8-11). It is also possible that the quartz schist at the base of the slope is somewhat stronger than the upper units and should have different input parameters. Finally, the artificial joint parallel to the slope is perhaps not deep enough (i.e., the columns should have been longer), and jointing in the region below this joint should have been included. This is evidenced by the displacement vectors in the columns terminating very close to the artificial joint. Ideally the deformation should not have been impacted at all by this joint. For stronger input parameters, however, this may not be as significant.

Of interest is the relative displacement of the different units (Figures 8-9 and 8-10). Uphill-facing scarps have developed in all three units, although the columns do not bend to 30° dips as observed in the field. The slopes of the deformed units get progressively steeper moving from toe to crest until the upper quartz schist units, where the slope flattens. This roughly reproduces the observed slopes, if allowance is made for preferential weathering of the schists.

With the limited amount of information available on subsurface conditions, many assumptions had to be made in order to define the input geometry and parameters. Only a very limited number of possibilities have been considered here. A more detailed study of Mount Breakenridge, beyond the scope of the present study, would provide valuable insight into the failure mechanism.

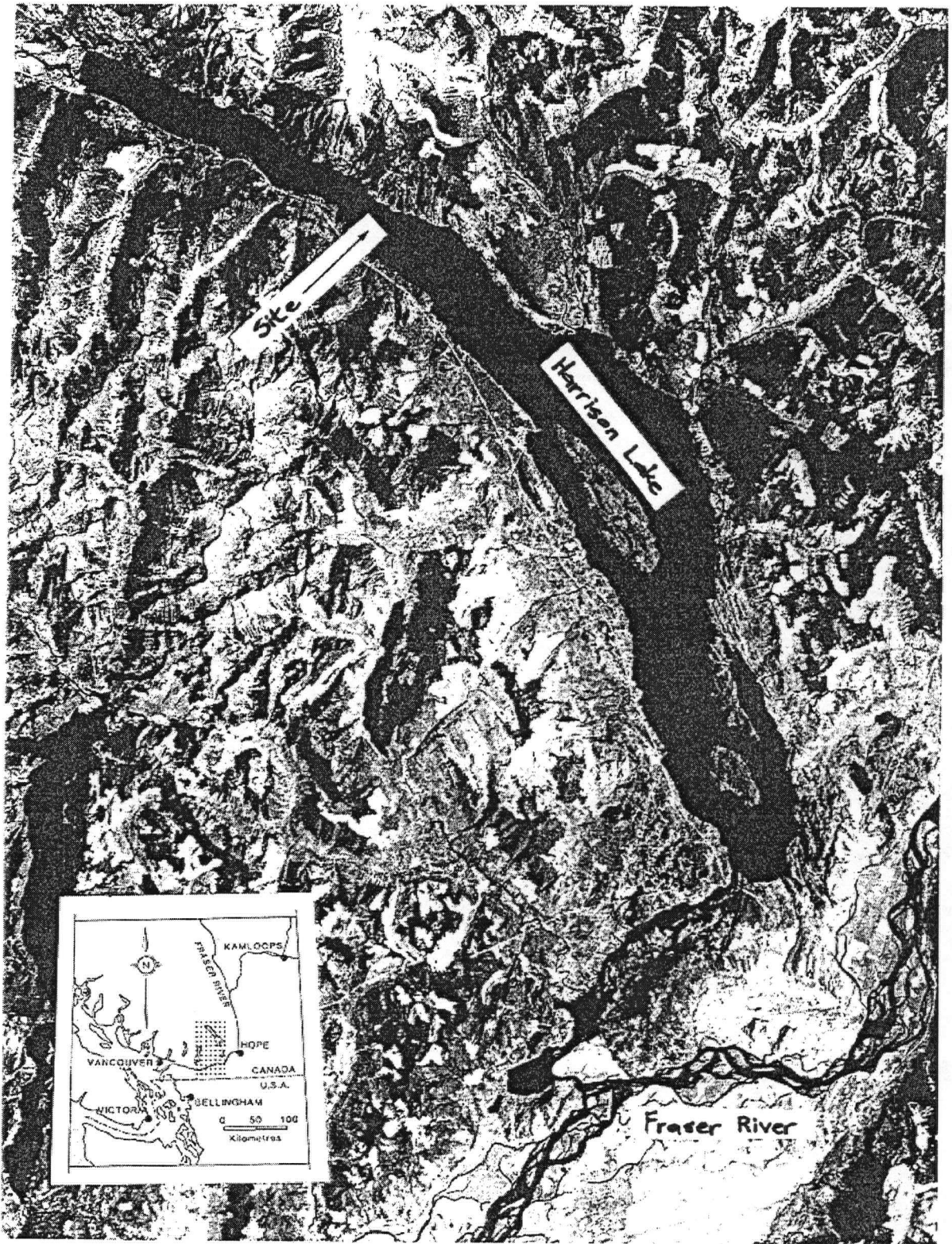


Figure 8-1: Location of Mt. Breakenridge slope movement (Anon., 1990, Fig. 1).



Figure 8-2: Photo of the Mt. Breakenridge disturbed slope.

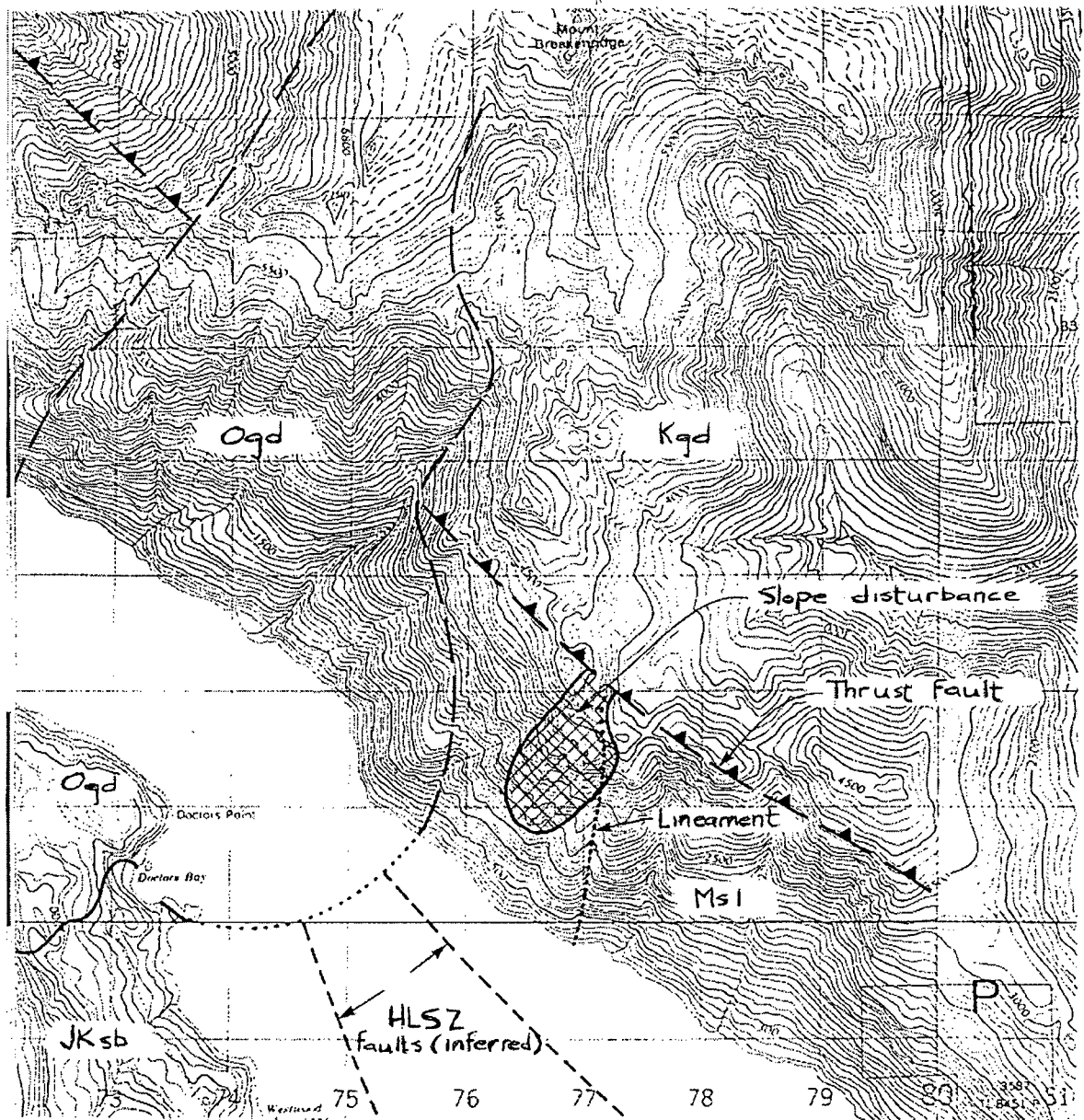


Figure 8-3: Geology of Harrison Lake area (Anon., 1990, Fig. 3, based on M. Journeay, GSC, unpublished).

**LEGEND:**

- Northwest Cascade System (Jurassic):
- Msl – Slollicum Schist, schists, phyllites, volcanic siltstone.
- Kgd – Mt. Breakenridge Gneiss.
- Coast Plutonic Complex:
- Ogd – Doctor's Point Pluton, granodiorite, quartz monzonite. Nooksack Terrane (Cretaceous):
- Jksb – Fire Lake Sequence, volcanics, metasediments.
- HLSZ – Harrison Lake Shear Zone.

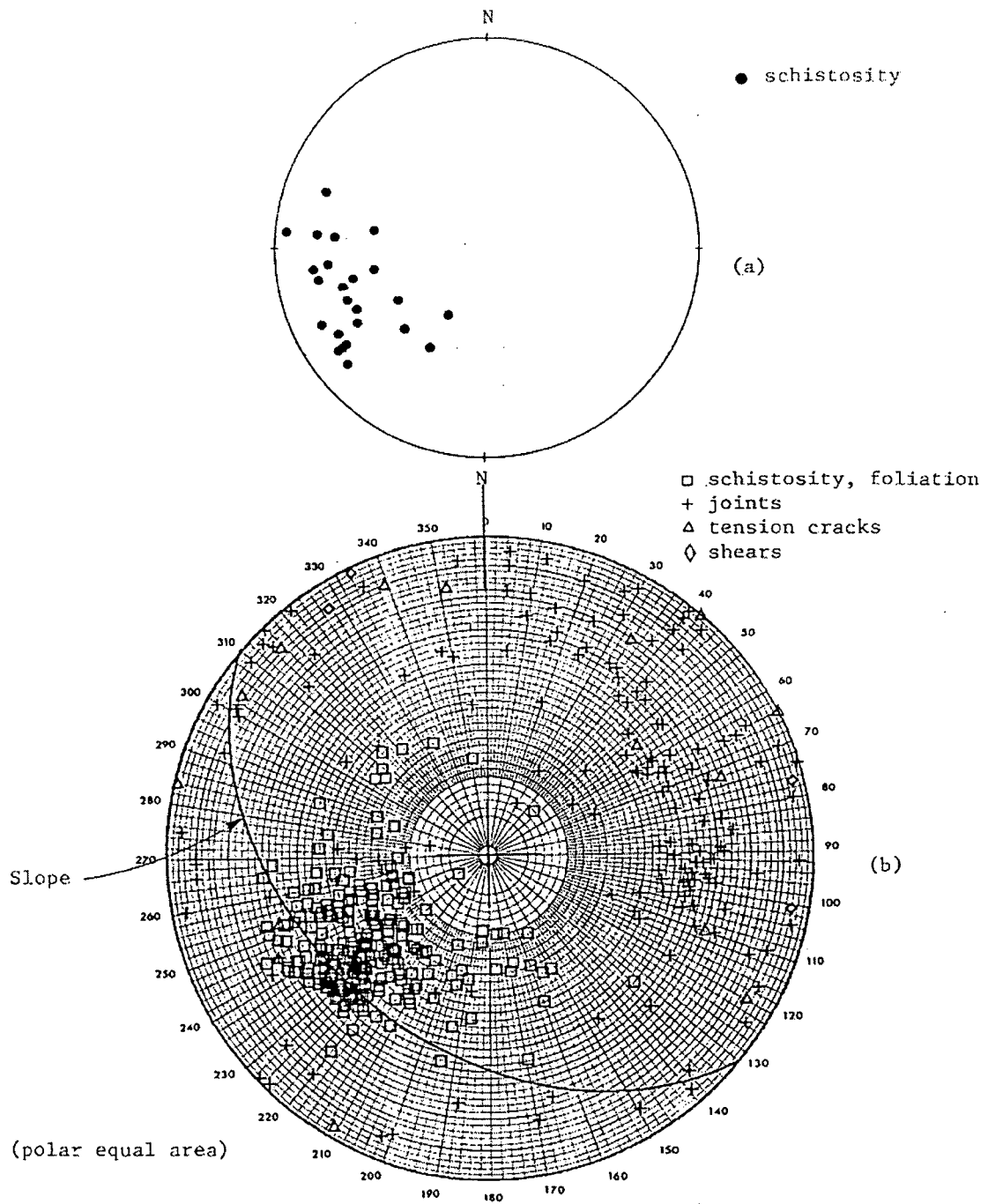


Figure 8-4: Structural data from the Slolicum Formation (from Anon. (1990), Figure 6):  
 (a) Monger (1986); (b) Anon. (1990).

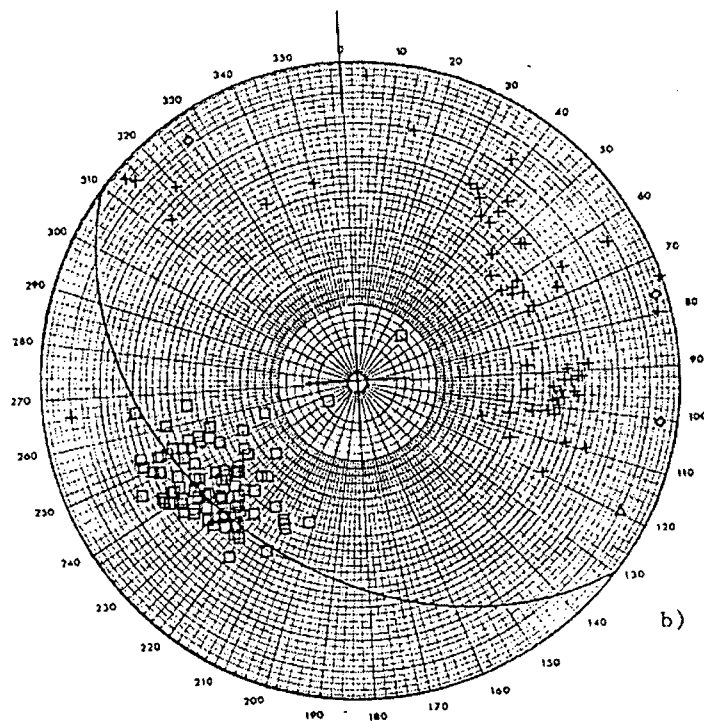
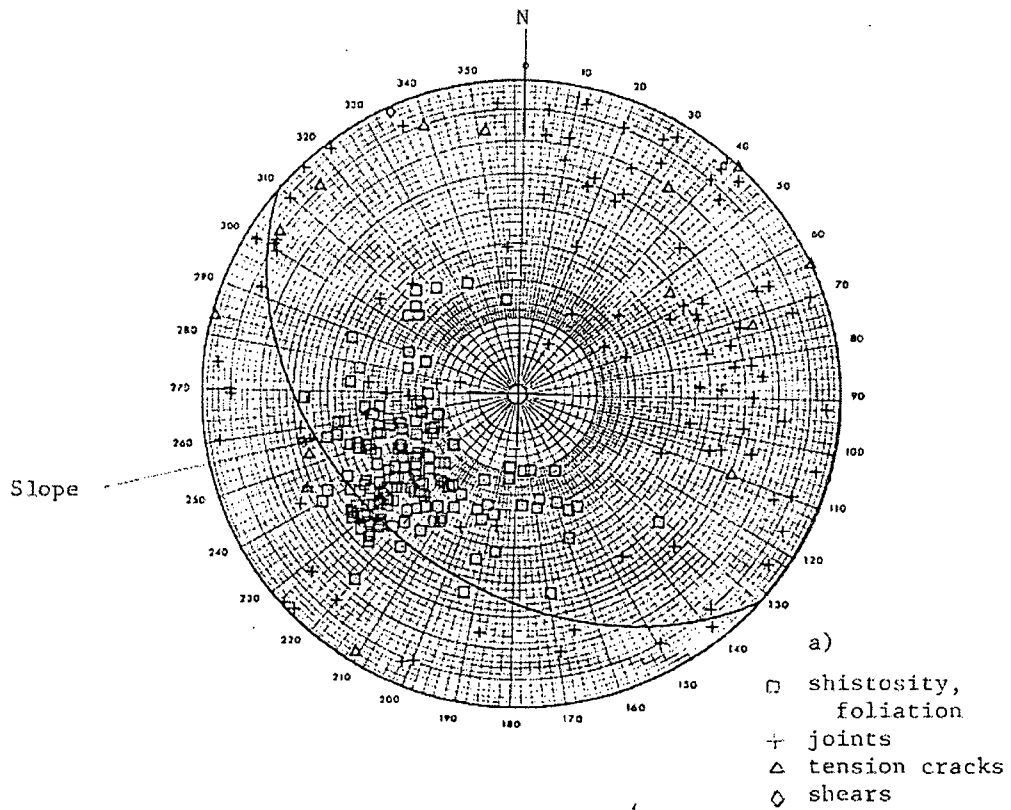


Figure 8-5: Comparison between structural orientations (from Anon. (1990), Figure 7):  
 (a) inside disturbed area; (b) outside disturbed area.

Figure 8-6:  
Mount Breakenridge  
geometry: Section b-b  
from Thurber report  
(Anon., 1990, Fig. 4).

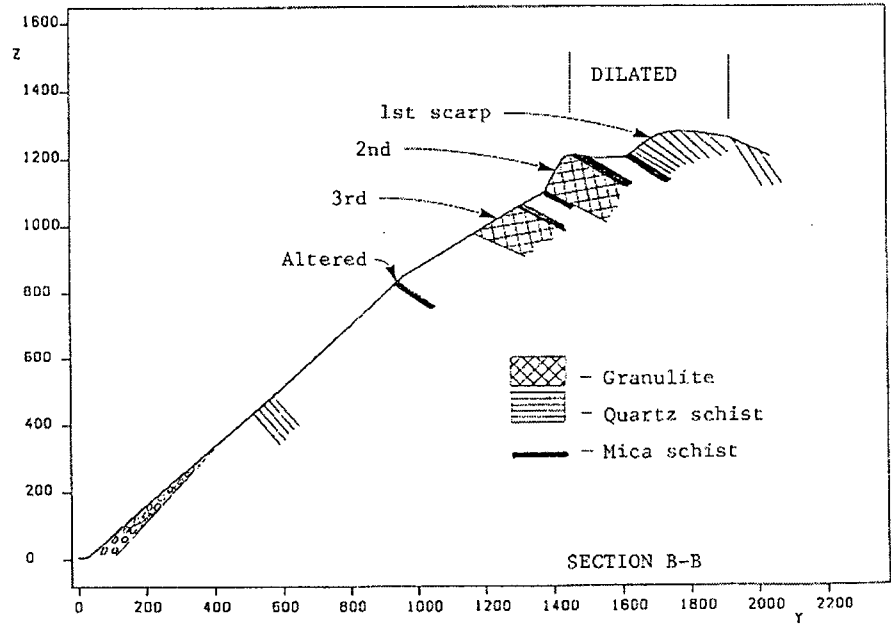
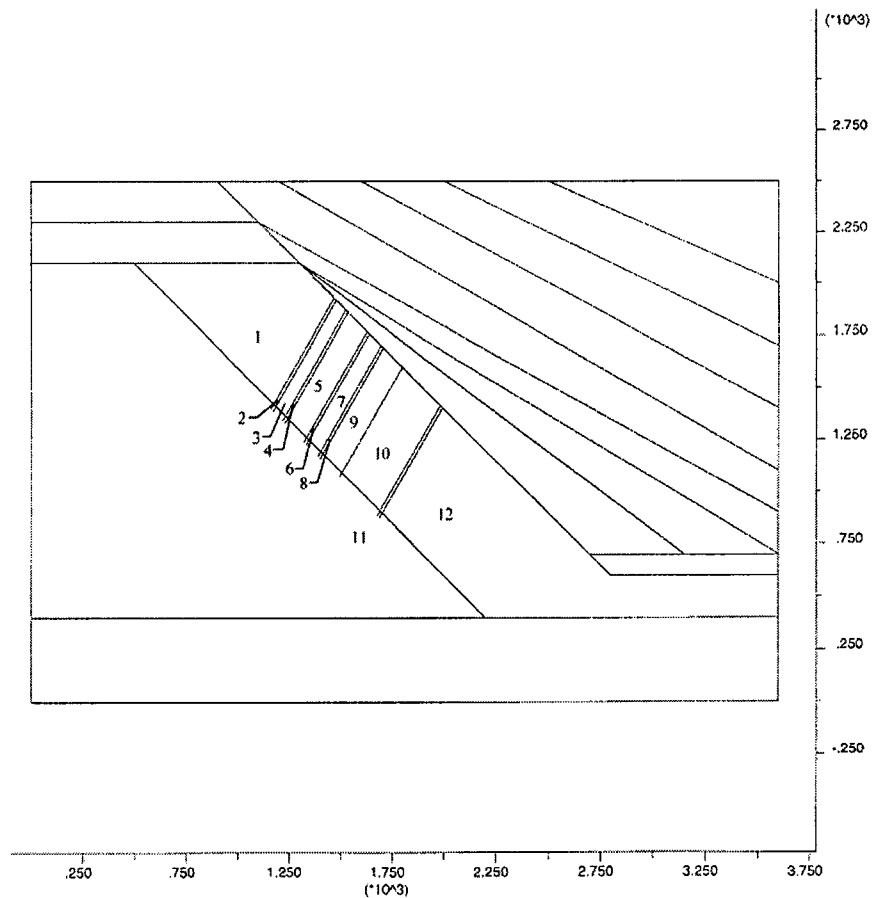


Figure 8-7:  
Initial input geometry  
for Mount Breakenridge  
UDEC model.

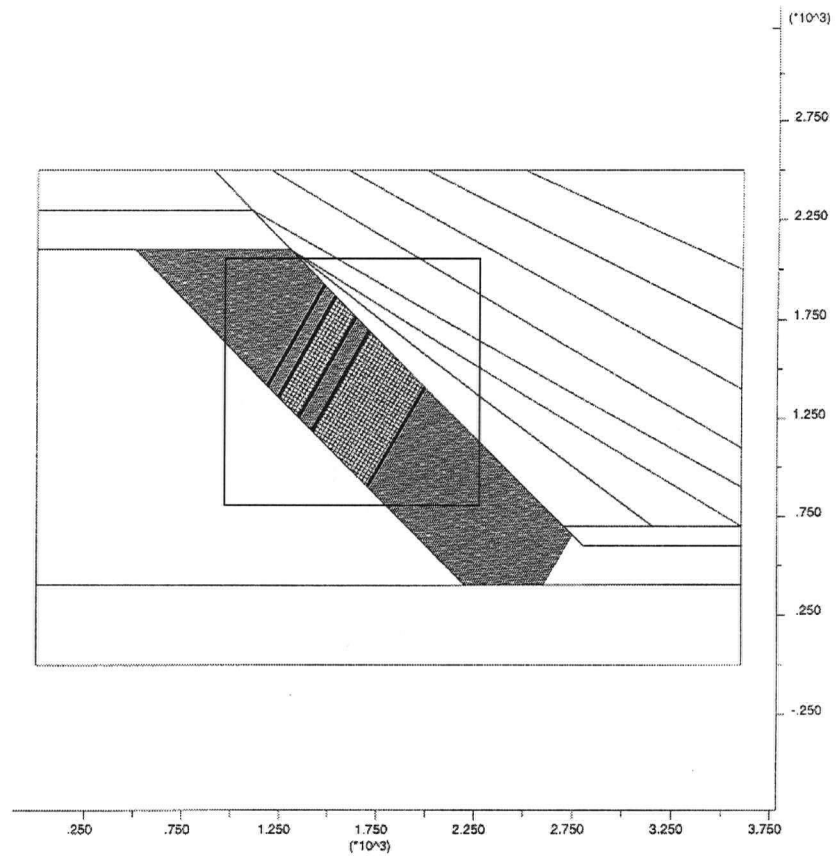
Quartz Schist:  
zones 1, 3, 7 and 12

Mica Schist:  
zones 2, 4, 8 and 11

Granulite:  
Zones 5, 9 and 10



(a)



(b)

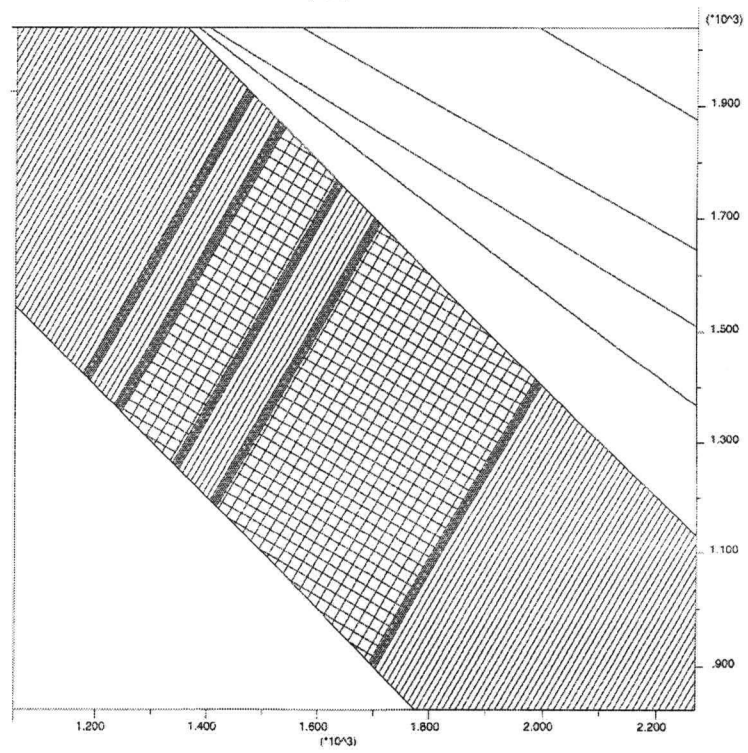
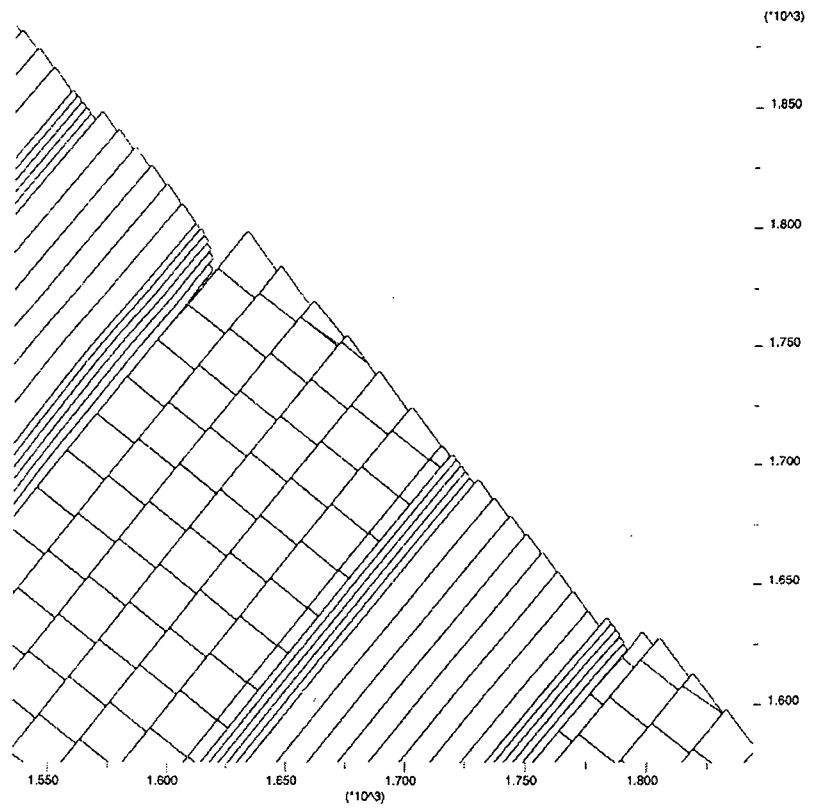


Figure 8-8: Initial input geometry for Mount Breakenridge UDEC model: (a) with joints (boxed area shown in (b)); (b) inset area shown in (a).

(a) block plot



(b) displacement vectors

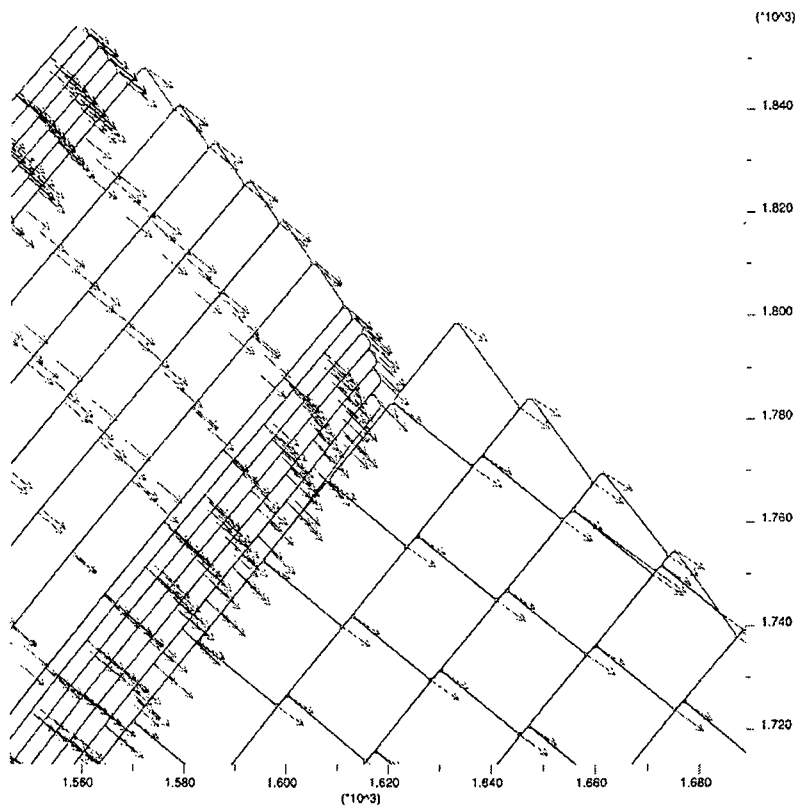


Figure 8-9: Detail of deformation in upper portion of Mount Breakenridge slope.

Figure 8-10:  
Kink band development  
near base of columns.

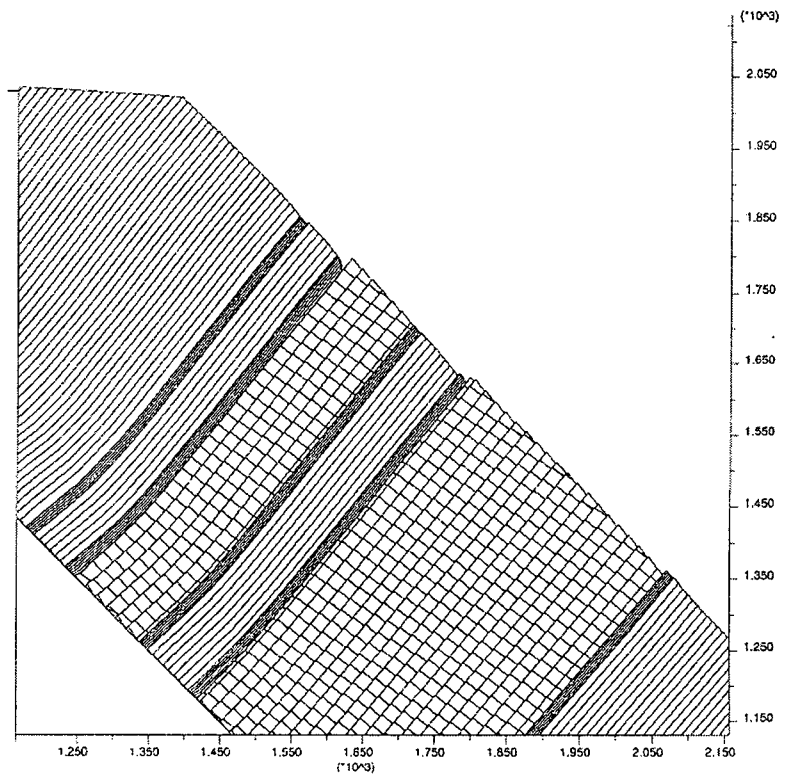


Figure 8-11: Bulging of  
the toe area.

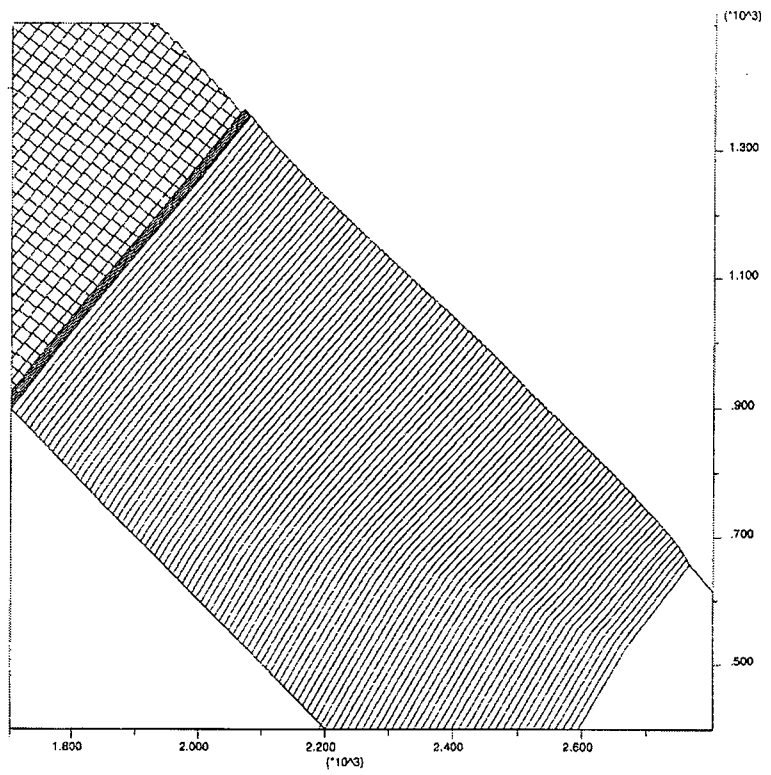


Table 8-1: Initial Input Parameters for UDEC Modelling of Mount Breakenridge

	Granulite	Quartz Schist	Mica Schist
<u>Rock Mass Properties:</u>			
UCS* (MPa)	150	100	10
GSI*	65	60	50
$m_i^*$	12.5	8	4
Bulk density (kg/m <sup>3</sup> )	2700	2700	2700
Bulk modulus (GPa)	15.8	12.2	2.1
Shear modulus (GPa)	9.5	7.3	1.3
Friction angle (°)	53	42	14
Dilation angle (°)	1	1	0
Cohesive Strength (kPa)	1000	600	120
Tensile Strength (kPa)	200	120	20
<u>Joint Properties:</u>			
Friction angle (°)	15	15	15
Cohesive Strength (kPa)	0	0	0
Tensile Strength (kPa)	0	0	0
Joint Normal Stiffness (GPa/m)	9	9	1
Joint Shear Stiffness (GPa/m)	5	5	0.5

\*These values were input into the spreadsheet shown in Table 5-3 to determine the other input parameters.

Table 8-2: Secondary Input Parameters Used in UDEC Modelling of Mount Breakenridge

	Granulite	Quartz Schist	Mica Schist
<u>Rock Mass Properties:</u>			
UCS* (MPa)	80	50	10
GSI*	60	50	50
$m_i^*$	12.5	8	4
Bulk density (kg/m <sup>3</sup> )	2700	2700	2700
Bulk modulus (GPa)	10.6	4.7	2.1
Shear modulus (GPa)	6.4	2.8	1.3
Friction angle (°)	46	31	14
Dilation angle (°)	0	0	0
Cohesive Strength (kPa)	510	270	120
Tensile Strength (kPa)	100	50	20
<u>Joint Properties:</u>			
Friction angle (°)	15	15	15
Cohesive Strength (kPa)	0	0	0
Tensile Strength (kPa)	0	0	0
Joint Normal Stiffness (GPa/m)	9	9	1
Joint Shear Stiffness (GPa/m)	5	5	0.5

\*These values were input into the spreadsheet shown in Table 5-3 to determine the other input parameters.

## 9.0 DISCUSSION

The case histories presented in Chapter 4 illustrate that toppling behaviour occurs under an apparently wide range of conditions. The Heather Hill landslide (s. 4.1) was modelled by Pritchard (1989) using UDEC without including cross-joints, and a failure surface similar to that observed in the field developed in the model. The upslope limit of the failure was found to be related to a change in rock type (relatively weaker rock in the lower portion of the slope and stronger rock upslope) and to the oversteepened toe of the slope. The toe of the Clapière landslide (s. 4.2) was also oversteepened – this process is considered to have been the first stage in the development of the failure. In the case of both Heather Hill and Clapière, a sliding surface developed through the toppling hinge. Thus, sliding was secondary to toppling (this process was not investigated in the current study). Modelling at Affliction Creek (s. 4.3), another case where the lower portion of the slope is oversteepened, included all major joint sets and showed that toppling was feasible under gravitational stresses alone, without seismic or tectonic driving forces. Fluctuating groundwater levels were shown to influence the amount of displacement.

At Glen Pean (s. 4.4), where release surfaces are provided by cross-joints dipping toward the valley, catastrophic toppling failure is considered to have been prevented by a wedge at the toe of the slope that provides stability to the plates higher up the slope. The persistence of steeply dipping joints at Ben Attow (s. 4.5) has allowed for development of “the largest extent of obsequent-scarplets in Scotland,” with deformation occurring progressively from the base up the slope; however, catastrophic failure has not occurred.

Reservoir filling at Billan (s. 4.6) weakened the toe of the slope; expensive drainage works were required to prevent a slide into the reservoir. Mining to a depth of 200 m at Brenda Mine triggered toppling of the south wall (s. 4.8). Modelling of the wall by Pritchard (1989) showed that stability was significantly affected by the groundwater level, and that the geometry and location of the failure surface was dependent on the combination of block cohesion, block tensile strength and the joint friction angle. These input parameters could be determined from the intact rock strength and rock mass parameters  $m_i$  and GSI (see Table 5.3). Research by Benko and Stead (1999) showed that there was a wide range of strength parameters that could reproduce the slope failure observed at Luscar Mine (s. 4.9), and that the same general area of the slope was affected under both dry and wet conditions. Using FLAC and UDEC, Board et al. (1996) modelled the west wall of the Chuquicamata Mine (s. 4.10). The main conclusion of this modelling is that toppling would not occur if a weak zone at the base of the wall did not compress.

Oversteepening (naturally or man-made) and/or a compressible or relatively weak rock unit (naturally or due to groundwater pressure) at the lower part of the slope are common to most of the cases described above (and in further detail in Chapter 4). Indeed, toe conditions play a large role in determining how much movement can occur. Sjöberg (1999) shows that toppling movements were greatly reduced in models without joints in the toe area or with a higher Young's modulus in the toe area. Sjöberg also showed that toppling movements begin at the toe of the slope and progressively increase upslope (the current study shows similar results). However, it is doubtful whether catastrophic failure of the deformed slope can be

predicted from conditions at the toe alone. It is obvious that other factors, such as rock strength and release surfaces, also play a role.

Many assumptions had to be made in the modelling in order to keep things simple. Arguably the most serious simplifying assumption made was not to include the effects of groundwater. All models were run under dry conditions. This may not be critical for the parametric modelling, where it could be assumed that the inclusion of groundwater would weaken the rock mass and accelerate movements but would not change the overall behaviour qualitatively, but ideally water would have been included in the case studies. The groundwater regime in the two cases during deformation is not known, however, nor would it be straightforward to estimate; thus, the simplest procedure involved using dry conditions. Despite this, it was possible to reproduce to some extent the observed deformation in the two case studies using very simplified models of the slopes. It is recognized that less than ideal geometries were used in the models for both cases, specifically with respect to artificial joints parallel to the ground surface that were not located at sufficient depth to avoid having an impact on the results. Further study of both sites with improved model set up and allowing for various groundwater conditions would provide greater insight into the behaviour of the slopes.

As a further simplification, input parameters were not changed with depth for any of the models. Stress release joints and weathering effects at the surface were thus not accounted for. In work by Stewart (1997), who modelled deformation at the Wahleach Hydroelectric Project, the simulation of weathering led to yield conditions in the upper 100 m of the model,

indicating that weathering can have a significant effect on the behaviour of the slope close to the ground surface. Not changing input parameters with depth could perhaps be considered similar to not including groundwater, discussed above. It also means that the weaker rock units were weak throughout, which may not be entirely realistic. Again, constant parameters was a simplification, but one which allowed for the analysis of the relative amount of movement occurring for different strengths. Had the parameters been increased, i.e., if there was weaker, weathered rock near the ground surface and stronger rock at depth, the hinge zone may have occurred closer to the ground surface in the flexural toppling models. This is inferred from the results of the parametric study showing a change in the amount of displacement based on the intact rock strength (stronger rock had less displacement). In the block toppling models, the failure surface would possibly have occurred higher in the slope, if strengthening was achieved by decreasing joint spacing and persistence as well as increasing UCS and joint strength properties. Confirmation would require further research.

Initial in situ stress conditions were identical for all models, and were based on a horizontal to vertical stress ratio ( $k$ ) of 0.5. This assumes that all residual in situ stresses have dissipated, which is not unrealistic for post-glacial valley slopes at this point in time. A higher stress ratio would perhaps be more appropriate for excavations such as open pit mines (e.g., Benko and Stead (1999) set  $k = 1.5$  for their modelling of Luscar Mine). For a higher stress ratio the rates of movement would likely increase, but the overall behaviour of the slope might not change significantly, assuming that principal stresses still develop parallel to the topography near the ground surface.

Joints within the slopes being studied were generally modelled without cohesive or tensile strength. No joint infilling or alteration was considered, again, to keep the input parameters as simple as possible. Because the strength of the joints plays a part in the amount of displacement that can occur, the models generally used constant joint strength parameters so that the influence of the other parameters being varied could be better identified.

The values used in this study for joint normal stiffness ( $j_{kn}$ ) and joint shear stiffness ( $j_{ks}$ ) could be considered to be somewhat arbitrary. However, Benko and Stead (1999) examined the sensitivity of their models to different values for  $j_{kn}$  and  $j_{ks}$  (they used  $j_{ks} = 1/10 j_{kn}$ ), and found that while there were larger movements with lower stiffness values, the overall behaviour of the slope was unchanged. In the current study, lower stiffness values were assigned to joints in the weaker rock units and higher values to stronger units; the amount of movement observed is thus due to both the stiffness values and the values for the other input parameters. As the sensitivity of the models to stiffness values was not tested, it cannot be stated for certain how much these values contribute to the deformation, but based on Benko and Stead (1999), the overall behaviour of the slope should not change. It should be noted that joint permeability and joint aperture were not included in the models as a simplification, mainly because water was not being considered.

Automatic damping in UDEC is normally used for static analysis and is dependent on block velocity. This study used automatic damping as a means of testing whether the given geometry and input parameters ultimately lead to stable conditions. Results were analyzed to determine whether the damping effects were realistic. Some of the damping imposed artificially by UDEC could occur naturally where block velocities are low, while some of the

damping imposed is unrealistic. For example, in cases where the velocity of the blocks is high ( $> 1$  m/s), artificial damping acts to reduce the unbalanced forces and significantly lower the block velocity in a way that cannot be considered realistic. In these cases, the conditions were considered to be unstable and the models were stopped. Because only static conditions were examined, it was not possible to compare actual movement rates. Further research involving dynamic conditions, particularly at Mystery Creek, would be beneficial.

The results of the modelling carried out in this study, described in cc. 6, 7 and 8, are interesting, despite the relative simplicity of the approach used. When considering a rock slope having only sub-vertical joints, increasing the UCS of the intact rock by an order of magnitude increased displacements by an order of magnitude (all other conditions being equal). The failure surface is closer to the ground surface and is closer to the top of the slope for stronger rock. Where the UCS is greater than about 60 MPa the amount of displacement is small compared to the scale of the slope and involves shearing along the joints but little bending of the columns. Work by Sjöberg (1999) shows similar results although intact tensile strength, intact shear strength, intact stiffness and joint shear strength were varied separately.

The spacing normal to the sub-vertical joints in the parametric study was held constant at 3 m. Sjöberg (1999) performed analyses with different joint spacing using UDEC and found that while toppling was less pronounced for larger joint spacing, reverse shearing and bending of columns could be observed even for relatively large joint spacing (slope height to joint spacing ratio of 6).

From the results of varying cross-joint persistence, it seems that there may be a “critical” geometry necessary for catastrophic failure of the slope. It is difficult to analyze this property using UDEC, which can generate a large number of geometries for given mean and standard deviation values which “define” persistence. Generally, a failure surface developed about 100 m below the crest of the slope and followed the dip of the cross-joints; the continuity of this surface increased with cross-joint persistence. Movement increases significantly between Test 1 and Test 2 (gap lengths, i.e., “rock bridges”,  $10\text{ m} \pm 5$  and  $6\text{ m} \pm 3$ , respectively; see Table 5-4), to the extent that catastrophic failure is deemed to occur for Test 2. The strength of the columns forming “rock bridges” between the cross-joints would influence whether tensile failure occurs through these bridges. This was not analyzed in the current study, for all models in which persistence was varied were run with identical “strong” parameters (UCS = 100 MPa – see Table 5.2).

The present study does not, unfortunately, offer any definitive results that can be used to predict whether a particular slope will or won't fail catastrophically. However, it was possible to demonstrate qualitatively that transition from ductile to brittle behaviour occurs with increasing rock strength and persistence of cross-joints. This qualitative study of the influence of intact rock strength, cross-joint persistence and toe conditions showed behaviour consistent with existing field observations. Simplified models of Mystery Creek and Mount Breakenridge showed fair correspondence with observed patterns of behaviour.

## 10.0 CONCLUSIONS AND RECOMMENDATIONS

### 10.1 *Conclusions*

This study examined toppling behaviour in large rock slopes. A qualitative parametric study was carried out using the Universal Distinct Element Code (UDEC). The parameters studied were: intact rock strength; joint persistence, spacing and orientation; and toe conditions. All models were run with a slope face of 45° and sub-vertical continuous joints dipping 85° into the slope at 3 m spacing, and under dry conditions.

The first set of analyses was made with no cross-joints to simulate flexural toppling. The unconfined compressive strength of the intact rock was varied from 10 MPa (weak rock) to 100 MPa (strong rock). Displacement was found to decrease significantly where the UCS was greater than about 60 MPa; above this strength, some shearing along the sub-vertical joints occurred, but bending of the columns was limited. Note that parameters were not varied with depth, thus the influence of weathering of the near surface was not taken into account. Stresses were found to be sub-parallel to the slope surface in the upper 100 m or so (i.e., the first 100 m or so below the ground surface) for all strengths, even after the slope had undergone some deformation. Below about 100 m depth, the principal stresses rotate towards vertical.

In the second part of the parametric study, four variations of cross-joint persistence were considered (it was not feasible to examine every possible combination), including fully

continuous “idealized” joints, and compared to the slope without cross-joints. All models used parameters based on a UCS of 100 MPa. Movement was found to increase as the persistence of the cross-joints increased, tensile failure of intact “rock bridges” increased, and the failure involved a larger and larger portion of the slope. There appears to be a “critical” persistence at and above which catastrophic failure occurs – where the gaps between joints (i.e., the “rock bridges”) are less than about 10 m. It should be noted that only a limited number of models were tested. As the persistence was increased, the stresses rotate to vertical closer to the ground surface. As well, the area where stresses remain parallel to the slope surface moves progressively downslope as persistence increases.

Increasing the spacing perpendicular to the fully continuous cross-joints from 20 m to 50 m was not found to significantly change the behaviour of the slope. Movement begins at the toe, a kink band develops and the slope fails catastrophically.

Using parameters based on  $UCS = 100$  MPa and cross-joint normal spacing of 50 m, it was found that changing the orientation of the cross-joints from  $25^\circ$  to horizontal altered the behaviour of the slope. A kink band did not develop in the model with horizontal cross-joints; rather, a hinge zone developed much the same as when there were no cross-joints. However, brittle failure still occurred.

Oversteepening of the toe was investigated by removing a portion of the toe after overburden removal to form a cliff. The model, which used fully continuous cross-joints and parameters based on  $UCS = 100$  MPa, developed a kink band similar to when the entire slope was at  $45^\circ$ .

Reduced strength of the toe was examined in a model without cross-joints, using parameters based on  $UCS = 10 \text{ MPa}$  and reduced rock mass quality constants. The weak, highly deformable rock was squeezed up at the toe, allowing room for columns upslope to move, but did not result in catastrophic failure.

Two case studies were analyzed using simplified models: Mystery Creek and Mount Breckenridge, both in British Columbia. Mystery Creek is a prehistoric landslide that failed catastrophically; Mount Breckenridge shows significant deformation but catastrophic failure of the slope has not occurred. The Mystery Creek model used constant strength parameters with variations in cross-jointing. Observed displacements and catastrophic failure of the slope could be reproduced. The columns bend forward, but rather than stabilize, the cross-joints allow for destressing in the lower portions of the slope and catastrophic failure occurs. Pre-failure stresses are sub-vertical due to destressing of the slope. The Mount Breckenridge model used a combination of three rock units with different strength and jointing characteristics. The stresses in the upper portions of the slope remain sub-parallel to the slope surface. Relatively good reproduction of observed deformations was achieved.

## *10.2 Recommendations for Further Work*

While further parametric modelling using UDEC may prove useful, the main recommendation for further work that arises from this study is a detailed analysis of each of the two slopes modelled (Mystery Creek and Mount Breckenridge, as well as other similar

sites). The very simple analyses carried out in this study yielded encouraging results about the deformation mechanisms.

A detailed study of Mystery Creek should involve further field mapping and if possible subsurface investigation to more adequately determine subsurface structure and possible groundwater conditions. A variety of groundwater levels and dynamic analyses should be included in numerical modelling, as well as more accurate representations of strength parameters, particularly with respect to joints.

A detailed study of Mount Breakenridge would be particularly useful, in part because the present study relied on information from a report published ten years ago. The new study should involve further field mapping and possibly subsurface investigation to more adequately determine subsurface structure and possible groundwater conditions. The ubiquitous joint model should be used and groundwater should be included in the numerical modelling.

In summary, the qualitative study of the influence of intact rock strength, cross-joint persistence and toe conditions showed that stable flexural toppling develops in rock masses characterized by weak to medium-strength rock (UCS less than about 50 MPa) with relatively few cross-joints. Stresses in these cases remain sub-parallel to the ground surface in the upper portions of the slope. This study demonstrated that deformation of slopes undergoing flexural toppling is relatively slow and generally does not accelerate. With slow rotation, discontinuity dips become sufficiently shallow that flexural toppling is no longer

kinematically feasible and these slopes ultimately stabilize. With more persistent cross-joints and stronger rock, this study showed that deformation generally accelerates and catastrophic brittle toppling failure is more likely to occur. This type of failure is strongly promoted by toe undercutting. Stress distributions show sub-vertical stresses dominating the upper portions of the slope. Simplified models of Mystery Creek and Mount Breakenridge were able to demonstrate these contrasting types of behaviour. These results may provide a simple starting point for assessing the potential for a slope deforming by toppling to result in catastrophic failure.

## REFERENCES

- Anon., 1976. CPR – Rogers Pass: Geotechnical Evaluation of Alternate Routes. Report to Canadian Pacific Railroad by EBA Engineering Consultants.
- Anon., 1990. Mount Breakenridge Slide Phase 2 Study. Report to the Regional District of Fraser-Cheam by Thurber Consultants Ltd.
- Anon., 1992. Failure Behaviour of Large Rockslides. Report to the Geological Survey of Canada and BC Hydro and Power Authority by Thurber Engineering Ltd.
- Anon., 1997a. Revelstoke Dam Deficiency Investigations – 1992 to 1995. BC Hydro Maintenance, Engineering and Projects Report No. MEP84, January 1997.
- Anon., 1997b. B.C. Hydro Columbia River – Revelstoke Project: Checkerboard Creek Rock Slope FLAC Modelling Study (Ref. No. 10131/1-1). Report to B.C. Hydro by Knight Piésold Ltd., October 1997.
- Barton, N.R., 1973. Review of a new shear-strength criterion for rock joints. *Engineering Geology* 7: 287-332.
- Barton, N.R., Lien, R. and Lunde, J., 1974. Engineering classification of rock masses for the design of tunnel support. *Rock Mechanics* 6(4): 189-239.
- Barton, N.R., 1986. Deformation phenomena in jointed rock. *Géotechnique* 36(2): 147-167.
- Benko, B. and Stead, D., 1998. Analysis of two landslide case studies using numerical modelling. *In Slope Stability & Landslides: Proceedings of the 13<sup>th</sup> Annual Vancouver Geotechnical Society Symposium, May 28, 1999, Vancouver, BC.* Richmond, BC: BiTech Publishers Ltd., pp. 19-29.
- Bieniawski, Z.T., 1973. Engineering classification of jointed rock masses. *Transactions of the South African Institute of Civil Engineers* 15: 335-344.
- Bieniawski, Z.T., 1976. Rock mass classification in rock engineering. *In Exploration for rock engineering, proceedings of the symposium* (ed. Z.T. Bieniawski), vol. 1. Cape Town: Balkema, pp. 97-106.
- Bieniawski, Z.T., 1989. *Engineering rock mass classifications.* New York: Wiley.
- Board, M., Chacón, E., Varona, P. and Lorig, L., 1996. Comparative analysis of toppling behaviour at Chuquicamata open-pit mine, Chile. *Trans. Instn Min. Metall. (Sect. A: Min. industry)*, 105, January-April.

Bovis, M.J., 1982. Uphill-facing (antislope) scarps in the Coast Mountains, Southwest British Columbia. *Geological Society of America Bulletin*, v. 93, pp. 804-812.

Bovis, M.J., 1990. Rock-slope deformation at Affliction Creek, southern Coast Mountains, British Columbia. *Canadian Journal of Earth Sciences* 27: 243-254.

Bovis, M.J. and Evans, S.G., 1995. Rock slope movements along the Mount Currie "fault scarp," southern Coast Mountains, British Columbia. *Canadian Journal of Earth Sciences* 32: 2015-2020.

Bovis, M.J. and Stewart, T.W., 1998. Long-term deformation of a glacially undercut rock slope, southwest British Columbia. *Proc., 8<sup>th</sup> International IAEG Congress*. Rotterdam: Balkema, vol. II, pp. 1267-1276.

Brown, E.T., (Ed.), 1987. *Analytical and Computational Methods in Engineering Rock Mechanics*. Allen & Unwin: London.

Chigira, M., 1992. Long-term gravitational deformation of rocks by mass rock creep. *Engineering Geology* 32: 157-184.

Cruden, D.M., 1987. Rock slope movements in the Canadian Rockies. *Proceedings, International Symposium on Engineering Geological Environment in Mountainous Areas, Beijing*, vol. 1, pp. 323-332.

Cruden, D.M., 1989. Limits to common toppling. *Canadian Geotechnical Journal* 26: 737-742.

Cruden, D.M. and Varnes, D.J., 1996. Landslide types and processes. *In Landslides: Investigation and Mitigation*. Edited by A.K Turner and R.L. Schuster. Transportation Research Board, Special Report 247, National Research Council, Washington, DC, pp. 36-75.

Cundall, P., 1971. A computer model for simulating progressive, large scale movements in blocky rock systems. *Proceedings of the International Rock Mechanics Symposium*, pp. 11-18.

Deere, D.U., Hendron, A.J., Patton, F.D. and Cording, E.J., 1967. Design of surface and near surface construction in rock. *In Failure and breakage of rock, proceedings of the 8<sup>th</sup> U.S. symposium on rock mechanics* (ed. C. Fairhurst). New York: Society of Mining Engineers, American Institute of Mining, Metallurgy and Petroleum Engineers, pp. 237-302.

De Freitas, M.H. and Watters, R.J., 1973. Some field examples of toppling failure. *Géotechnique* 23(4): 495-514.

Desloges, J.R. and Gilbert, R., 1991. Sedimentary record of Harrison Lake: implications for deglaciation in southwestern British Columbia. *Canadian Journal of Earth Sciences* 28(5): 800-815.

Eisbacher, G.H., 1983. Slope Stability, Southern Coast Mountains and Fraser Lowland Fieldtrip Notes (October 16, 1983; leaders: Eisbacher, G.H. and Clague, J.J.). Cordilleran Section, Geological Association of Canada.

Evans, S.G., 1987. Surface displacement and massive toppling on the northeast ridge of Mount Currie, British Columbia. *In Current Research, Part A, Geological Survey of Canada, Paper 87-1A*, pp. 181-189.

Evans, S.G., 1992. High-magnitude low frequency catastrophic landslides in British Columbia; Proceedings, British Columbia Geological Survey Workshop on Geologic Hazards in British Columbia, British Columbia Ministry of Energy Mines and Petroleum Resources, Open File 1992-15, pp. 71-98.

Evans, S.G. and Savigny, K.W., 1994. Landslides in the Vancouver-Fraser Valley-Whistler region. *In Geology and Geological Hazards of the Vancouver Region, Southwestern British Columbia*, (ed.) J.W.H. Monger; Geological Survey of Canada, Bulletin 481, pp. 251-286.

Follacci, J.-P., 1987. Les mouvements du versant de la Clapière à Saint-Etienne de Tinée. *Bull. liaison Labo. Ponts et Chaussées*, Vol. 150, Paris, pp. 31-46.

Follacci, J.-P., Guardia, P. and Ivaldi, J.-P., 1988. Le glissement de la Clapière dans son cadre géodynamique. Proceedings, 5<sup>th</sup> International Symposium on Landslides, Lausanne, C. Bonnard ed., Vol. 2, pp. 1323-1328 (in French).

Fruneau, B., Delacourt, C. and Achache, J., 1996. Observation and modelling of the Saint-Etienne de Tinée landslide using SAR interferometry. Proceedings, ERS SAR Interferometry Workshop, Zurich.

Giraud, A., Rochet, L. and Antoine, P., 1990. Processes of slope failure in crystallophyllian formations. *Engineering Geology* 29: 241-253.

Goodman, R.E., 1980. *Introduction to Rock Mechanics*. Wiley, New York, NY.

Goodman, R.E. and Bray, J.W., 1976. Toppling of Rock Slopes. *In Rock Engineering: ASCE, Geotechnical Engineering Division, Conference, Boulder, Colorado, Vol. II*, pp. 201-234.

Goodman, R.E. and Shi, G., 1985. *Block Theory and Its Application to Rock Engineering*. New Jersey: Prentice-Hall, Inc.

Heim, A., 1932. *Bergsturz und Menschenleben (Landslides & Human Lives)*. Translated by Nigel Skermer. Vancouver: BiTech Publishers Ltd., 1989.

- Hoek, E., 1983. Strength of jointed rock masses. *Geotechnique* 33(4): 187-233.
- Hoek, E. and Bray, J.W., 1981. *Rock Slope Engineering*, 3<sup>rd</sup> edition. London: Institution of Mining and Metallurgy.
- Hoek, E. and Brown, E.T., 1980. *Underground excavations in Rock*. London: Institution of Mining and Metallurgy, 527 p.
- Hoek, E. and Brown, E.T., 1988. The Hoek-Brown Failure Criterion – A 1988 Update. *In Proceedings of the 15<sup>th</sup> Canadian Rock Mechanics Symposium (Toronto, Canada, 1988)*, pp. 31-38. Toronto: Department of Civil Engineering, University of Toronto.
- Hoek, E., Kaiser, P.K. and Bawden, W.F., 1995. *Support of Underground Excavations in Hard Rock*. Rotterdam: Balkema.
- Hoek, E. and Brown, E.T., 1997. Practical estimates of rock mass strength. *Int. J. Rock Mech. Min. Sci.*, 34, No. 8, pp. 1165-1186.
- Holmes, G. and Jarvis, J.J., 1985. Large-scale toppling within a sackung type deformation at Ben Attow, Scotland. *Quarterly Journal of Engineering Geology* 18: 287-289.
- Hu, X.-Q. and Cruden, D.M., 1992. Rock mass movements across bedding in Kananaskis Country, Alberta. *Canadian Geotechnical Journal* 29: 675-685.
- Itasca, 1995. *FLAC Version 3.3 Manual*. Minneapolis: Itasca Consulting Group.
- Itasca, 1997. *UDEC Version 3.0 Manual*. Minneapolis: Itasca Consulting Group.
- Knoblauch, P. 1927. Die Bewegungen am Motto d'Arbino bei Bellinzona. *Die Alpen* III 28: 361-373.
- Ladanyi, B. and Archambault, G., 1970. Simulation of shear behaviour of a jointed rock mass. *Proceedings of the 11<sup>th</sup> Symposium on Rock Mechanics*. Published by AIME, New York, pp. 105-125.
- Ladanyi, B. and Archambault, G., 1972. Evaluation de la résistance au cisaillement d'un massif rocheux fragmenté. *Proceedings of the 24<sup>th</sup> International Geological Congress, Montreal*. Section 13D, pp. 249-260.
- MacLaughlin, M.M., 1997. *Discontinuous Deformation Analysis of the Kinematics of Landslides*. Ph.D. Thesis, University of California, Berkeley.
- MacLaughlin, M.M. and Sitar, N., 1995. *Discontinuous Deformation Analysis for the Windows PC Environment, UC-Berkeley Version 1.1 Manual*. Berkeley: University of California Department of Civil and Environmental Engineering, October 1995.

Martin, D.C., 1993. Time Dependent Deformation of Rock Slopes. Ph.D. Thesis, University of London.

Matheson, G.D., 1983. Rock stability assessment in preliminary site investigations – graphical methods. Transport and Road Research Laboratory, Crownthorne, Berkshire, United Kingdom, Report 1039.

Monger, J.W.H., 1986. Geology between Harrison Lake and Fraser River, Hope Map Area. *In Current Research, Part B.*, Geologic Survey of Canada Paper 86-1.

Moore, D.M., 1989. Toppling Failure in the Marmot Vertical Limb at Quintette Coal Ltd., Tumbler Ridge, British Columbia. M.A.Sc. Thesis, University of British Columbia, Vancouver, Canada.

Palmstrom, A., 1982. The volumetric joint count – a useful and simple measure of the degree of rock jointing. Proceedings of the 4<sup>th</sup> Congress of the International Association of Engineering Geologists, Delhi, vol. 5, pp. 221-228.

Pande, G.N., Beer, G. and Williams, J.R., 1990. Numerical Methods in Rock Mechanics. John Wiley & Sons Ltd.: England.

Patton, F.D., 1966. Multiple modes of shear failure in rock. Proceedings of the 1<sup>st</sup> International Congress of Rock Mechanics, Lisbon, vol. 1, pp. 509-513.

Pritchard, M.A., 1989. Numerical Modelling of Large Scale Toppling. M.A.Sc. Thesis, University of British Columbia, Vancouver, Canada.

Pritchard, M.A., Savigny, K.W. and Evans, S.G., 1990. Toppling and deep-seated landslides in natural slopes. *In Mechanics of Jointed and Faulted Rock*, Rossmanith (ed.). Rotterdam: Balkema, pp. 937-943.

Rapp, P., 1987. Rock Toppling and Massive Slope Instability in the Beaver Valley, B.C. Unpublished B.A.Sc. Thesis, University of British Columbia, Vancouver, Canada.

Rochet, L., 1987. Développement des modeles numériques dans l'analyse de la propagation de éboulements rocheux. Proceedings, 6<sup>th</sup> Congress ISRM, Vol. 1, pp. 479-484 (in French).

Savage, W.Z., Swolfs, H.S. and Powers, P.S., 1985. Gravitational stresses in long symmetric ridges and valleys. *International Journal of Rock Mechanics and Mineral Sciences & Geomechanics Abstracts* 22: 291-302.

Shi, G.-H., 1988. Discontinuous Deformation Analysis: A New Numerical Model for the Statics and Dynamics of Block Systems. Ph.D. Thesis, University of California, Berkeley.

Shi, G.-H., 1993. Block System Modeling by Discontinuous Deformation Analysis. Computational Mechanics Publications, London, England, 209.

Sjöberg, J., 1999. Analysis of Large Scale Rock Slopes. Ph.D. Thesis, Luleå University of Technology, Sweden.

Stewart, T.W.G, 1997. Investigation of Rock Slope Deformation at the Wahleach Hydroelectric Project using the FLAC Computer Code. M.A.Sc. Thesis, The University of British Columbia (Department of Civil Engineering).

Turner, A.K. and Schuster, R.L (editors), 1996. Landslides Investigation and Mitigation. Transportation Research Board Special Report 247, National Academy Press, Washington, DC.

Wang, B. and Garga, V.K., 1993. A numerical method for modelling large displacements of jointed rocks. I. Fundamentals. Canadian Geotechnical Journal 30: 96-108.

APPENDIX

GENERALISED HOEK-BROWN CRITERION		SURFACE CONDITION					
$\sigma_1' = \sigma_3' + \sigma_c \left( m_b \frac{\sigma_3'}{\sigma_c} + s \right)^a$ <p> <math>\sigma_1'</math> = major principal effective stress at failure  <math>\sigma_3'</math> = minor principal effective stress at failure  <math>\sigma_c</math> = uniaxial compressive strength of <i>intact</i> pieces of rock  <math>m_b</math>, <math>s</math> and <math>a</math> are constants which depend on the composition, structure and surface conditions of the rock mass </p>		VERY GOOD Very rough, unweathered surfaces	GOOD Rough, slightly weathered, iron stained surfaces	FAIR Smooth, moderately weathered or altered surfaces	POOR Slit-sided, highly weathered surfaces with compact coatings or fillings containing angular rock fragments	VERY POOR Slit-sided, highly weathered surfaces with soft clay coatings or fillings	
STRUCTURE							
	BLOCKY -very well interlocked undisturbed rock mass consisting of cubical blocks formed by three orthogonal discontinuity sets	$m_b/m_i$ $s$ $a$ $E_m$ $\nu$ $GSI$	0.60 0.190 0.5 75,000 0.2 85	0.40 0.062 0.5 40,000 0.2 75	0.26 0.015 0.5 20,000 0.25 62	0.16 0.003 0.5 9,000 0.25 48	0.08 0.0004 0.5 3,000 0.25 34
	VERY BLOCKY-interlocked, partially disturbed rock mass with multifaceted angular blocks formed by four or more discontinuity sets	$m_b/m_i$ $s$ $a$ $E_m$ $\nu$ $GSI$	0.40 0.062 0.5 40,000 0.2 75	0.29 0.021 0.5 24,000 0.25 65	0.16 0.003 0.5 9,000 0.25 48	0.11 0.001 0.5 5,000 0.25 38	0.07 0 0.5 2,500 0.3 25
	BLOCKY/SEAMY-folded and faulted with many intersecting discontinuities forming angular blocks	$m_b/m_i$ $s$ $a$ $E_m$ $\nu$ $GSI$	0.24 0.012 0.5 18,000 0.25 60	0.17 0.004 0.5 10,000 0.25 50	0.12 0.001 0.5 6,000 0.25 40	0.08 0 0.5 3,000 0.3 30	0.06 0 0.55 2,000 0.3 20
	CRUSHED-poorly interlocked, heavily broken rock mass with a mixture of angular and rounded blocks	$m_b/m_i$ $s$ $a$ $E_m$ $\nu$ $GSI$	0.17 0.004 0.5 10,000 0.25 50	0.12 0.001 0.5 6,000 0.25 40	0.08 0 0.5 3,000 0.3 30	0.06 0 0.55 2,000 0.3 20	0.04 0 0.60 1,000 0.3 10

Note 1: The in situ deformation modulus  $E_m$  is calculated from Equation 4.7 (page 47, Chapter 4). Units of  $E_m$  are MPa.

Figure A-1: Estimation of constants  $m_b / m_i$ ,  $s$ ,  $a$ , deformation modulus  $E$  and the Poisson's ratio  $\nu$  for the Generalised Hoek-Brown failure criterion based upon rock mass structure and discontinuity surface conditions for undisturbed rock mass (Hoek et al., 1995, Table 8-4).